UNIVERSITÀ DEGLI STUDI DI PALERMO

PhD in *Biologia Cellulare e Scienze Tecnologiche del Farmaco*
-Scienze Farmaceutiche-
Department of *Scienze e Tecnologie Biologiche, Chimiche e Farmaceutiche*
(STEBICEF)
CHIM/08

DESIGN, SYNTHESIS, AND BIOLOGICAL EVALUATION OF NOVEL HETEROCYCLIC DERIVATIVES AS MODULATORS OF B-DNA AND G-QUADRUPLEXES DNA FUNCTIONS

Doctor
ROBERTA BARTOLOTTA

PhD Coordinator
PROF. PATRIZIA DIANA

Supervisor
PROF. ANTONINO LAURIA

CICLO XXVI
2016

"Working hard
for something we do not care about
is called stress;
working hard for something we love
is called passion."

Simon Sinek

ABSTRACT

This research work focuses on the design, the synthesis, interaction studies and biological evaluation of new aromatic heterocyclic small molecules addressed either towards the B-DNA as well as the G4-DNA isoforms as targets.

The synthesis and the biological evaluation of a new benzo[*b*]thiophene and benzo[*b*]furan series were reported. Generally, all tested compounds in the first series showed a good antiproliferative effect on HeLa tumor cell line with GI50 values in a low micromolar range. These findings could be in accordance with biological assays that highlight a possible antimitotic mechanism or a potential inhibition of the topoisomerase II enzyme, thus affecting and modulating some of the B-DNA functions. This could justify the cell cycle arrest at G2/M checkpoint.

The synthesis and the biological evaluation of the new benzo[*b*]furan were accomplished. In this series, the thiophene central core of the benzo[*b*]thiophene derivatives above mentioned has been replaced with a furan ring, in order to evaluate the isosteric influence on the biological activity, affording significant growth inhibition effect when antiproliferative screening on HeLa and MCF7 tumor cell lines were carried out, producing cell cycle arrest with proapoptotic effects.

The design, synthesis and biological studies of some new potential ligands of G-quadruplex have attracted further interest.

Synthesis of *bis*-isoquinoline derivatives and double-chained naphthalenes were carried out. Unfortunately spectroscopic tests on G4-DNA isoforms gave any expected result previously observed through *in silico* assessments.

Besides, linear and annellated naphthaleno-pyridazinone derivatives were synthesized *via* nucleophilic substitution reaction and intramolecular Heck-type arylation, exploiting as starting material the 2-benzyl-4,5-dibromopyridazin-3(2*H*)-one, because its controllable regiochemistry. Noteworthy, antiproliferative tests on Hela cell tumor lines over 48 hours treatment have shown interesting GI50 values both in micromolar and nanomolar range.

1. Introduction

It has long been known that the deoxyribonucleic acid (DNA) is the main *bio-target* for anticancer drugs currently used in the clinical field, both if they are able to bind the polynucleotide covalently or reversibly. However, the side effects on normal cells from the classical DNA-interactive drugs, such as alkylators, intercalators, and strandbrakers are so relevant as to limit their therapeutic use (1).

The current anticancer treatments have several limitations, including drug resistance and side-effects of toxicity (2), due to the correspondence in shape and chemical structure of DNA both in healthy and tumor cells. The rapid, abnormal, and uncontrolled cell division characterizes cancer cells, which are continuously undergoing mitosis. Because this rapid cell division, tumor cells do not have sufficient triggering time for repair mechanisms. Indeed, when a DNA damage is sensed in a cell, mechanisms involving proteins such as p53 are activated. Particularly, activation of p53 in normal cells can result in several cellular responses namely upregulation of DNA repair systems, programmed cell death (*apoptosis*) or cell cycle arrest, which allows time to DNA to be repaired. Differently, tumor cells are defective in their ability to undergo cell cycle arrest or apoptosis in response of DNA damage, thus resulting more sensitive to DNA-damaging agents (3,4). Although targeted therapies in anticancer drug discovery are being developed, the lack of selectivity remains a major issue for current anticancer therapeutics. Therefore, the development of synthetic molecules that alter or halt with lower side effects the cell proliferation processes giving rise to tumors, is still a topic highly studied by many research groups.

1.1 DNA-Interactive Drugs Limitations

1.1.1 Side effects of Toxicity

Most of the side effects of toxicity of the current DNA-interactive drugs are observed in the bone marrow, the mucosa, the gastrointestinal tract (GI) and the hair, namely where rapid cell proliferation occurs.

Doses in the toxic range ensure the effectiveness of a cancer drug itself thus to kill tumor cells but allowing healthy cells of bone marrow and GI tract to survive, although there are some evidences according which nausea and vomiting, for instance, are not depending on the destruction of GI cells rather on the DNA-interactive agents effect on the central nervous system (CNS) (5). According to the *fractional cell kill hypothesis* (6),

a given drug concentration administered over a defined time period will kill a constant fraction of cells, regardless of the absolute number of cells. Therefore, since each cycle of treatment will kill a specific amount of the remaining cells, the effectiveness of the treatment is a direct function of the dose and the frequency of the cycle repetition. Besides, in anticancer drug therapies single-drug treatments are not completely effective, have short duration, and complete remission is only short lived. Furthermore, relapse is associated with resistance to the original drug.

1.1.2 Combination Chemotherapy: a Drug Interactions and Resistance issue

In order to overcome anticancer drugs resistance, in the late 1950s combination chemotherapy has been introduced. Indeed, whether single-drug treatment may increase the rate of mutation cells into resistant forms, multiple drugs therapies show many advantages and improved effectiveness, acting through different mechanisms of action that allow independent cell killing by each drugs. Moreover, cells resistant to one drug may be sensitive to another and if drugs do not have overlapping toxicities, each of them can be used at full dosage ensuring their effectiveness in combination. On the other hand, drugs that cause for instance renal toxicity must not used in combination with drugs whose primary mechanism of excretion depends on renal elimination. Indeed, the most relevant issue associated with the use if combination chemotherapy, is still drug interaction (7).

1.2 DNA Structure and Properties

The three dimensional structure of B-DNA consists of two complementary strands of antiparallel poly-deoxyribonucleotide, wrapped around one another to form a double helix.

The two strands are held together by specific hydrogen bonds of Watson-Crick, which are established between purine and pyrimidine nucleotides. The two purine bases, adenine (A) and guanine (G) and the two pyrimidine bases, cytosine (C) and thymine (T) form stable 3,5'- phosphodiester bonds, through the linkages between the 5'-phosphate group of one nucleotide and a 3'-hydroxyl group on the sugar of the adjacent nucleotide (fig.1).

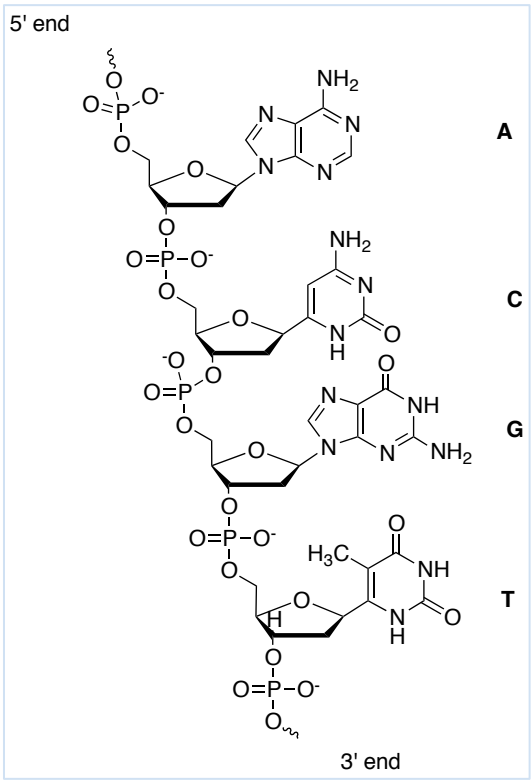

Figure 1. **3',5'-Phosphodiester linkages between A(adenine)/G(guanine) and C(cytosine)/T(thymine) of the DNA.**

The different spacing between the two sugar phosphate backbones of the double helix along the helical axis is due to the two glycosidic bonds joining the base pair to its sugar rings that are not directly opposite to each other. As a consequence, the grooves between the backbones result larger, in the case of the *major groove*, and smaller if it deals with the *minor groove* (fig.2).

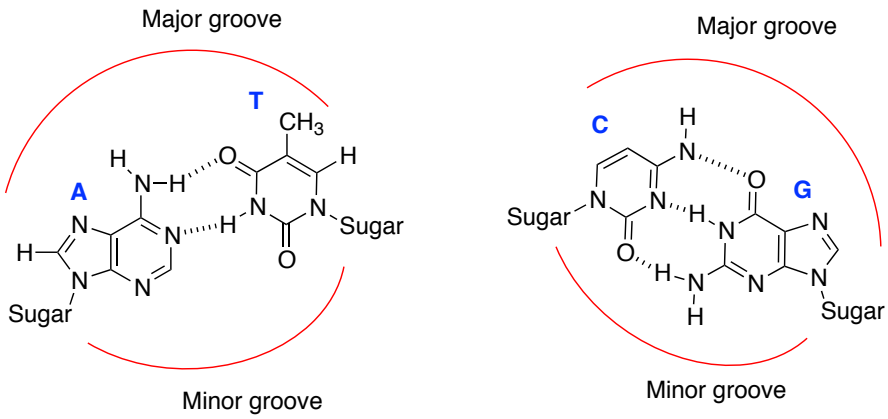

Figure 2. **Features of DNA base pairs A-T, C-G responsible for the formation of major and minor grooves.**

In the major groove the base pair nitrogen and oxygen atoms project inward from their sugar phosphate backbones towards the centre of the DNA, while in the minor groove nitrogen and oxygen atoms of base pairs project outward from their sugar-phosphate backbones towards the outer side of the DNA. Therefore, electrostatic interactions with B-DNA are historically classified into minor and major groove and interactions of intercalation (2,3). For intercalation is meant the insertion of planar molecules, in particular those containing aromatic heterocyclic rings, between two adjacent base pairs of DNA, perpendicular to the axis of the double helix, causing a vertical separation of the pairs of complementary bases with deformation and elongation of the sugar-phosphate backbone (10).

Thus, in the B-DNA, the backbone of the paired strands provides a shallow-wide major groove and a deep-narrow minor grove (11,12), with different chemical features that form the basis for molecular recognition by small molecules and proteins.

1.2.1 The Importance of the DNA base pairing

Base pairing plays a key role in maintaining the integrity of the DNA. The specificity of base pairing is depending on several factors: hydrogen bonding and shape represent two significant aspects in this regard.

1.2.1.1 Hydrogen Bonding and Tautomerism

Due to the tautomerism of the different heterocyclic bases, largely depending on the dielectric constant of the medium and on the p*K* of the respective heteroatoms (13), at physiological pH, the more stable tautomeric form for the bases having amino substituents as A, C, and G is, by far (>99.9%), the amino form not the imino form and the oxygen atoms of G and T also strongly prefer (>99.9%) being in the keto form rather than the enol one (14). Apparently, these four bases in the appropriate tautomeric forms are the only requirement for complementary base recognition.

Donor and acceptor groups are complementary for C and G and for A and T, but not for C and A or G and T (fig. 3).

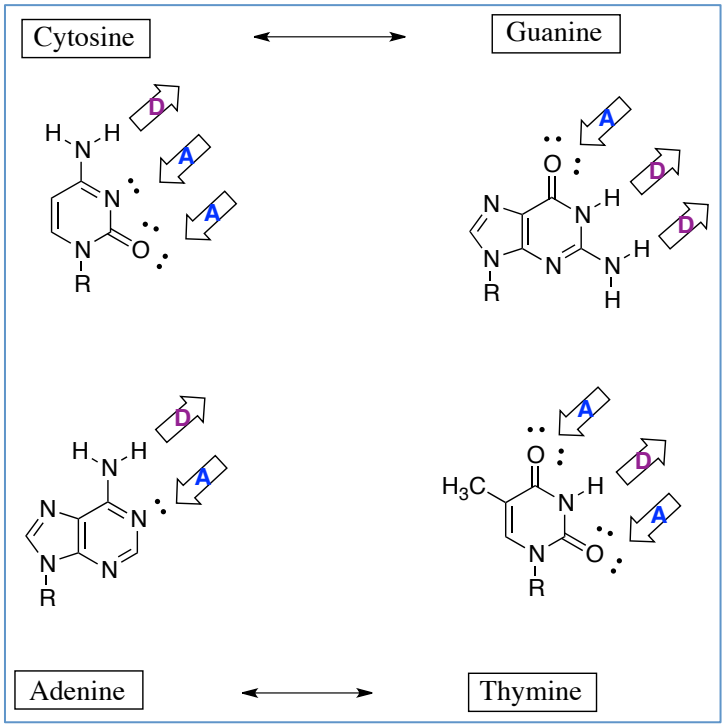

Figure 3. Complementary base recognition by hydrogen bonding sites of the DNA bases. D, hydrogen bond donor; A, hydrogen bond acceptor.

Modifications of the bases, such as replacement of the carbonyl group in purines by a thiocarbonyl group, would increase the enol population to about 7% (15), resulting in a significant effect on base pairing.

1.2.1.2 Base-pairs Isosters to Determine Important DNA Features

Hydrogen bonding is not the only factor that controls the specificity of base pairing; shape may also play an important role. As demonstrated by Kool in its studies (16-18), in the synthesis of several nonpolar nucleoside isosteres, thus lacking hydrogen bonding functionality, complementarity of size and shape is as important as the hydrogen bond ability in controlling the DNA base pairing (19,20).

In order to determine the importance of hydrogen bonding for DNA, a thymidine isostere, the difluorotoluene isostere nucleoside **1** (log P= +1.39) has been synthezized, resulting in a nearly perfect mimic of thymidine (log P = −1.27) in the crystalline state and in solution (21).

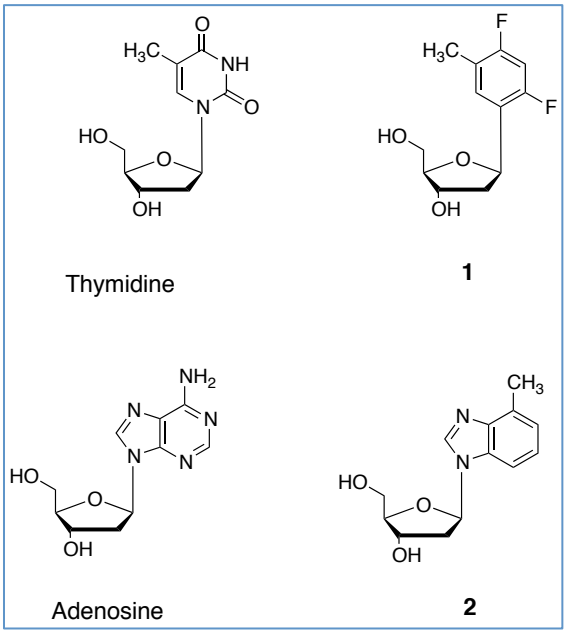

Figure 4. Nonpolar nucleoside isosters (1 and 2) of thymidine and adenosine (7)

Indeed, the isostere **1,** incorporated and substituted in a template strand of DNA where it is paired opposite to adenine, adopts a structure identical to that of a T–A base pair (22) and common polymerases is able to selectively insert adenosine opposite it (23) with a similar efficiency to that of a natural base pair. The benzimidazole isostere of deoxyadenosine, **2** is less similar in shape but it still base pairs by non-hydrogen-bond interactions by mimicking adenosine in DNAs (22) even as a substrate for polymerases. This suggests that Watson–Crick hydrogen bonds are not necessary to replicate a base pair with high efficiency and selectivity and that steric and geometric factors may be at least as important in the polymerase active site (24,25).

1.3 G4s-DNA

Unlike the well known double–helical B-DNA that, as above mentioned, consists of two complementary antiparallel, sugar-phosphate poly-deoxyribonucleotide strands, held together with specific Watson-Crick hydrogen bonds between purine and pyrimidine nucleotides, G-quadruplexes (G4s) are higher-order DNA and RNA secondary structures. G-quadruplexes show a considerable polymorphism, important in the carcinogenic processes. These structures are characterized by a core of at least two overlapping G-tetrads.

The G-tetrads are formed by a pseudo planar quartet of guanines, adopting either *anti* or *syn* alignements respect to the glycosidic bonds, stabilized by Hoogsteen-hydrogen bonds

and a positively charged monovalent metal ion (mainly K^+ or Na^+) located within the central channel of stacked G-tetrads, which allows the neutralization of the strong electrostatic potential associated with the guanine carbonilic oxygenes, fostering the stabilization of G4-structures (10,26).

In detail, each tetrad is overlapped parallel to another of the same strand through π-π stacking interactions, thereby forming a polymer with helical structure (fig.5).

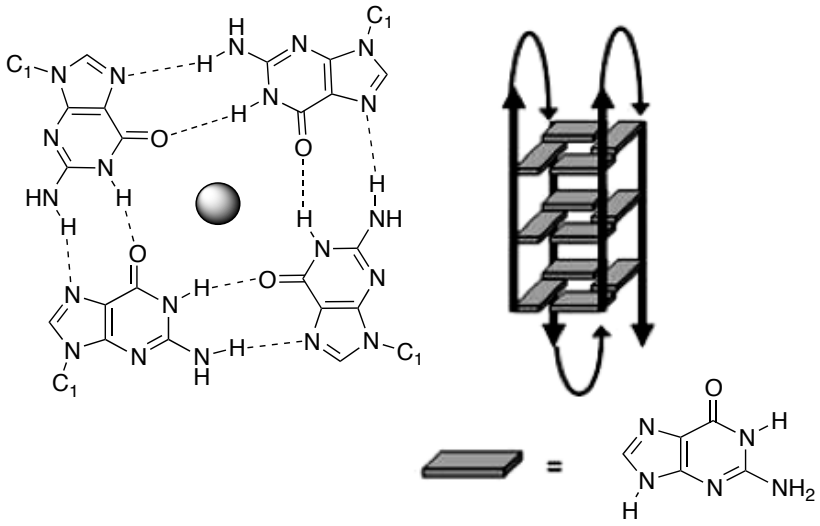

Figure 5. Tetrad consists of 4 guanines stabilized by Hoogsteen hydrogen bonds and the presence of monovalent metal ion (left side). Schematic representation of a structure given by the intramolecular bonds of G-quadruplex tetrads (right side).

Structurally, there are different topologies of G-quadruplex depending on the orientation of the filaments, the length of the loops and the nucleotide sequence thereof. In addition, the G-quadruplex structures can be both of intramolecular and intermolecular nature.

In the latter case, the secondary structure is given by the union of multiple strands that can arrange in all possible combinations of parallel and anti-parallel orientation (26). The filaments of connection (fig. 6), called loops, can be classified into: *edgewise*, lateral, linking two adjacent antiparallel strands; *double chain reversal,* that combine two adjacent parallel filaments, and *diagonal* loops, which bind two antiparallel strands but opposite (27), and finally *V-shaped* loops that connect the corners of two stacked guanine tetrads, which lack a connection (28).

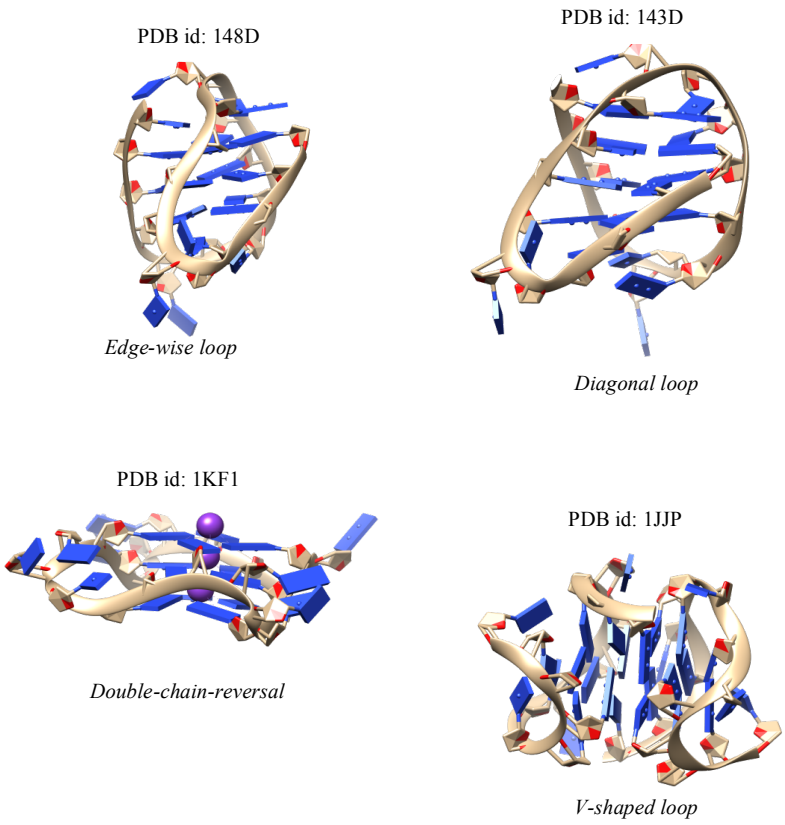

Figure 6. G4-DNA: loops

From a different perspective, G4s are higher-order DNA and RNA secondary structures located in key areas of the eukaryotic genome, including telomeres and regulatory regions of many genes among which oncogenes (29).

Bioinformatical analyses combined with biophysical and structural investigations have highlighted the relative abundance of putative G-Quadruplex forming sequences in promoter regions of oncogenes close to transcriptions start sites, which include also the c-myc gene (30).

The MYC gene promoter was one of the most studied system for the G-quadruplex formation, especially because its dysregulation is one of the hallmarks of many cancers (30). Unlike telomeric G-Quadruplexes, which can be formed from the single-stranded DNA, G-Quadruplexes in gene promoter regions are constrained by the duplex nature of genomic DNA. Each of single stranded elements in gene promoter double stranded DNA could be a precursor of the formation of secondary DNA structures like G-Quadruplexes and protruding structures that keep the two DNA strands separated and prevent the formation of the basal transcriptional complex.

G4 structures are over-expressed not only in telomeres, about which it will discuss hereinafter, but also in gene promoter regions, making them even more attractive as therapeutic targets in oncology (10). The first study about it reported that the proto-oncogene *c-myc*, is upregulated in up to 80% of solid tumors, and it has a putative G4 in the nuclease hypersensitive element (NHE) targeted with a small molecule. Since then, the folding patterns of several promoter G-quadruplexes have been proposed, such as the genes encoding MYC, B cell lymphoma 2 (BCL-2) (31), vascular endothelial growth factor (VEGF)(32), hypoxia-inducible factor 1a (HIF1a) (33), the transcription factor MYB(34), and KRAS (35,36).

Therefore, the transcriptional repression can be achieved by induction of putative G-quadruplex formation, that can inhibit the MYC transcription thus suppress oncogenic expression (30).

1.3.1 The Important Presence of G4-DNAs in Telomeres

Telomeres are repetitive hexanucleotide non-coding sequences, placed at each end of a chromatid, with the function to protect chromosomes from erosion or from fusion with adjacent chromosomes, during gene duplication.

Human telomere consists of a double stranded DNA sequence 5-10 kilobases long. It is characterized by tandem repeats of the hexanucleotide d(TTAGGG)n (37,38), ending up in a single-stranded G-rich 3’ overhang of 35-600 bases (38-40), (fig. 7).

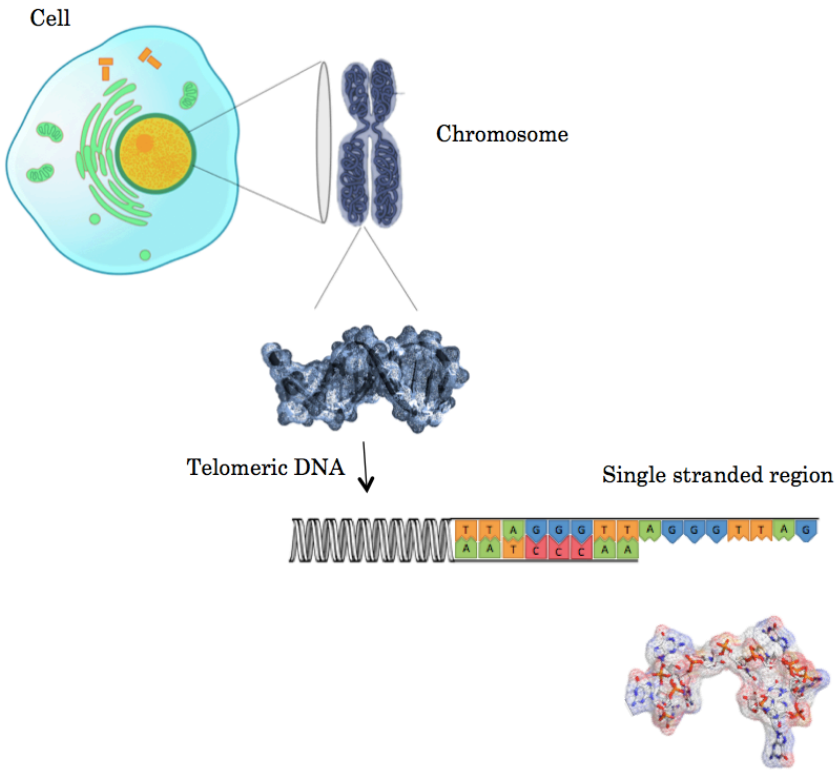

Figure 7. Schematic representation of the DNA overhang region (26).

In order to protect the otherwise exposed telomeric overhangs, the telomere ending is folded in a higher-order conformation known as telomeric loop or "T-loop" (41), (fig. 8).

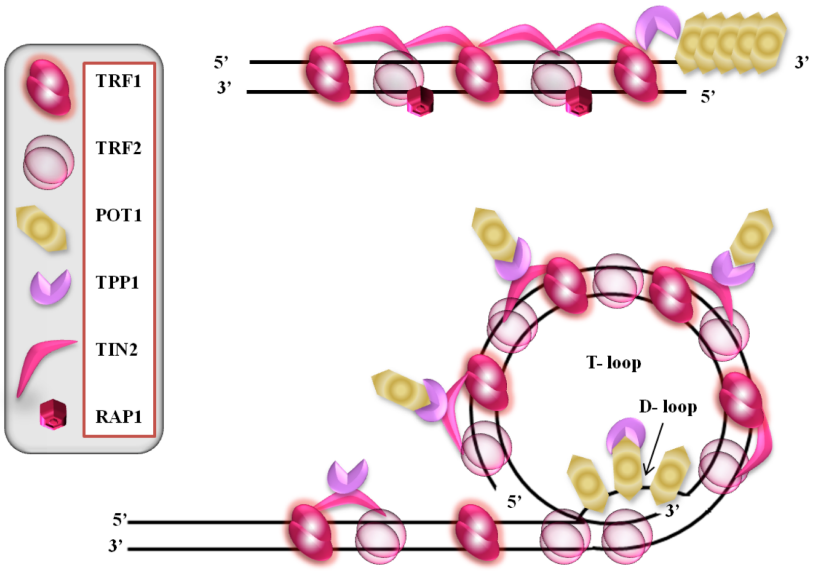

Figure 8. Schematic representation of the chromosome end, folded in T-loop, including members of the shelterin proteins complex (26). TRF1, telomere-repeat-binding factor 1; TRF2, telomere-repeat-binding factor 2; POT1, protection of telomeres protein; TPP1, tripeptidyl pepti-dase; TIN2, interacting nuclear factor; RAP1, repressor activator protein 1.

This structural organization, which provides the maintenance and capping of telomeric DNA, is achieved through a smaller displacement loop (D-loop) of the G-rich strand, which is mediated by six shelterin proteins: telomere-repeat-binding factors (TRF1, TRF2), protection of telomeres protein (POT1), interacting nuclear factor (TIN2), repressor activator protein 1 (RAP1), and tripeptidyl peptidase 1 (TPP1) (26).

Telomeres are essential for genome integrity. The double stranded terminates with a single-stranded 3' extension of a G-rich sequence that can fold into G-quadruplex structures. Such single-stranded 3' overhang is the substrate for the telomerase. Telomeres shorten with each cell replication and, when they reach a critically short length, such shortening leads normal cells to arrest proliferation, undergo senescence, by acquiring a variety of altered functions up to a DNA damage response that culminates in cell cycle arrest or cell death.

1.3.2 Telomerase Enzyme and the G-Rich Telomeric DNA

Telomerase is a RNA-dependent DNA polymerase almost universally conserved in eukaryotes. It is made up of a minimal catalytic core including two subunits: the TERT protein (Telomerase Reverse Transcriptases) and the RNA component known as TERC (Telomerase RNA Component) or simply TR (Telomerase RNA) (42,43).

The active site of the enzyme catalytic subunit, mainly characterized by aspartic acid triplets, acts as a reverse transcriptase likewise the viral ones (44,45).

The human proteic subunit hTERT is a heterodimer, made up of the proteins p123 and p43, which binds the RNA component TR with a ratio of 1:1:1 (46). The human ribonucleic subunit (hTERC) is a large RNA made up of 451 nucleotides in humans and between 148 and 209 nucleotides in ciliates (47). It contains a small portion of eleven nucleotides (5'-CUAACCCUAAC in human), located at the 5' end, which encodes the related telomere repeat and works as a template for the additions of nucleotides at the end of the chromosome (42). The elongation of telomere occurs in several steps that can be summarized as shown in (fig. 9).

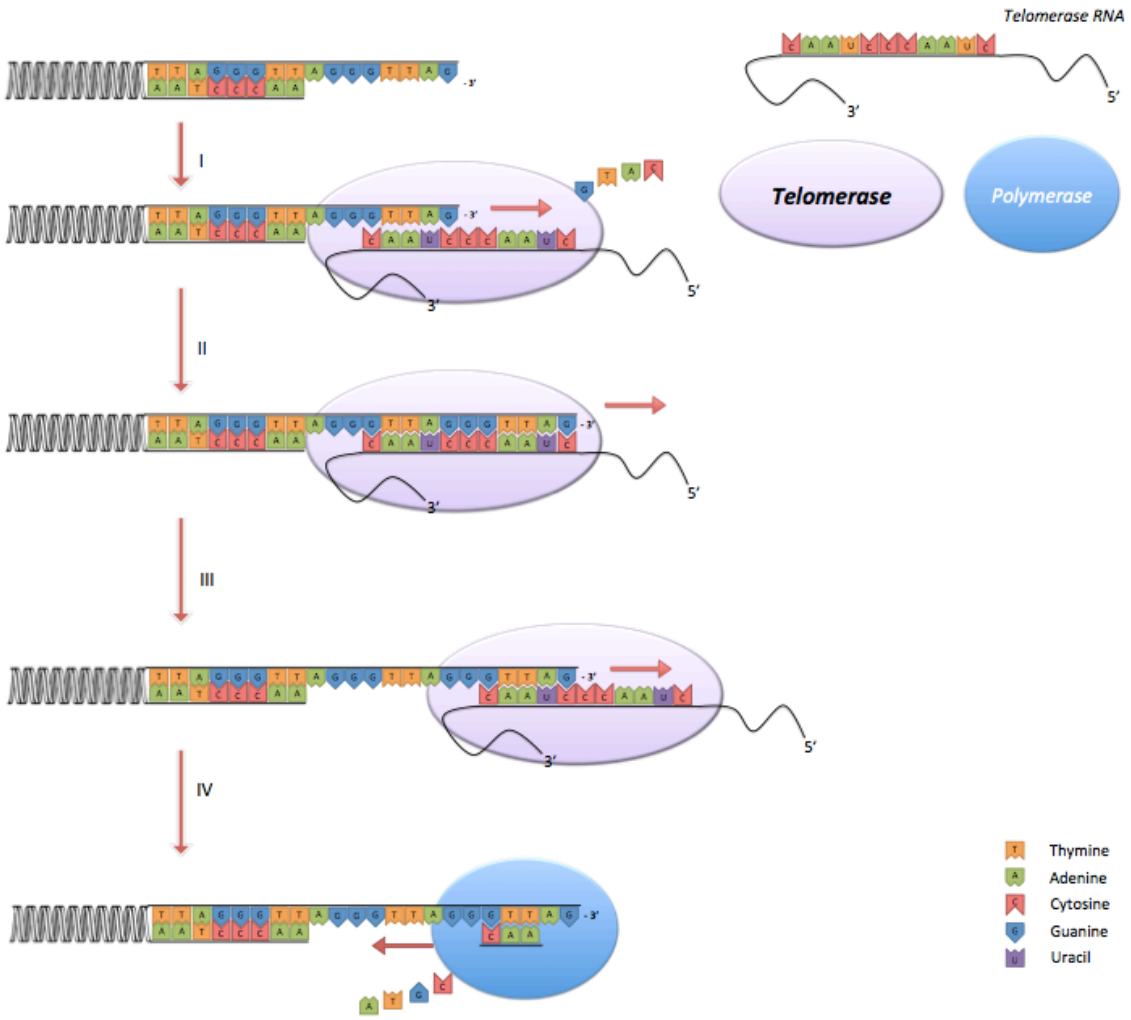

Figure 9. The elongation of telomere: (I): initial annealing; (II): first extention cycle; (III): dissociation and reannealing; (IV): extension cycles and DNA polymerase complementing the laggins strand

Telomerase, a unique reverse transcriptase, plays a key role in maintaining telomere length and integrity: it binds to the G-rich 3' end of telomeric DNA and fosters the addition of telomeric DNA onto the chromosome ends using its own integral RNA template. Likewise, telomeres of tumor cells do not shorten during proliferation but instead tend to have short but yet stable telomeres. This is the reason why telomerase, which has been found upregulated in 85-90% of human tumors, ensures cellular immortality, hence the proliferation of cancer cells.

Noteworthy, the G4-DNA formation in a telomeric primer obstructs telomerase association and inhibits primer extension.

Nevertheless, it is worth to notice that telomerase is inactive in few tumors in which other pathways are responsible for the telomere maintenance (48). This recombination-

dependent telomere lengthening mechanism, named Alternative Lengthening of Telomeres, or "ALT" pathway, replaces telomerase activity in about 10-15% of human cancers. Therefore, therapeutics directed only against telomerase in cancer cells might not be able to interact with those using ALT pathway that, for this reason, will be resistant to therapy (49).

On the other hand, targeting telomeres might be a new solution for resistant tumor cell lines. In this context, G-rich 3' overhangs play a key role. The latter is the natural substrate for telomerase, which uses it as its primer, and it is probably the necessary structural motif for the recombination-based mechanism of telomere maintenance ALT (50). Interestingly, it has been shown that the guanine-rich 3' overhangs of telomeres, with TTAGGG repeats, can equilibrate between single-stranded and G4 structures by means of hPOT1 protein (51). G4 folding of the G-overhang is a structural motif for telomere protection, alternative or in addition to the T-loop conformation. As a matter of fact, when the telomere tail is in a G4 conformation, the activity of telomerase, and probably of ALT, is inhibited (50,52,53).

This interesting finding suggests that ligand-induced stabilization of telomeric G4 scaffold is a promising strategy for anticancer drug development (44,54-56). Furthermore, this telomerase inhibition pathway represents a useful approach to bypass the occurrence of ALT.

Thus, G-quadruplexes are considered effective targets for novel anticancer drugs development, although telomere-targeting G-quadruplex ligands, known hitherto, have not yet been successful in clinical phase, due in part to poor tumor penetrating ability and lack of target selectivity (57).

1.4 Heterocyclic Aromatic Compounds in Anticancer Drug Discovery

Heterocycles are heavily involved in life processes. DNA, RNA, proteins, and coenzymes are classical examples of fundamental biological macromolecules structured by heterocyclic moieties. The biomolecular standpoint of drug action confirms the broad biocompatibility and the versatile aptitude of heterocycles to mimic endogenous molecules and consequently to interact with biological entities (58). These features make heterocyclic chemistry one of the major pivots for the development of new drugs, justifying the intense attention of the scientific community on this field.

1.4.1 Isosterism and Bioisosterism in Medicinal Chemistry

The discovery of more potent, clinically safe, and commercially attractive new targeted drugs is the driving force at the base of medicinal chemistry research. To reach this goal, different approaches might be followed. On this purpose, the study of structure-activity relationship (SAR), between molecular structures and their biological activity, is a valuable and rational approach in the lead compounds identification and optimization. The SAR analysis enables the identification of chemical moieties, responsible for the interactions with a biological target and, therefore, for their therapeutic effects in an organism (59). Structural modifications may be conducted on lead compound in order to get more suitable the pharmacodynamic properties and/or to improve the pharmacokinetic ones. More often the lead optimization process is based on the isosteric replacements of functional groups to systematically understand the contribution of each modification of the lead compounds on the biological activity.

The concept of isosterism, was introduced for the first time by Irving Langmuir (1919). He defined isosteres those atoms or groups of atoms or molecules or compounds (organic or inorganic) having the same electronic and steric arrangements (60,61). Later, the isosteric concept was extended to the biological field in the therapeutic search of new drugs, defining the concept of bioisosterism. Friedman (1951) identified bioisosteres those molecules or atoms, which fulfill the electronic and steric criteria of isosterism, retaining the same biological effects of their correspondent isosters (61).

Table 1. **Ring Equivalents producing biososteric structural modifications.**

RING EQUIVALENTS			
			
Benzene	**Thiophene**	**Furan**	**Pyrrole**
			
	Benzene	**Pyridine**	
	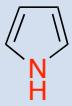	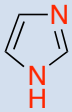	
	Pyrrole	**Imidazole**	

In medicinal chemistry field, the approach to bioisosteric structural modifications, like ring equivalents (table 1) or ring-to-ring transformations, are widely investigated in lead compounds optimization, producing a notable number of clinically drugs (62). Indeed, the substitution of –CH= by –N= or –CH=CH- by –S- within aromatic rings has been one of the most successful application of classical isosterism (e.g. H_1-blockers) (63).

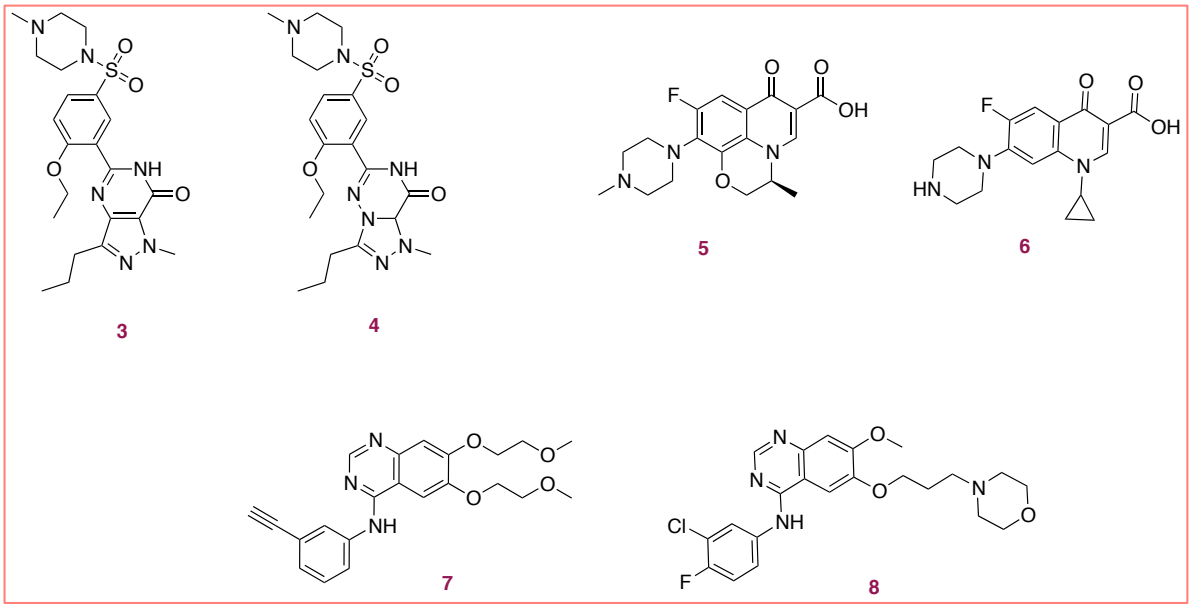

Figure 10. Successful bioisosters: Sildenafil (3) and Vardenafil (4); Levofloxacin (5) and Ciprofloxacin (6); Gefitinib (7) and Erlotinib (8).

In figure 10 are reported some examples of successful application of bioisosterism in the drug structural optimization process: Sildenafil (**3**) (Viagra) >> Vardenafil (**4**) (Levitra), Levofloxacin (**5**) (Tavanic) >> Ciprofloxacin (**6**) (Cipro) and Gefitinib (**7**) (Iressa) >> Erlotinib (**8**) (Tarceva).

1.4.2 From The Canonical B-DNA to the Modern G4-DNA Interactive Agents

The main goal of anticancer research is to develop targeted therapeutic strategies in order to find new agents with selective biological activity against tumor cells. Regulation of duplication and transcription machinery is a crucial way to achieve gene expression control in human cells. Therefore, deoxyribonucleic acid (DNA) is an elective target for anticancer therapy. Classical DNA-binding drugs, such as intercalators, alkylators, and strand breakers, exert their biological activity in an unselective way, producing serious

side effects on normal cells (1). Accordingly, an intriguing challenge is to design DNA-interactive molecules showing maximum specificity in DNA-binding, without interfering with the functions of healthy cells.

In the last few decades, the design of small molecules able to bind non-canonical DNA secondary structures, such as G-quadruplexes (G4s), has aroused considerable interest. Several compounds described in literature have already shown to be good candidates as powerful sequence-specific G4s binders, stabilizing the non canonical DNA structures mainly through top/end stacking interactions (64).

In this regard, many research groups have worked to identify or design small-molecule ligands, which specifically bind to the G4s. Thus, several ligands, which have high affinity for G4s and inhibit cell proliferation, have been proposed. Some of these compounds have shown to inhibit telomerase or to affect telomere lengthening (54,65,66).

Evidence that G4 structures may occur at the telomeres and in gene promoter regions, has undoubtedly provided further impetus to the development of drugs that interact with or promote the formation of the G-quadruplexes.

1.4.2.1 Classical DNA-Interactive Drugs

DNA-interactive drugs can be classified into three clinically important major classes:

- *reversible binders*, which interact with DNA through the reversible formation of non-covalent interactions;
- *alkylators*, which react covalently with DNA bases;
- *DNA strand breakers*, which generate reactive radicals producing cleavage of the polynucleotide strands.

The primary DNA sequence recognition by proteins results from complementary hydrogen bonding between amino acid residues on the protein and nucleic acid bases in the major and minor grooves of DNA (7,67). In detail, proteins and large molecules, for example oligonucleotides, bind B-DNA preferentially through the major groove, because it is a good receptor in terms of size, flexibility, and possibility to form H-bonds through donor and acceptor sites, which are more abundant than those present in the minor groove (1,68,69). Small molecules typically bind B-DNA through the minor groove, where sequence recognition is limited compared to the major groove, in large part due to

less varied H-bonding patterns and more limited shape variations with sequence (1,68,69).
However, it is not yet clear what DNA sequences (genes) should be targeted.

1.4.2.1.1 Reversible DNA Binders

DNA functions can be altered by three important ways of reversible interaction of small molecules binding to duplex DNA:

1. electrostatic binding along the exterior of the helix;
2. interaction with the edges of the base pairs in either the major or minor groove;
3. intercalation between the base pairs.

Indeed, since nucleic acids inside the cell interact with small molecules as water, metal cations, small organic molecules, and proteins, important for stabilization of the nucleic acid structure, interference with these interactions can disrupt the DNA structure (7).

1.4.2.1.1.1 External Electrostatic Binding

The interactions hereinafter described are generally not dependent upon DNA sequence.
The polyanionic nature of duplex DNA, containing a negatively charged sugar-phosphate backbone, strongly affects both the structure and function of DNA. Cations and water molecules bind to DNA and allow it to exist in various secondary structures. Release of bound cationic counter ions of the negative phosphate groups upon binding of specific cation ligands can lead to disruption of the DNA structure, providing both favourable (increased entropy) and unfavourable (decreased enthalpy because of loss of specific ionic interactions) contributions to the overall free energy (7).

1.4.2.1.1.2 Groove Binding

The major and minor grooves differ in their electrostatic potentials, hydrogen bonding features, steric effects, and degree of hydration. As above mentioned, proteins exhibit binding specificity interacting primarily with major groove, but small molecules prefer minor groove binding. Minor groove binding molecules generally have aromatic rings connected by single bonds that allow for torsional rotation in order to fit into the helical curvature of the groove with displacement of water molecules (70). The minor groove turns out more suitable to flat aromatic molecule binding with its narrow A-T regions

respect to the G–C regions, binding to such molecules through van der Waals interactions and interactions with the edges of the base pairs on the floor of the groove. Furthermore, a higher selectivity for cationic molecules in A–T regions can be achieved, because of greater negative electrostatic potential in these regions of the minor groove relative to the G–C regions (71).

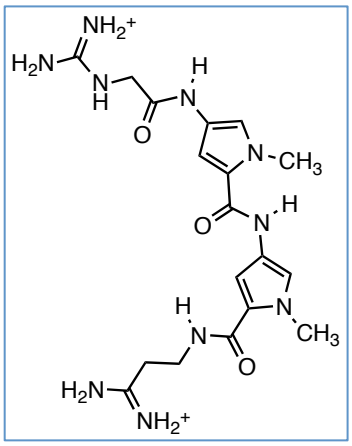

Figure 11. Netropsin, a typical minor groove binder.

A typical minor groove binder is the antitumor, antibacterial, and antiviral agent netropsin (fig.11). This agent causes a widening of the minor groove (0.5–2.0 Å) in the AATT region and a bending of the helix axis (8°) away from the site of bindin (72), thus interferring with the interaction of topoisomerase II and leading to DNA damage.

1.4.2.1.1.3 Intercalation and Topoisomerase-Induced DNA Damage

Intercalation was firstly described in 1961 by Lerman (73), as a noncovalent interaction through which the drug is held rigidly perpendicular to the helix axis. This causes the vertical separation of the base pairs, distorting the sugar-phosphate backbone. Intercalation occurs without disruption of the Watson–Crick hydrogen bonding: the regular helical structure is destroyed, the DNA at the site of binding is unwinded and, as a result, interferences with the action of DNA-binding enzymes such as DNA topoisomerases and DNA polymerases occur. In detail, interference with topoisomerases alters the degree of supercoiling of DNA; interference with DNA polymerases inhibits the elongation of the DNA chain in the 5′ to 3′ direction and also prevents the correction of mistakes in the DNA by inhibiting the hydrolysis of the phosphodiester bond of mismatched residues at the terminus.

Intercalation of a drug into DNA represents only the first step before that DNA damage occurs. Other mechanisms are involved. For instance, simple cationic intercalators initially interact with the negatively charged DNA sugar-phosphate backbone; then the intercalator diffuses along the surface of the helix until it encounters gaps between base pairs, thereby creating a cavity for intercalation.

Many classes of antitumor agents involve the DNA topoisomerases subsequent to intercalation (74). In this regard, a variety of examples are reported in the literature: mammalian DNA topoisomerase I is involved in the action of the antitumor agent topotecan hydrochloride (fig.12), (75) whereas DNA topoisomerase II is involved in the action of a variety of classes of antitumor drugs, such as anthracyclines, anthracenediones, acridines, actinomycins, and ellipticines (76).

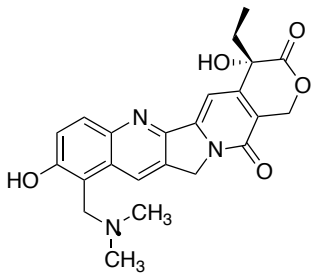

Figure 12. Topotecan hydrochloride.

Flat, generally aromatic or heteroaromatic molecules bind to DNA by intercalating and stacking between the base pairs of the double helix. The main driving forces for intercalation are stacking and charge-transfer interactions, but hydrogen bonding and electrostatic forces also play a role in stabilization. Furthermore, the van der Waals forces that hold the molecules intercalated into the base pairs, are stronger than those between the stacked base pairs.

Three classes of drug molecules are ranked as DNA intercalators: the acridines (e.g. amsacrine), the actinomicines (e.g. dactinomycin), and the anthracyclines (e.g. doxorubicin and daunorubicin), (fig.13).

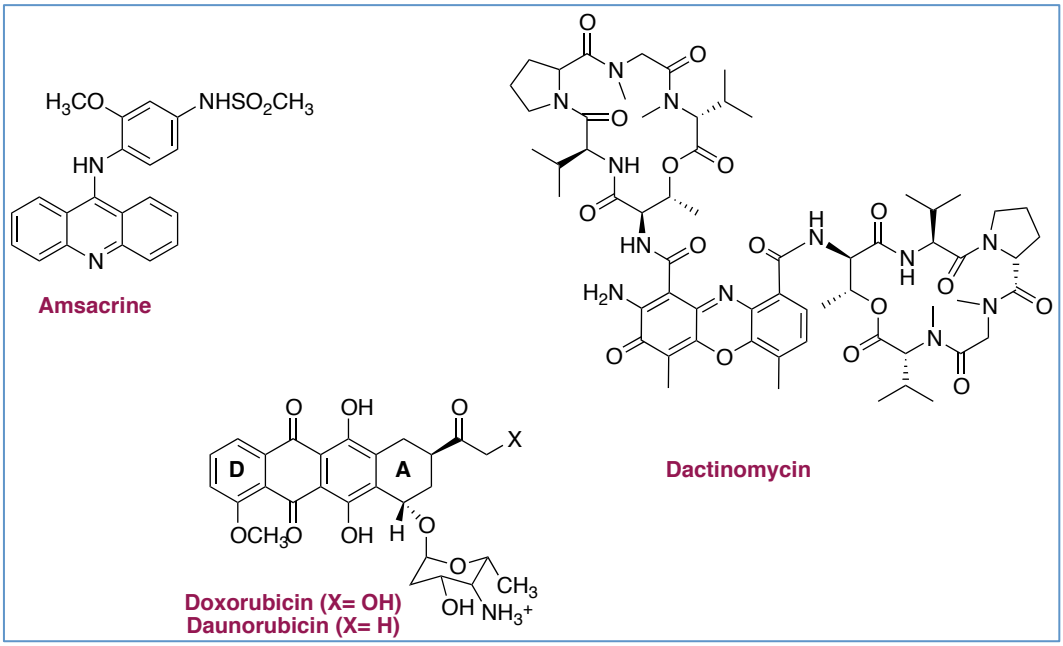

Figure 13. **DNA-interactive drugs acting as intercalators between the base pairs.**

In 1952, Dactinomycin and its parent Actinomycin analog, were found active as antitumor agents and were used clinically. Dactinomycin acts through the binding to double-stranded DNA, and inhibits DNA-directed RNA synthesis or DNA synthesis in a concentration-dependent manner. The peptide substituents, lying in the minor grove, may halt the progression of RNA polymerase along the DNA thus to block the chain elongation (77). Therefore it is evident that intercalators cytotoxicity is due to the interference with the normal cellular processes of DNA, such as replication and transcription.

In the 1960s and early 1970s, among a variety of anilino-substituted acridine derivatives tested as antitumor agents, Amsacrine turned out as the most potent with mode of action of intercalators of double-stranded (duplex) DNA, so as to be still used in the treatment of leukemia (78).

The antracycline class of antitumor anibiotics is well represented by Doxorubicin (fig. 13). It is not yet clear the mechanism of action of these compounds: they may act either intercalating into the DNA double helix by forming a ternary complex with DNA topoisomerase II, causing topoisomerase II-induced DNA damage with consequent inhibition of replication and transcription processes, or through radical-induced DNA strand breakage (79).

In general, groove binders exhibit significantly greater binding selectivty than intercalators. Groove binders interact with more base pairs than intercalators as they lie along the groove and display A-T binding preference; differently, most intercalators show no sequence preferences in their binding unless a slight G–C preference (7).

1.4.2.1.2 DNA Alkylators

As Ross described (80), a biological alkylating agent is a compound that can replace a hydrogen atom with an alkyl group under physiological conditions (pH 7.4, 37 °C, acqueous solution). DNA alkylators differ from DNA intercalators by the nature of their respective interactions; indeed the former are reversible-type and the latter are covalent bonds, namely irreversible-type.

The lead compound of DNA alkylators was the sulphur mustard, a highly cytotoxic chemical warfare agent used in World Wars I and II. This chemical caused leukopenia (low white blood cell count), bone marrow aplasia, dissolution of lymphoid tissues, and ulceration of GI tract (81). These potent effects suggested the use of the sulphur mustard as antitumor agents. The high toxicity of this agent led Gilman and others to asses the antitumor effects of the isosteric nitrogen mustard (82), (fig.14), the Mechloretamine, still used in the treatment of advanced Hodgkin's disease.

Figure 14. Successful bioisosteric substitution: sulphur mustard and its bioisoster mechloretamine.

Nitrosoureas are a metabolically activated alkylating agents type. They were developed from the lead compound N-methylnitrosourea (Fig.15, R=CH3, R'=H), which displayed modest antitumor activity than its analogues carmustatine and lomustatine (fig.15). The lipophilic features of the 2-chloroethyl analogues allowed their use in the treatment of brain tumors.

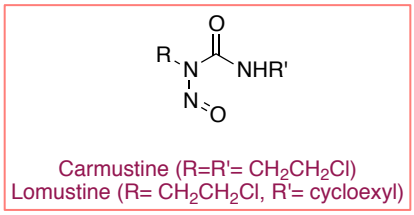

Figure 15. **Nitrosoureas analogues used in the treatment of brain tumors.**

1.4.2.1.3 DNA Strand breakers

DNA strand breakers are metabolically activated radical generators. The mechanism of action of strand breakers includes the initial intercalation into DNA and the subsequent generation of radicals that abstract hydrogen atoms from the DNA sugar-phosphate backbone or from DNA bases, leading to DNA strand breakage. Examples of these compounds are anthracycline antitumor antibiotics, bleomycin, tirapazamine (7). The anthracyclines Doxorubicine and Daunorubicine (fig.13), as mentioned above, can act either *via* the topoisomerase-induced mechanism or as radical-induced DNA strand breakage. In this latter mechanism of action, DNA damage occurs through a one-electron reduction of anthracyclines, presumably catalized by flavoenzymes such as NADPH cytocrome P-450 reductase, which produce the anthracycline semiquinone radical (scheme 1).

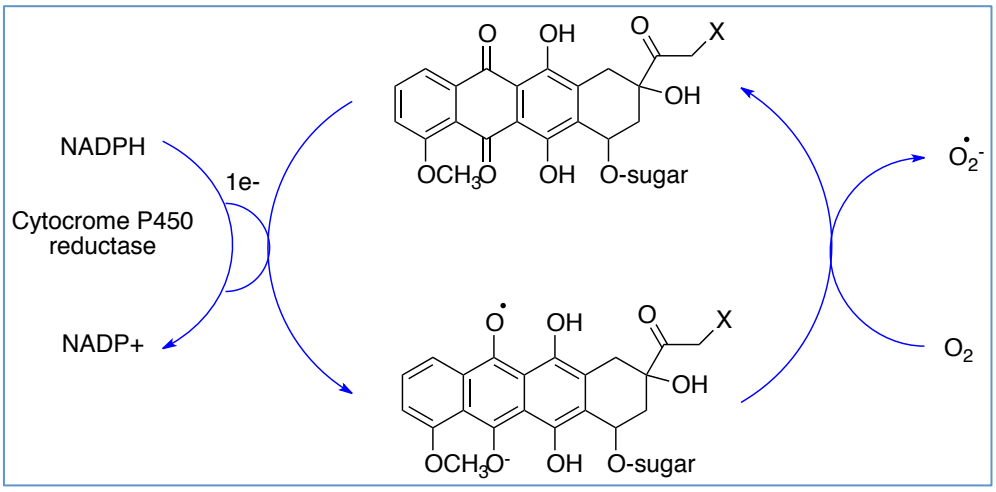

Scheme 1. **Mechanism of DNA strand breakage by anthracyclines (7).**

1.4.2.2 G4-DNA Binders

Several compounds have already described in literature as good G4s DNA binders. Such molecules are able to stabilize the non canonical DNA structures manly through top/end stacking interactions.

In order to obtain the stabilization of the G4s-DNA, the following structural features are requiered: the ligand has to display a delocalized π-system, giving rise to top-stacking interaction with the quartet of guanine and some side chains, positively charged, which would be useful either to increase the solubility and possibly the bioavailability of the G4-interacting agent, and to allow interactions with the skeleton of the sugar phosphate, negatively charged. Furthermore, the presence of a positive charge into a central channel formed by guanine would improve the interactions with G4s. A further characteristic never investigated hitherto (26), is the symmetry. BRACO-19 (fig.16), is one of the most representative symmetrical compounds able to interact with G4-DNA, showing *in vivo* anticancer activity in tumor xenografts, in a significant shorter time exposure (83).

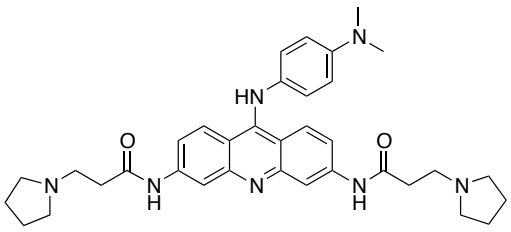

Figure 16. BRACO-19

2. Aim of the Work

This PhD work focuses on the design, the synthesis, and the biological evaluation of novel heterocyclic small molecules able to halt tumor cell proliferation, both reproducing the mechanisms of the classical DNA-interactive drugs, namely the reversible binding to DNA through the formation of non-covalent interactions, and interacting with secondary structures of the DNA (G-quadruplexes), recently turned out as more appealing targets in anticancer drug discovery.

In particular, these objectives are summarized as follows:

- *in silico* studies, as approach to rationalize upstream the proposed synthetic pathways concerning both some new old-fashioned DNA-interactive drugs and novel modern G-quadruplex DNA binders;
- synthesis of heterocyclic symmetrical and unsymmetrical small molecules selected *in silico*, in detail of:
  - benzo[*b*]thiophene and benzo[*b*]furan series;
  - *bis*-isoquinoline derivatives;
  - double-chained naphthalene-derivatives;
  - linear and annellated, symmetrical and unsymmetrical, naphthaleno-pyridazinone derivatives.
- Interaction studies between the synthesized compounds and B and G4s DNA isoforms through UV-vis spectroscopy;
- Evaluation of cytotoxic activity *in vitro* on tumor cell lines.

3. Experimental part

3.1 Results And Discussion

This research work focuses on the design, the synthesis, and the biological evaluation of novel heterocyclic ring systems able to halt tumor cell proliferation.

The access points to the B-DNA, as reported above, are the minor and major grooves, while the G4-DNA interact with its ligands through top/end stacking interactions with the G-tetrads and interactions with the grooves. Thus, it is easy asserting that the features for the interaction with the two targets seem to be roughly similar.

However, some ligands prefer one structure to another. Looking back through the classical binders of B-DNA (fig.17a-b) and the G4-DNA (fig.18), some similarities can be observed. At first glance, all the structures display planar aromatic rings, heterogeneous chains or both. But a difference in symmetry can be easily detected (26). Indeed, intercalators (fig.18a) and the structures binding the grooves (figure 18b) appear to be devoid of symmetry elements. In contrast, the classical G4-DNA binders show at least the element of symmetry C_{nv} (26).

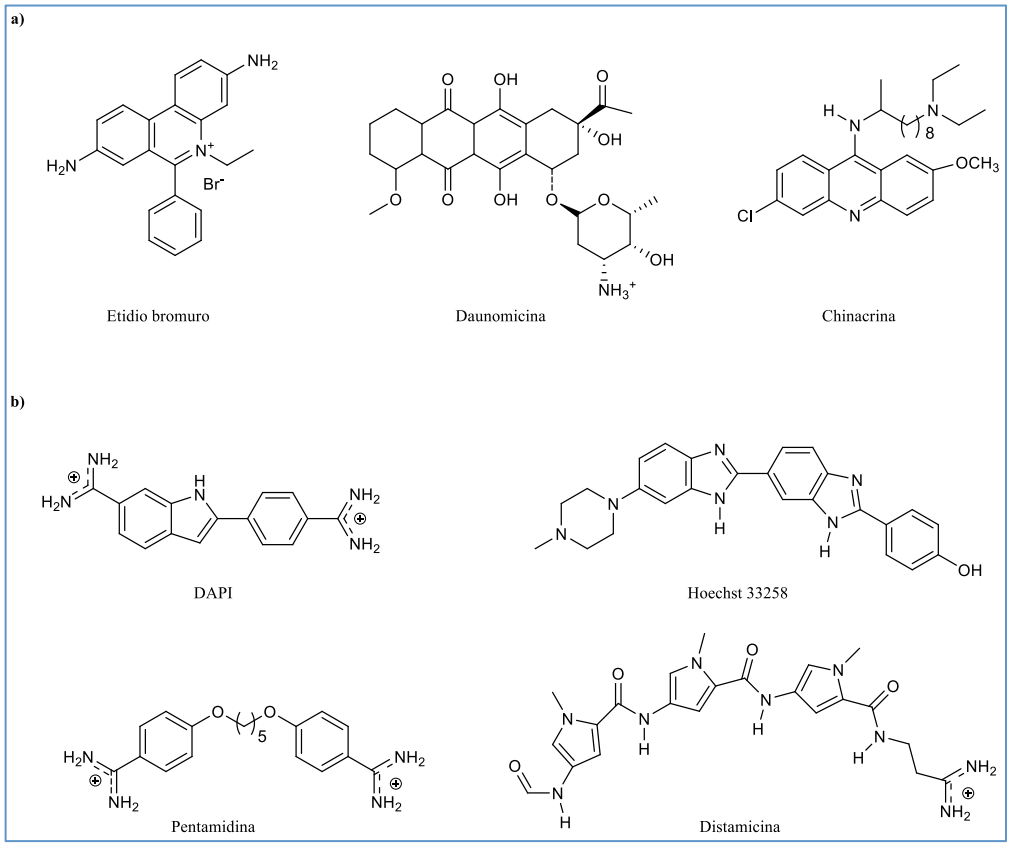

Figure 17. Chemical structures of the most representative B-DNA binders: a) intercalators; b) groove binders.

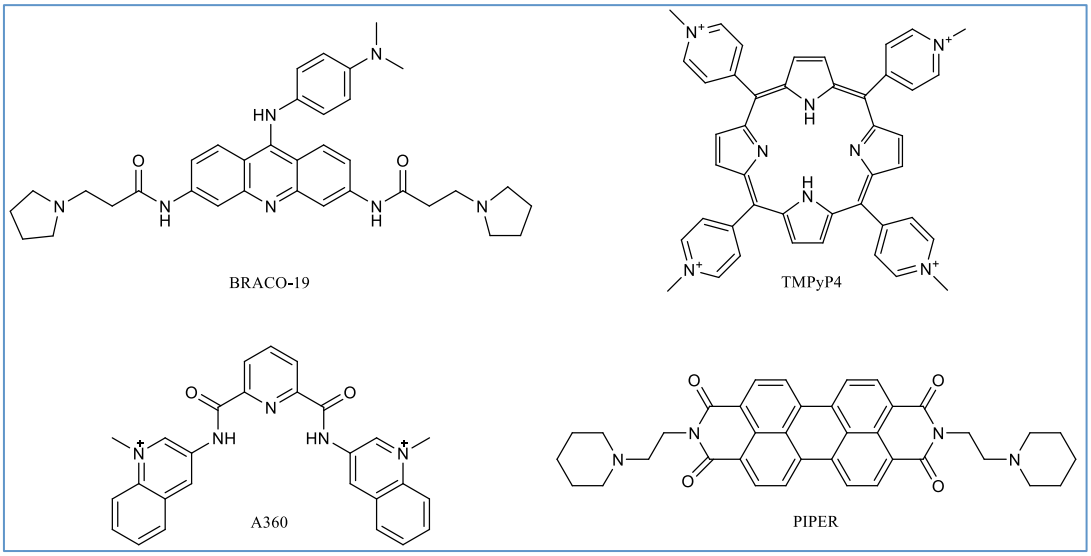

Figure 18. G4- DNA binders known in the literature.

Our symmetry considerations reported by Lauria and co-workers (26) were useful to address this research work to the discovery of both new DNA-interactive drugs and new potential G-quadruplex binders and stabilizers. It is worth noting that molecules without symmetry are not necessarily less effective DNA binding drug, but as shown hereinafter, they exploit a different mechanism of action than that observed in G4-DNA binding.

3.1.1 Synthesis, Biological Evaluation and *In Silico* Insights of Novel Heterocyclic Ring System as Potential Classical DNA-Interactive Drugs

This section focuses on the design, the synthesis, and the biological evaluation of novel heterocyclic ring systems able to halt tumor cell proliferation, reproducing the mechanisms of the classical DNA-interactive drugs, namely the reversible binding to DNA through the formation of non-covalent interactions.

3.1.1.1 New 3-Benzoylamino-benzo[*b*]thiophene Derivatives as Potential Antimitotic Agents or Topoisomerase II Inhibitors

A new series of 3-benzoylamino-5-imidazol-5-yl-benzo[b]thiophenes of type **1** and the parent amino derivatives were synthesized and screened as antitumor agents.

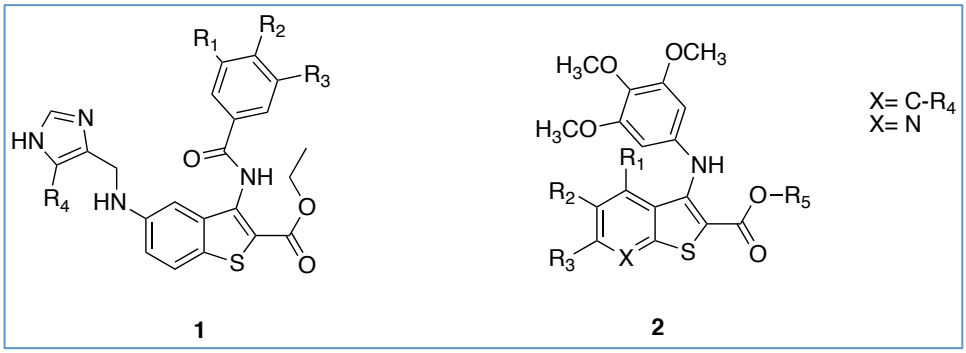

Figure 19. Ethyl 3-benzoylamino-5-[(1H-imidazol-4-yl-methyl)-amino]-benzo[b]thiophene-2-carboxylates (1), 2-(alkoxycarbonyl)-3-anilino-benzo[*b*]thiophenes and thieno[2,3-*b*]pyridines (2), (84).

Several published works assigned to scaffold **1** a peculiar biological activity, suggesting the proposed molecules as potential bioisosteres of major microtubules assembly inhibitors. Indeed, in the past few years, an ever increasing number of thieno derivatives as potent tubulin polymerization inhibitors have been proposed (85-87). In this contest, Romagnoli and co-workers reported an interesting series of 2- (alkoxycarbonyl)-3-anilinobenzo[b]thiophenes of type **2**. These compounds, acting on the colchicine binding site of tubulin, showed an excellent antiproliferative activity, interfering with microtubules dynamics during cancer cell division processes (88,89).

All tested compounds of type **1** showed concentration-dependent antiproliferative activity profile against HeLa cell line, exhibiting GI50 values in the low micromolar range. The most active compounds were tested in cell cycle perturbation experiments. A rapid accumulation of cells in the G2/M phase, with a concomitant reduction of cells in both the S and G0/G1 phases, was observed, suggesting that cell exposure to selected derivatives produces mitotic failure. To rationalize the biological results, the 3-benzoylamino-benzo[b]thiophenes were analyzed through the in silico VLAK protocol. Compounds having the 3,4,5-trimethoxy-benzoyl moiety were in silico classified as potential antimitotic agents or topoisomerase II inhibitors, in good agreement with the biological studies.

3.1.1.1.1 Chemistry

As shown in scheme 2, the general synthetic route for the preparation of 3-benzoylamino-benzo[b]thiophene derivatives **10 a-l** involved five steps, starting from the commercially available 2-fluorobenzonitrile **3**.

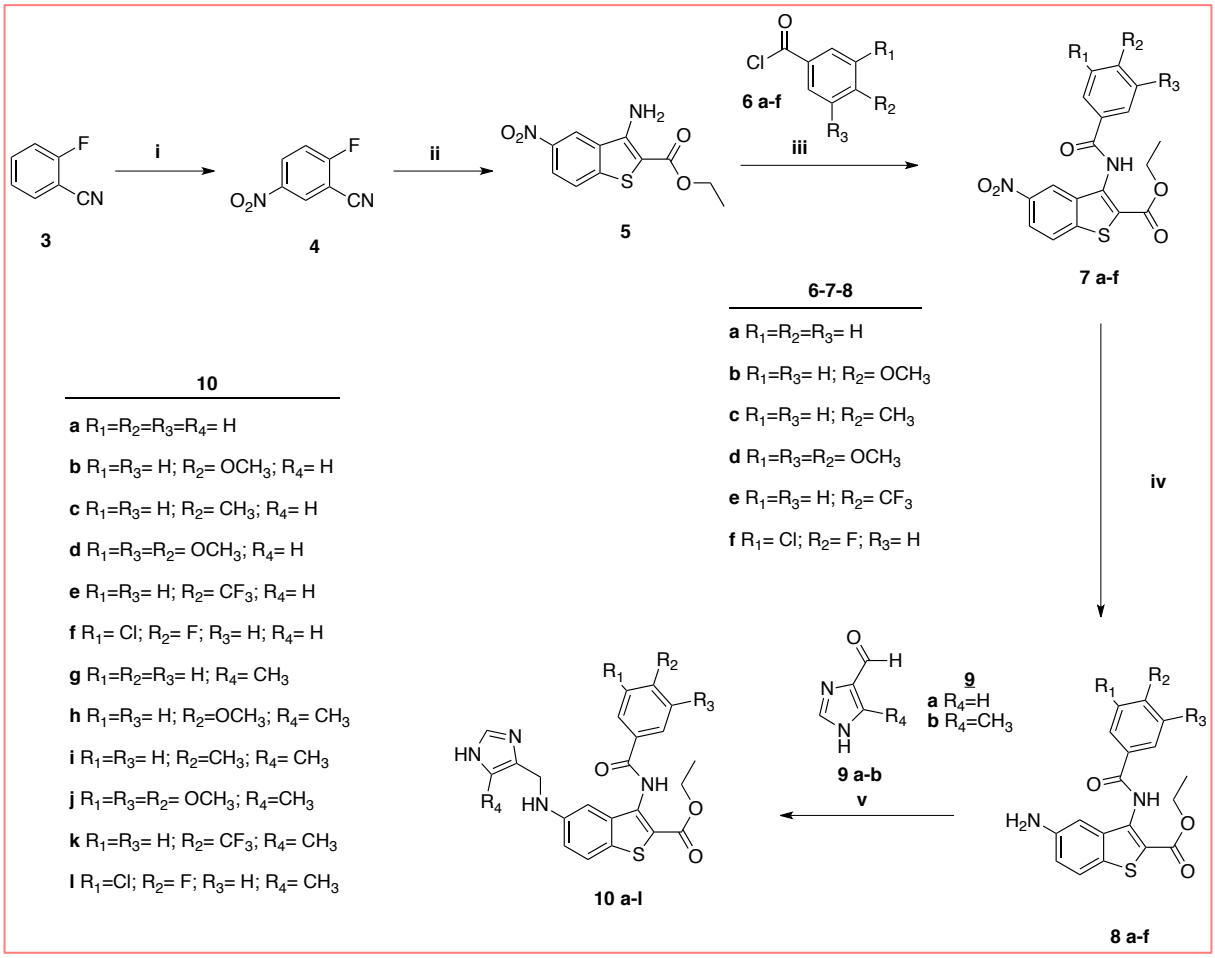

Scheme 2. Synthesis of ethyl 3-benzoylamino-5-[(1H-imidazol-4-yl-methyl)-amino]-benzo[*b*]thiophene-2-carboxylates 10 a-l. Reagents and conditions: (i): HNO_3 : H_2SO_4 (1:1), N_2, 0 °C, 2h; (ii): ethylthioglicolate/NaH 60%, anydrous DMSO; (iii): pyridine, rt, 12 h; (iv): 10% Pd/C, ethanol, rt 2h; (v): $NaCNBH_3$, ethanol/AcOH, 2h (84).

Pale yellow needles of 2-fluoro-5- nitrobenzonitrile **4** were obtained, in quantitative yield, by nitration of **3**, using a mixture of concentrated nitric and sulfuric acids, under inert atmosphere (90). The presence of both cyano and nitro substituents on substrate **4** enhanced the reactivity of the ortho-fluorine atom, which readily underwent nucleophilic displacement by ethyl thioglycolate, in the presence of NaH (60% in oil dispersion) and dimethyl sulfoxide (DMSO). Subsequent intramolecular cyclization in situ led to the formation of the central core, and the isolation of the key intermediate 3-amino-benzo[*b*]thiophene **5**.

To introduce the benzoyl moiety, amino derivative **5** was treated with substituted benzoyl chlorides **6 a-f**. The nucleophilic acyl substitution was carried out employing pyridine both as base and solvent. The use of other reaction media gave a significant decrease of the yields. Reduction of nitro group on compounds **7 a-f** was achieved through

hydrogenation with 10% Pd/C in ethanol. After removal of the catalyst, amino derivatives **8 a-f** were easily isolated as pure needles, in good yields. The last synthetic step provided the imidazole moiety insertion via a reductive amination in the presence of imidazole-4-carbaldehydes **9 a, b**.

The reaction of the amino group with the aldehydes led to the formation of the corresponding imines, which, by mean of sodium cyanoborohydride addition, provided to a tightly selective reduction affording ethyl 3-benzoylamino-5-[(1H-imidazol-4-yl-methyl)-amino]-benzo[b]thiophene-2-carboxylates **10 a-l**.

3.1.1.1.2 Biology: Antiproliferative Activity

The antiproliferative activity of 3-benzoylamino-5-imidazol- 4yl-benzo[b]thiophene derivatives **10 a-l** and their corresponding precursors **8 a-f** was evaluated on HeLa tumor cell line for 48 h using MTT based cell viability assay.

Table 2. Cytotoxicity over 48 h of 3-benzoylamino-benzo[*b*]thiophene derivatives 8 a-f, 10 a-f, 10 g-l against Hela cell line expressed as GI50 values [GI50± SE (µM)].

	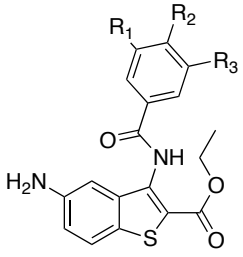 8 a-f	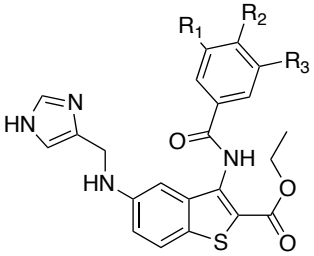 10 a-f	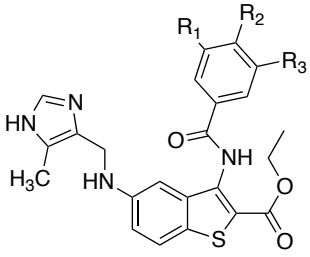 10 g-l
R_1=R_2=R_3=H	**a** >50	**a** 17.89 ± 2.03	**g** 23.32 ± 2.91
R_1=R_3=H; R_2= OCH_3	**b** >50	**b** 12.92 ± 0.94	**h** 8.22 ± 0.75
R_1=R_3=H; R_2= CH_3	**c** 24.44 ± 0.31	**c** 11.72± 1.17	**i** 11.42 ± 1.03
R_1=R_2=R_3= OCH_3	**d** 4.66 ± 0.31	**d** 6.79 ± 0.33	**j** 2.23 ± 0.04
R_1=R_3=H; R_2= CF_3	**e** 6.68± 0.57	**e** 16.84 ± 0.98	**k** 12.82 ± 1.09
R_1= Cl; R_2= F; R_3= H	**f** 12.29 ± 1.69	**f** 10.65 ± 1.32	**l** 2.91 ± 0.24

All tested compounds showed concentration-dependent antiproliferative activity, but they did not affect the cell membrane integrity in the concentration range 1-20 µM, as determined preliminary by the Trypan Blue exclusion method. For an easier analysis of

the biological results, the tested molecules have been divided into three main subgroups: 5-amino- benzo[b]thiophenes **8 a-f**, imidazole side-chain compounds **10 a-f**, and methyl-imidazole side-chain derivatives **10 g-l** (table 2).

The majority of our benzo[*b*]thiophene compounds proved a good growth inhibition effect, exhibiting GI50 values in the low micromolar range. As a general trend, 5-amino-benzo[*b*]thiophenes **8 a-f** showed lower activity than the corresponding compounds with the imidazole side-chain **10**. Only when the benzoyl moiety was functionalized with 4-CF_3, the activity of the amino intermediate **8e** was more potent than imidazole derivatives **10e** and **10k**. The presence of the methyl moiety on the imidazole ring resulted in a significant increase of activity for the 3,4,5-trimethoxy (**10d** vs **10j**) and the 3-chloro-4-fluoro-benzoylamino-benzo[*b*]thiophene derivatives (**10f** vs **10l**), while it was irrelevant in the other cases. Relatively to the influence of the substituents on the benzoyl moiety there is no clear difference on activity between electron-withdrawing and electron-releasing substituents. Anyway, 3,4,5-trimethoxy benzoyl (TMB) derivatives **8d**, **10d**, and **10j** stand out as the most active of each subgroup.

3.1.1.1.2.1 Cell cycle analysis

The derivatives **8d**, **10j**, and **10l**, which showed the highest antiproliferative effect, were tested in cell cycle perturbation experiments to evaluate their potential influence on cell-cycle distribution. The flow cytometric analysis was performed after 24 and 48 h of incubation in order to detect the shifts in cell cycle distribution before a significant amount of cells underwent apoptosis. The working concentrations were fixed taking into account the GI50 values measured at 48 h. The histograms show the percentage of cells in the respective cell cycle phase (G1, S, and G2/M), along with the percentage of cells in the sub-G0/G1 (apoptotic cells) obtained by flow cytometry (fig.20). Untreated HeLa cells revealed a normal diploid distribution, presenting fast proliferation features, with S + G2/M phase cells accounting for about 40% of the total cells (ctrl). After cell exposure to selected 3-benzoylamino-benzo[b]thiophene derivatives **8d**, **10j**, and **10l**, a rapid accumulation of cells in the G2/M phase, with a concomitant reduction of cells in both the S and G0/G1 phases, was observed. These changes occurred in a concentration-dependent manner. In fact, while in the experimental conditions a treatment with 1xGI50 produced only slight variations, a concentration of about 2xGI50 induced significant effects on cell cycle distribution. The time-dependent tendency of benzo[b]thiophenes

effects was confirmed, after 48 h of treatment, by the deep alterations in the cell cycle distribution profile, with significant reduction of the cells number in all phases, and by the simultaneous increase of the cells population in subG0/G1, which is indicative of apoptotic cells (data not shown).

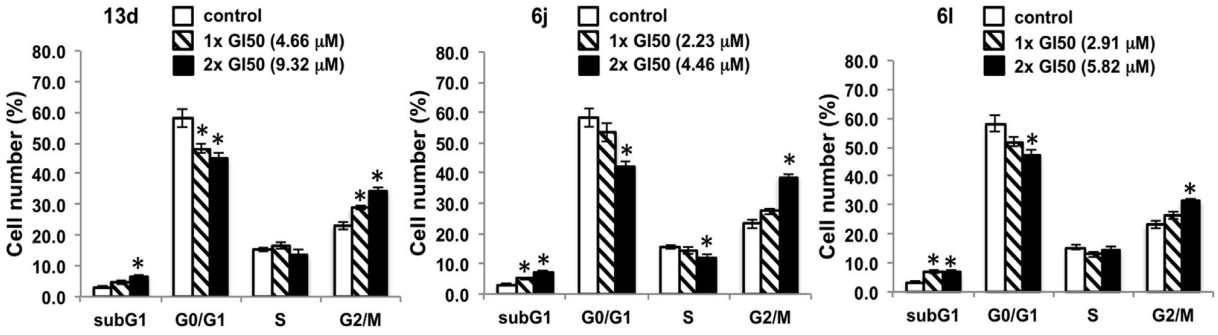

Figure 20. Effects of compounds 8d, 10j, and 10l on the cell cycle distribution of Hela cells following 24 h treatment. The cells were cultured without any compound (ctrl) or with compound used at the indicated concentrations. Cell cycles distribution was analysed by the standard propidium iodide procedure as described in Methods. The histograms represent the percentage of cells in the respective cell cycle phase (G0/G1, S, and G2/M), along with the percentage of cells in the subG1 (dead cells) obtained by flow cytometry. Results are expressed as the mean of two independent experiments, performed in duplicate ± SE. Statistical analyses were performed using the Student's test to determine the differences between the datasets. *$p < 0.05$ denotes significant differences from untreated control cells (84).

3.1.1.1.3 *In Silico* Insights

In attempt to rationalize biological results of selected hits on cell-cycle distribution and considering the structural features of the proposed derivatives of type **8** and **10**, similar to known antimitotic agents, the benzothiophenes were analyzed through the in silico VLAK protocol (91). Mostly developed in the last years, as well as the recent protocol BIOTA (92), this protocol was employed in the design and optimization of lead compounds as anticancer drugs. The interesting results, concerning a wide set of heterocyclic derivatives, confirmed this *in silico* methodology as powerful approach in prediction capability of biological activities (93-95). The VLAK protocol is focused on the search of molecular descriptors, which could be considered as the "pins of the lock". The lock represents the biological target, or a specific mechanism of action (MA), which need a key (the molecule) to be tuned (95).

The first step of the VLAK protocol is the conversion of the biological targets, or the MAs, in "lock models" in which the keys (designed ligands) fit to modulate the biological activity (91). In this study, the VLAK protocol was applied to predict the MA of 3- benzoylamino-benzo[*b*]thiophene derivatives by using the National Cancer Institute (NCI) Anticancer Agent Mechanism (ACAM) database as training set. Drug screening

data are available for each structure as measurement of their growth inhibition ability over a panel of about 60 human tumor cell lines, and all tested molecules are explicitly designed as training set for neural network and multivariate analysis (96-98). In particular, this database is constituted by 114 antitumor drugs ranked according to their MA that can be considered as the locks in this protocol (99). Therefore, for each class of drugs (Alkylating Agents, Antimitotic Agents, Topoisomerase I Inhibitors, Topoisomerase II Inhibitors, RNA/DNA Antimetabolites, and DNA Antimetabolites), a "lock model" was generated starting from available known compounds. A set of 2D and 3D molecular descriptors was selected in order to best differentiate ACAM drugs database by MA. Once defined the lock model for each MA, compounds have been classified in terms of structure affinity to lock models. In table 3 the percentages of affinity (A%) for the screened derivatives are reported.

Table 3. Percentage of affinity (A%) calculated for the tested compounds. In bold, the highest A% values for the most active compounds (8d, 10d and 10j) as antimitotic and topoisomerase II inhibitors classes (84).

Compound	Alkylating agents	Antimitotic agents	DNA antimetabolites	Topoisomerase I inhibitors	Topoisomerase II inhibitors	RNA-DNA antimetabolites
8a	66.27	44.94	41.35	38.57	26.95	46.99
8b	64.59	53.90	38.99	53.55	36.60	50.29
8c	66.37	47.50	38.31	45.36	29.59	47.35
8d	46.27	**60.57**	23.35	56.25	56.32	45.25
8e	53.87	40.77	33.44	43.74	34.65	57.40
8f	60.85	40.22	43.58	45.92	30.79	54.95
10b	41.37	55.29	31.03	52.66	60.69	42.63
10c	43.16	48.52	29.74	48.83	52.80	40.57
10d	35.25	**56.39**	22.62	33.77	**62.67**	35.61
10e	40.22	38.92	31.11	38.89	45.41	49.06
10f	42.25	41.95	34.67	51.70	46.64	48.70
10g	44.48	45.58	30.19	46.60	47.89	40.24
10h	41.62	54.88	28.07	50.26	61.26	37.03
10i	43.40	49.57	26.70	47.40	54.34	38.56
10j	35.20	**56.74**	20.07	31.21	**61.32**	33.64
10k	41.46	42.30	28.77	41.64	44.37	44.63
10l	42.23	42.98	32.02	53.42	48.74	44.10

Analyzing the results for compounds that showed the most significant biological effect (**8d**, **10j**, and **10l**) it is noteworthy that TMB derivatives **8d**, **10j** represent the most significant compounds in terms of affinity for the class of antimitotic agents (B), showing good values of A%. The structural features of these compounds, similar to the well known antimitotic agents such as colchicine and combretastatin A-4, could justify these results (fig.21).

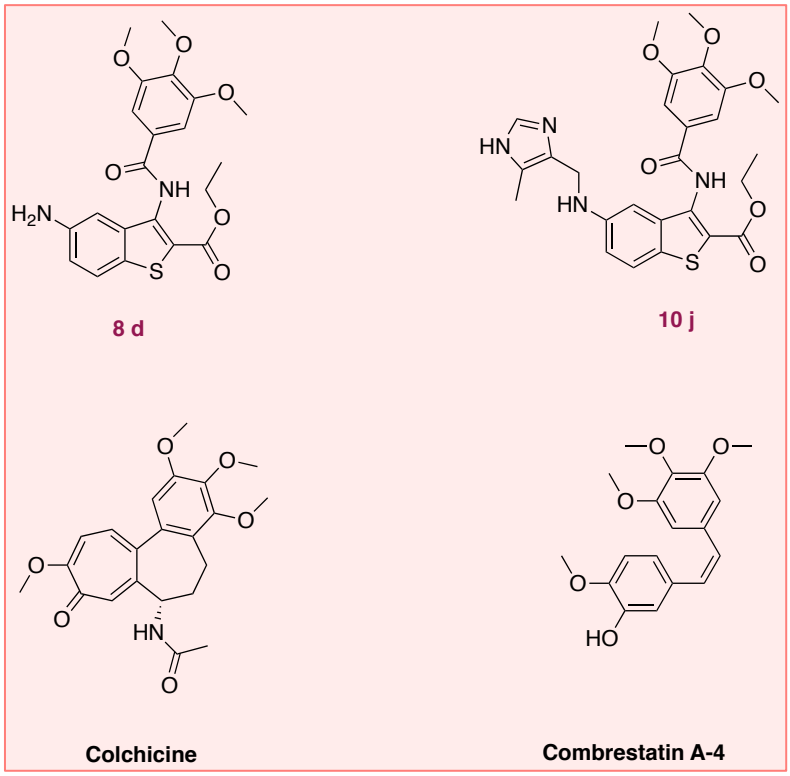

Figure 21. TMB derivatives (8d and 10j) showing good percentage of affinity (A%) and well-known antimitotic agents (Colchicine and Combrestatine A-4)

Molecule **10l** did not show high affinity percentage towards the antimitotic mechanism of action group (42.98), maybe because of the structural modifications involving the benzoyl moiety. Thus, in terms of structural analogies with known antimitotic compounds, these results highlight the importance of the TMB moiety and underline that the presence of the imidazole ring as substituent, essential for the biological activity, does not affect the structural analogy with known antimitotic agents. The difference in the affinity toward antimitotic agents for compound **10l** could be justified by the different functionalization of the benzoyl moiety rather than the presence of the methyl group on the imidazole ring. Another important aspect to be underlined is the good affinity percentage for topoisomerase II inhibitors showed by 3-benzoylamino-benzo[*b*]thiophene derivatives **10 b, d, h, j**. It is worth noting that these findings are in agreement with the biological insights. In particular, the *in silico* studies make possible to hypothesize that observed arrest in the G2/M phase, after cell exposure to selected derivatives, involving mitotic failure can be associated, with both an antimitotic mechanism by interference with mitotic spindle formation and the DNA-Topoisomerase-II inhibition.

3.1.1.2 New Class of Benzo[*b*]furan Derivatives with Antiproliferative Activity

A new series of 3-benzoylamino-5-imidazol-benzo[*b*]furans and the parent amino derivatives were synthesized and screened as antitumor agents, in order to investigate the influence of isosteric replacements and to optimize the antiproliferative activity with respect to the previous benzo[*b*]thiophene series. As a general trend, tested 3-benzoylamino-5-imidazol-benzo[*b*]furans showed concentration-dependent antiproliferative activity against HeLa and MCF-7 cell lines and some of these exhibited GI_{50} values in the low micromolar range. In most cases the insertion of a methyl substituent on the imidazole moiety improved the antiproliferative activity. Therefore the methyl-imidazol-benzo[*b*]furans compounds were tested in cell cycle perturbation experiments, producing cell cycle arrest with proapoptotic effects.

Focusing the attention on the thieno heterocyclic ring systems **8** and **10,** (fig.22) previously reported as a novel series of benzo[*b*]thiophene derivatives showing concentration-dependent antiproliferative profile, with GI_{50} values in the low micromolar range against HeLa cells (84), a few studies were carried out on the basis of the isosteric concept, suggesting useful aromatic ring replacements, in order to optimize the antiproliferative effects of our lead compounds.

Analyzing the benzo[*b*]thiophenes series, from a structural point of view, only a few derivatives exhibited notable antiproliferative effect, when functionalized with a methyl-imidazole side chain; instead no significant differences were observed by changing the substituents on the benzoyl moiety (both electron-withdrawing and electron-releasing substituents). These findings led this research work to further study these type of molecules and to investigate the isosteric replacement of benzo[*b*]thiophene skeleton by a benzo[*b*]furan one, in order to optimize the antiproliferative activity. In detail, hereinafter, is described the synthesis, and the biological screening of a new series of benzo[*b*]furan derivatives **11**, **12**, and **13** (fig.22).

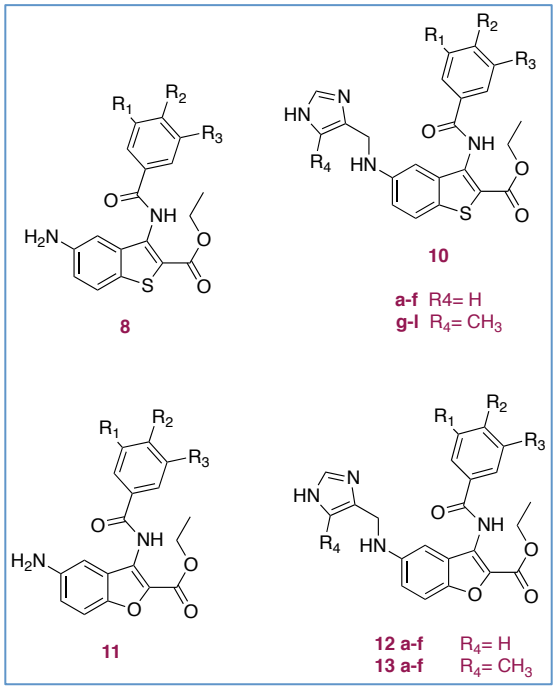

Figure 22. General chemical structures of benzo[*b*]thiophene derivatives (84) and their related benzo[*b*]furan isosters.

The interest on these new molecules is also supported by several experimental data, which assigned to the benzo[*b*]furan scaffold peculiar biological activities. Romagnoli and co-workers reported interesting series of 3-arylaminobenzo[*b*]furans **15** as result of accurate bioisosteric replacements and SAR studies (84,89). These compounds, acting on the colchicine binding site of tubulin, showed highly antiproliferative activity, comparable to the thiophene derivatives **14a**,**b** (fig.23).

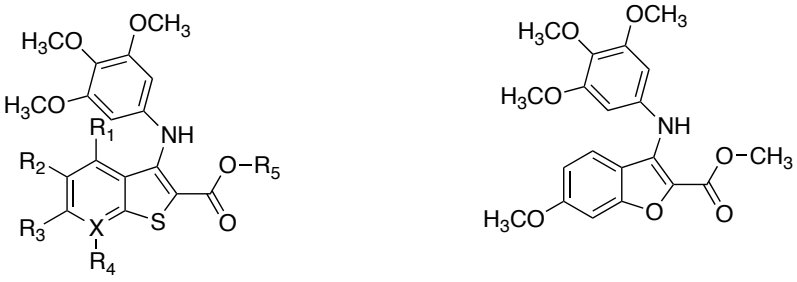

a) X=C, R_3=OCH_3, $R_{1,2,4}$= H, R_5= CH_3: IC_{50} 0.3-10.3 nM; IC_{50}=0.3-27 nM
b) X= N $R_{3,5}$= CH_3, $R_{1,2}$= H, R_4= not present: IC_{50} 0.2-16.2 nM

Figure 23. Chemical structures of 2-(alkoxycarbonyl)-3-(3,4,5-trimethoxyanilino)benzo[*b*]thiophene 14a, 2-(alkoxycarbonyl)-3-(3,4,5-trimethoxyanilino)thieno[2,3-*b*]pyridine 14 b (89), 2-(alkoxycarbonyl)-3-(3,4,5-trimethoxyanilino)benzo[*b*]furan 15 and respectively IC_{50} ranges against a panel of seven cancer cell lines (100).

3.1.1.2.1 Chemistry

As shown in scheme 3, the general synthetic route for the preparation of 3-benzoylamino-benzo[*b*]furan derivatives **11-13** started from the commercially available 2-fluorobenzonitrile (**3**). Pale yellow needles of 2-fluoro-5-nitrobenzonitrile (**4**) were obtained, in quantitative yield, by nitration of (**3**), using a mixture of concentrated nitric and sulfuric acids, under inert atmosphere (90). The presence of both cyano and nitro substituents on substrate (**4**) enhanced the reactivity of the *ortho*-fluorine atom, which readily underwent nucleophilic displacement by ethyl glycolate, in the presence of K_2CO_3 and *N,N*-dimethyl-formamide (DMF). Subsequent intramolecular cyclization *in situ* led to the benzo[*b*]furan central core, allowing the isolation of the 3-amino-benzo[*b*]furan derivate **16**.

To introduce the benzoyl moiety, the key intermediate 3-amino-benzo[*b*]furan **16** was treated with benzoyl chlorides **6a-f**, variously substituted with electron-withdrawing and electron-releasing groups. The nucleophilic acyl substitution was carried out employing pyridine both as base and solvent. In the same way to what observed in the benzo[*b*]thiophene series, the use of other reaction media gave a significant decrease of the yields. Reduction of nitro group of **17a-f** was realized through hydrogenation with 10% Pd/C in ethanol. After removal of the catalyst, amino derivatives **11a-f** were easily isolated as pure needles, in good yields. The last synthetic step provided the imidazole moiety insertion *via* a reductive amination in the presence of imidazole-4-carbaldehydes **9a,b**. The reaction of the amino group with the aldehydes led to the formation of the corresponding imines; therefore, the subsequent addition of sodium cyanoborohydride performed a tightly selective reduction and the final formation of ethyl 3-benzoylamino-5-[(1*H*-imidazol-4-yl-methyl)-amino]-benzo[*b*]furan-2-carboxylates **12a-f** and **13a-f**. In this synthetic step, when is employed the carbaldehyde **9b**, it was possible to isolate the methyl-imidazole side-chain derivative **18**, where the hydrolysis of the amide function releases the 3-amino group from the benzoyl moiety.

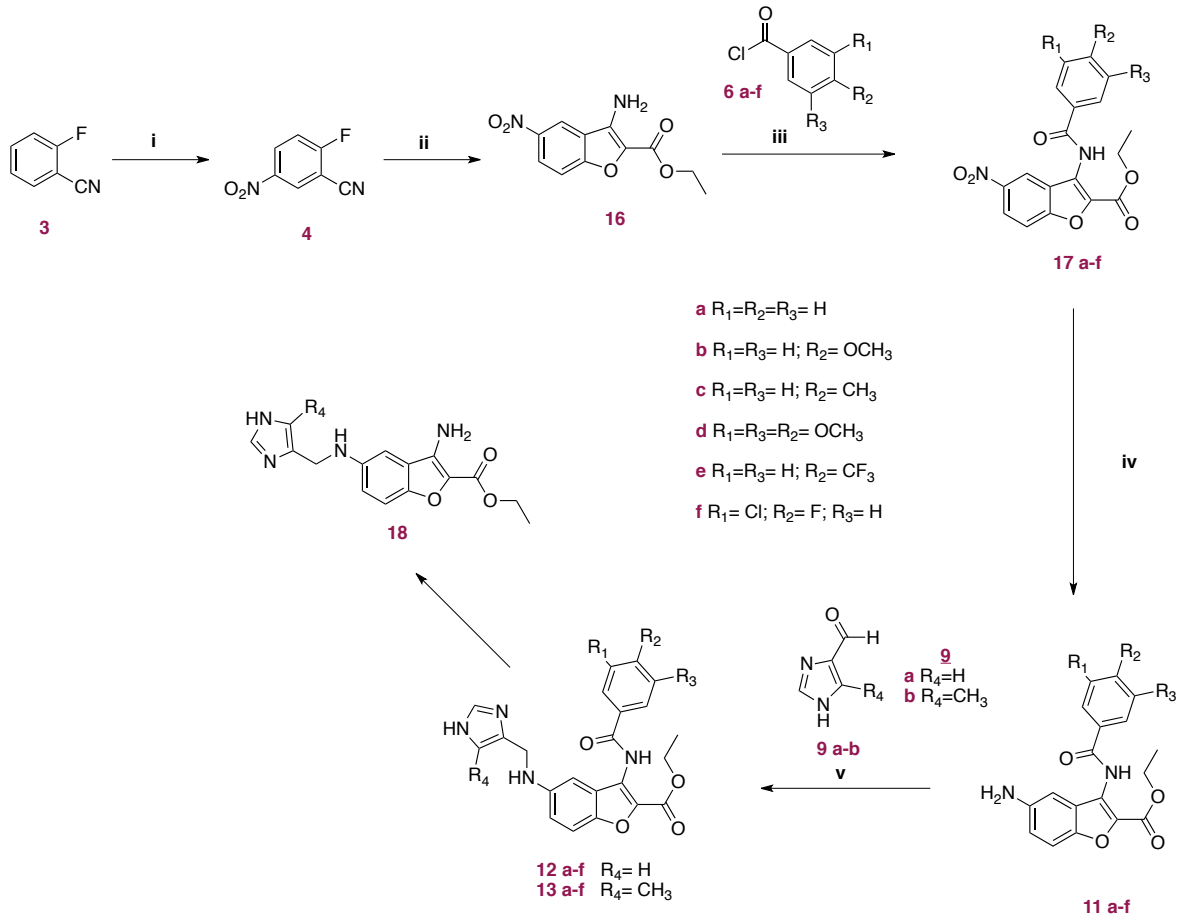

Scheme 3. Synthesis of ethyl 3-benzoylamino-benzo[*b*]furan-2-carboxylates 11 a-f, 12 a-f and 13 a-f. Reagents and conditions: (i) HNO_3: H_2SO_4 (1:1), N_2, 0 °C, 2h; (ii) ethylglycolate, K_2CO_3, anydrous DMF, 12h; (iii) pyridine, rt, 12 h; (iv) 10% Pd/C, H_2, ethanol, rt, 2 h; (v) $NaCNBH_3$, ethanol/AcOH, 2h.

3.1.1.2.2 Biology: Antiproliferative Activity

The antiproliferative activity of the synthesised 3-benzoylamino-benzo[*b*]furan derivatives **11a-f**, **12a-f**, and **13a-f** was evaluated on HeLa and MCF-7 tumour cell lines for 48h, using MTT based cell viability assay. In table 1 were displayed the GI_{50} values of all tested compounds, which, for an easier analysis, were divided into three main subgroups: 5-amino-benzo[*b*]furans **11a-f**, imidazole side-chain compounds **12a-f**, and methyl-imidazole side-chain derivatives **13a-f**.

Table 4. Antiproliferative activity over 48h of 3-benzoylamino-benzo[*b*]furan derivatives 11 a-f, 12 a-f and 13 a-f against Hela and MCF-7 cell lines expresses as GI_{50} values [$GI_{50} \pm$ SE (mM)].

	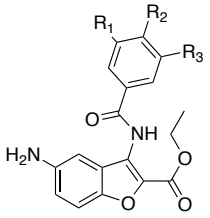 11 a-f		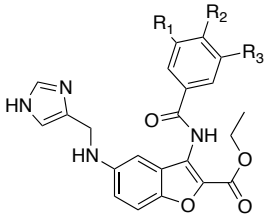 12 a-f		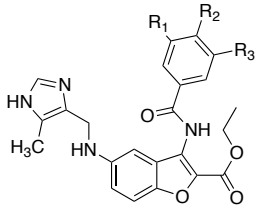 13 a-f	
	Hela	**MCF-7**	**Hela**	**MCF-7**	**Hela**	**MCF-7**
a R_1=R_2=R_3= H	35.09 ± 3.52	>50	41.59 ± 3.08	49.65± 4.91	7.69 ± 0.46	12.27 ± 1.46
b R_1=R_3= H; R_2= OCH_3	>50	>50	7.98 ± 0.67	13.36 ± 1.94	14.31 ± 1.97	17.35 ± 1.78
c R_1=R_3= H; R_2= CH_3	35.32 ± 3.92	30.84 ± 4.09	13.65 ± 1.02	18.22 ± 1.28	9.20 ± 0.34	15.53 ± 0.98
d R_1=R_3=R_2= OCH_3	>50	>50	12.18 ± 1.19	3.88 ± 0.40	12.19 ± 1.59	9.21 ± 1.02
e R_1=R_3= H; R_2= CF_3	>50	>50	>50	>50	2.01 ± 0.13	14.16 ± 2.02
f R_1= Cl; R_2= F; R_3= H	42.05 ± 5.08	35.63 ± 4.30	13.61 ± 0.86	11.25 ± 1.11	2.14 ± 0.35	1.55 ± 0.14

As a general trend, the screened 5-amino-benzo[*b*]furan derivatives **11a-f** showed poor antiproliferative effects on both tumor cell lines. Only in few cases, it was possible to observe low activity, with GI_{50} values greater than 30 µM.

As clearly highlighted by the data reported in table 3, the insertion of the imidazole side chain moiety exerted a weighty influence on the antiproliferative activity. Indeed, with the exception of derivatives **12a** and **12e**, where the benzoyl moiety was respectively not functionalized or brings a 4-trifluoromethyl substituent, the inhibition growth effects of benzo[*b*]furan compounds of type **12** were promising, showing GI_{50} values in the low micromolar range. Within this subgroup, remarkable was the selective antiproliferative effect of the 3,4,5-trimethoxy-benzoyl-benzo[*b*]furan **12d** on MCF-7 cell line, with a GI_{50} value of 3.88 µM.

The insertion of methyl group on the imidazole ring further increased the biological activity, especially in the cases of **13a**, **e**, **f**, where the benzoyl moiety was respectively unsubstituted (**13a** *vs* **12a**), or functionalized with 4-trifluoromethyl- **(13e** *vs* **12e)** and 3-chloro-4-fluoro- **(13f** *vs* **12f)** substituents. The cytotoxic activity was worthily interesting in the case of derivative **13f**, the most active of the benzo[*b*]furan series, where GI_{50} values on HeLa and MCF-7 tumour cell lines were respectively at 2.14 and 1.55 µM.

Generally, the biological activity of tested benzo[*b*]furan derivatives was less influenced by the substituents (both with electron-withdrawing and electron-releasing effects) located on the benzoyl moiety than by the imidazole side chains insertion. However, it was evident that the biological activity of the not substituted (**11a**, **12a**, and **13a**) and of the 4-trifluoromethyl- (**11e**, **12e**, and **13e**) derivatives, with respect to the other cases, varied in peculiar ways along the progression of the synthesis, from the 5-amino-benzo[*b*]furans to the methyl-imidazole side-chain derivatives.

Finally, the biological screening of derivative **18**, where the 3-amino group is free from the benzoyl moiety, certified the crucial importance of this molecular portion on the antiproliferative activity. The analysis of the cytotoxic data obtained for both tumor cell lines evidenced GI_{50} values up to 50 μM.

3.1.1.2.2.1 Cell Cycle Analysis

The methyl-imidazole side-chain compounds **13a-f** were also tested on HeLa cells, in cell cycle perturbation experiments, to evaluate their potential influence on cell-cycle distribution. The flow cytometric analysis was performed after 24h of incubation, in order to detect the shifts in cell cycle distribution before a significant amount of cells underwent apoptosis. The working concentrations were chosen taking into account the GI_{50} values measured at 48h.

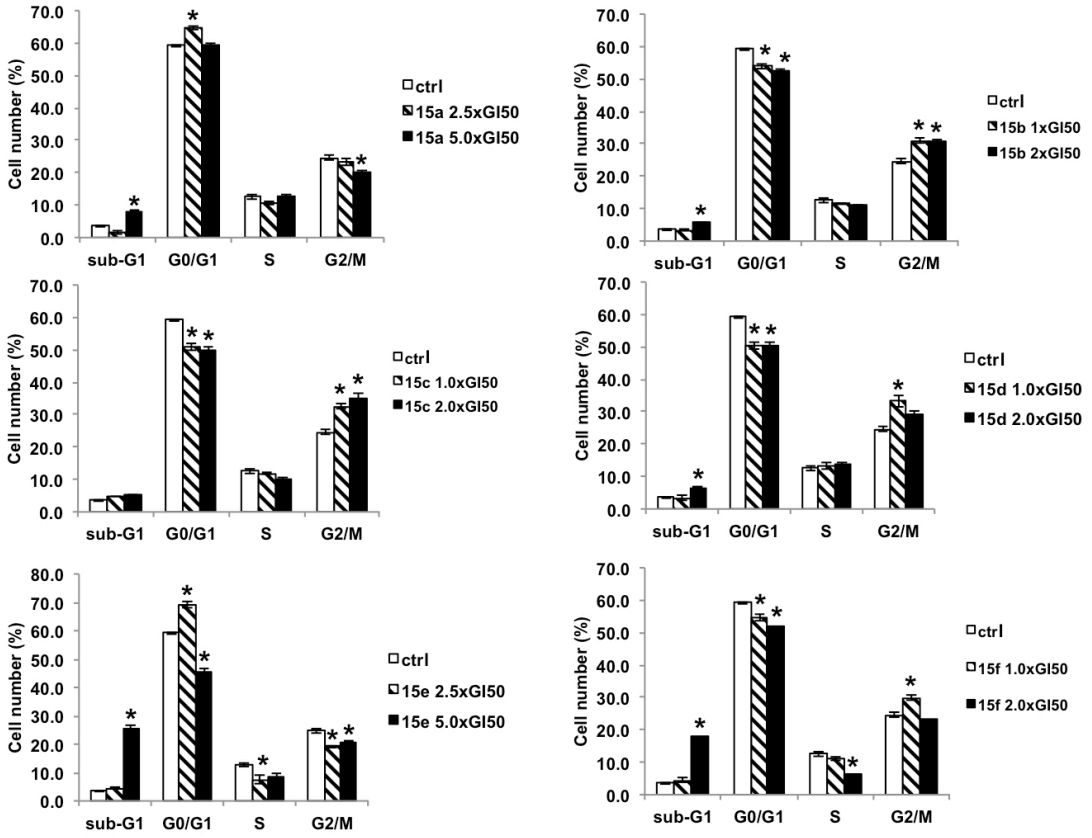

Figure 24. Effects of compounds 13 a-f on the cell cycle distribution of Hela cells following 24h treatment. The cells were cultured without any compound (ctrl) or with compound used at the indicated concentrations. Cell cycles distribution was analysed by the standard propidium iodide procedure as described in Methods. The histograms represent the percentage of cells in the respective cell cycle phase (G0/G1, S, and G2/M), along with the percentage of cells in the subG1 (dead cells) obtained by flow cytometry. Results are expressed as the mean of two independent experiments, performed in duplicate ± SE. Statistical analyses were performed using the Student's test to determine the differences between the datasets. *$p < 0.05$ denotes significant differences from untreated control cells.

In figure 24 the percentage of cells in the respective cell cycle phase (G1, S, and G2/M) were shown, along with the percentage of cells in the sub-G0/G1 (dead cells) obtained by flow cytometry. Untreated HeLa cells showed a normal diploid distribution presenting fast proliferation characteristics, with S + G2/M cell phases accounting for about 40% of the total cells (ctrl). Significant suppression of the G0/G1 phase with accumulation of cells in the G2/M was observed after cell exposure to $1xGI_{50}$ μM of methyl-imidazole side-chain derivatives **13b-d,f.** The antiproliferative effect was concentration-dependent and, in our experimental conditions, treatment with a concentration of about $2xGI_{50}$ produced deep alterations in the distribution profile. Indeed, it was possible to observe a significant reduction of the cell number in all phases and a simultaneous increase of the cell population in sub G0/G1, which was indicative of apoptotic cells. Interestingly, the not substituted **13a** and the 4-trifluoromethyl- **13e** derivatives, assayed at 1x and $2xGI_{50}$, failed to produce significant cell cycle alterations. On the contrary, cell exposure to

2.5xGI_{50} and 5xGI_{50} μM of derivatives **13a,e**, induced G0/G1 arrest associated with reduction of the cell number in other phases.

3.1.1.3 Synthesis, Biological Evaluation and *In Silico* Insights of New Potential G4-DNA Binders and Stabilizers

Although the interest in molecules able to interact through the mechanism of intercalation has not changed over the years, the lack of selectivity together with the discovery of more specific targets have made the B-DNA a less attractive target in the search for new anticancer drugs.

The current appealing challenge is to design DNA-interactive molecules showing higher specifity in DNA binding, without interfering with the functions of healthy cells.

In this regards, we focused our attention on the design, the synthesis, and the biological evaluation of novel heterocyclic ring systems potentially able to halt tumor cell proliferation through the binding to DNA when it assumes secondary structures known as G-quadruplexes (G4s), preferring them over the B form. Indeed, as already pointed out, the stabilization of such DNA secondary structures can modulate and control various processes in the carcinogenic pathways. On the basis of our considerations (26), symmetry could be an interesting feature to investigate in order to understand which structural feature affects more the G4 arrangement, hard to figure out due to the structure heterogeneity of both G4 stabilizers and the DNA G4s isoforms (26).

3.1.1.3.1 *In silico* Insight, Synthesis and Spectroscopic Assays of Bis Isoquinoline Derivatives

Molecular modelling studies made possible the identification of structures potentially related to telomeric G4s (*h-telo)* and the proto-oncogenes *c-kit and c-myc*, taken from the PDB database.

From the virtual screening of the database *DRUG-LIKE (ZINK),* a series of structures that share a common π-delocalized system core have been selected. These scaffolds, when functionalized with proper positively charged side chains, affect more the G4 arrangment, both stacking at the top/end of a G-tetrad and interacting with the groves. All the molecules screened display symmetry features, noteworthy, as the most interesting already known G4- stabilizers.

A series of these molecules have been submitted to a retrosynthetic study when not commercially available.

Indeed, the virtual screening of diversity set selected the structure **19**, shown in figure 25, commercially available.

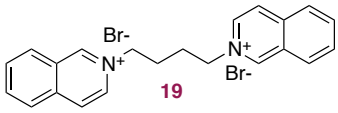

Figure 25. (19) 2,2'-(butane-1,4-diyl)bis(isoquinolin-2-ium) bromide

3.1.1.3.1.1 Chemistry

The two bis-isoquinolino derivatives **22a** and **22b** (scheme 4) were accomplished respectively from compounds **20a** and **20b** (Scheme 4)**.** They were allowed to react with 1,3-dichloro-2-propanol, **21,** at 140 °C within a Shlenk flask for 10-20 hours.

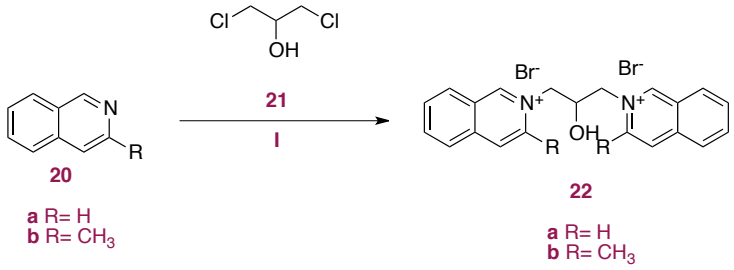

Scheme 4. Synthesis of bis isoquinoline derivatives: (22 a), 2,2'-(2-hydroxypropane-1,3-diyl)bis(isoquinolin-2-ium) and (22 b), 2,2'-(2-hydroxypropane-1,3-diyl)bis(3-methylisoquinolin-2-ium). Reagents and conditions: 20 a: Isoquinoline; 20 b: 2-methyl isoquinoline; 21: 1,3-dichloro-2-propanol; i: 140 °C, 10.20 h.

3.1.1.3.1.2 Spectroscopic Assays

Spectroscopic studies were carried out between the synthesized derivatives, obtained according to the scheme 4, and both the G4-DNA and B-DNA isoforms.

Although molecular modeling studies showed interesting interactions between the isoquinoline structures and the grooves of the promoter c-kit, unfortunately the spectroscopic tests on G4-DNA did not give the expected results. No interesting interactions with the B form of the DNA have been found.

3.1.1.3.2 *In silico* Insight, Synthesis and Spectroscopic Assays of Double Chained Naphthalenes as G4 Binders

The presence of G-quadruplexes in promoter regions of a number of oncogenes with functions in transcriptional regulation led our interest in designing and developing binders to specific G-rich sequences in oncogenes promoters able to modulate their expression. The first approached target was the human proto-oncogene c-*Kit*, which presents a G4 sequence (c-*Kit1*) with a large irregular cleft, not present in any other G4s. Computational studies were used to drive synthetic work, employing large databases of heterocyclic molecules and G4 isoforms as templates in the molecular modelling strategies. The designed binder (fig. 26) display a π-delocalized system able to stack at the top/end of the G4 and side arms able to fit specific binding pockets. These two fragments are connected by a proper linker. The selectivity of the synthesized binder was assessed by competitive binding experiment with other G4s from telomeric and gene promoter sequences, mainly using spectroscopic techniques.

3.1.1.3.2.1 Chemistry

The 2,7-bis(4-morpholinobut-1-yn-1-yl)naphthalene, **26** (fig.26), a symmetrical compound featured by a naphthalene core and two bromo-ethyl side chains in 2,9 positions, has been synthesized according to the scheme 5.

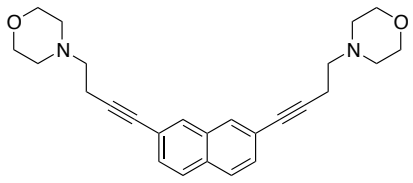

26

Figura 26. **2,7-bis(4-morpholinobut-1-yn-1-yl)naphthalene.**

Substrate, **23**, a 2,7-dihydroxynaphthalene commercially available, underwent a nucleophilic substitution base-catalysed (I) by trifluoromethansulfonic anhydride to give compound **24**, achieved in order to improve the reactivity of leaving groups of this substrate in the next step. Thus, in presence of 2,6-lutidine and DMAP, after adding a solution in THF of the trifluoromethansulfonic anhydride to the reaction mixture, either at -78 °C or 0 °C to 0 °C, in the former case, and to room temperature in the latter case, the best yield obtained was about 30%. A better yield (60%) was achieved after using

pyridine as a base, and carrying out the reaction at room temperature after the addition at 0 °C of trifluoromethansulfonic anhydride.

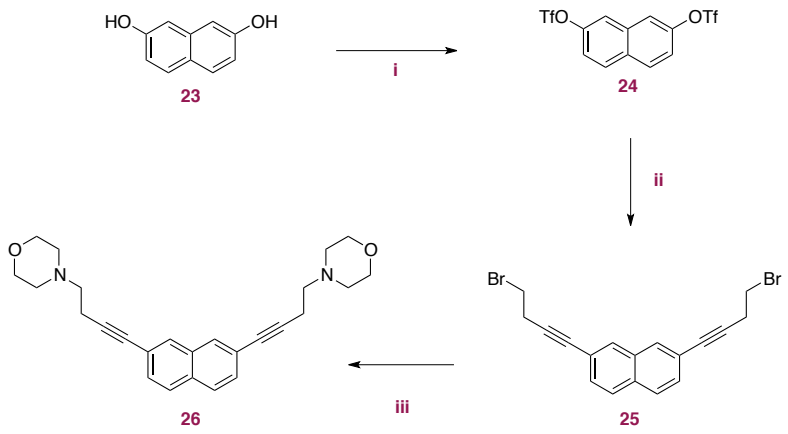

Scheme 5. Synthetisis of 2,7-bis(4-morpholinobut-1-yn-1-yl)naphthalene derivative (26). Reaction conditions: (i): Pyridine, DCM, N_2; addiction of Tf_2O at 0 °C -> r.t., over night; 60% yield. (ii): 4-Bromo-1-butyne, CuI, DIPEA, DMF dry, $Pd(PPh_3)_2Cl_2$, N_2, 3h, r.t.; 40% yield. (iii): Morpholine, DCM dry, r.t. -> reflux, 3h; 40% yield.

The following cross-coupling Sonogashira reaction (II) between **24** and 4-bromo-1-butyne, gave the formation of the C-C bond, catalyzed by CuI and triphenyl phosphine palladium di-chloride.

The cross-coupling reaction must be carry out under inert atmosphere because as a result of the presence of copper iodide, the Glaser coupling between two alkynes may occur, giving some side products.

This reaction was carried out at room temperature and DIPEA was used as a base, yielding the 2,7-bis(4-bromobut-1-yn-1-yl)naphthalene derivative (40% yield).

In the next step, to a solution of DCM anhydrous, a solution of morpholine (2 equivalents) in DCM anhydrous was added dropwise at room temperature over 1 hour. After that, the reaction mixture was refluxed over 3 hours, yielding compound **26** in a good yield.

3.1.1.3.2.2 Spectroscopic Analysis Results

Even in this case, although molecular modelling studies showed interesting interactions between compound **26** and G4-structures, spectroscopic tests on G4-DNA did not turn out the expected interactions.

3.1.1.4 *In Silico* Insight, Synthesis and Biological Evaluation of New Pyridazyne-Based Small Molecules as G-quadruplex Binders

In the effort to find new G4-DNA binders showing better tumor penetrating ability and target selectivity than the G4-stabilizers known hitherto (101), this section focused on the design and synthesis of new potential G4-DNA binders and stabilizers.

During my PhD visiting at the Department of Organic Chemistry (Semmelweis University, Budapest), the interest on development of symmetrical G4-binders met the great experience on the chemistry of 3-(2*H)*–pyridazinones of Prof. Péter Mátyus, giving rise the input to the implementation of some interesting symmetrical pyridazinone derivatives as potential new G4-DNA binders and stabilizers.

Since the early eighties, the considerable interest on the pyridazinone system was due to its synthetic versatility, well-balanced physic-chemical properties, and the presence of possible binding sites for interactions with various receptors. Among several new pyridazinone derivatives, identified as lead compounds, the most advanced a 3-(2*H)*–pyridazinone derivative, GYKY-16084, has been developed for the treatment of benign prostatic hyperplasia (102). Recently, GYKY-16084, entered Phase II clinical trials (102).

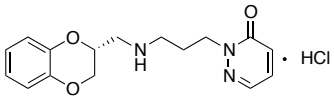

Figure 27. GYKI 16084 (102)

3.1.1.4.1 Chemistry and Biological Assays

Linear and annellated naphthaleno-pyridazinone derivatives were synthesized via nucleophilic substitution reaction and intramolecular Heck-type arylation (schemes 6-7).

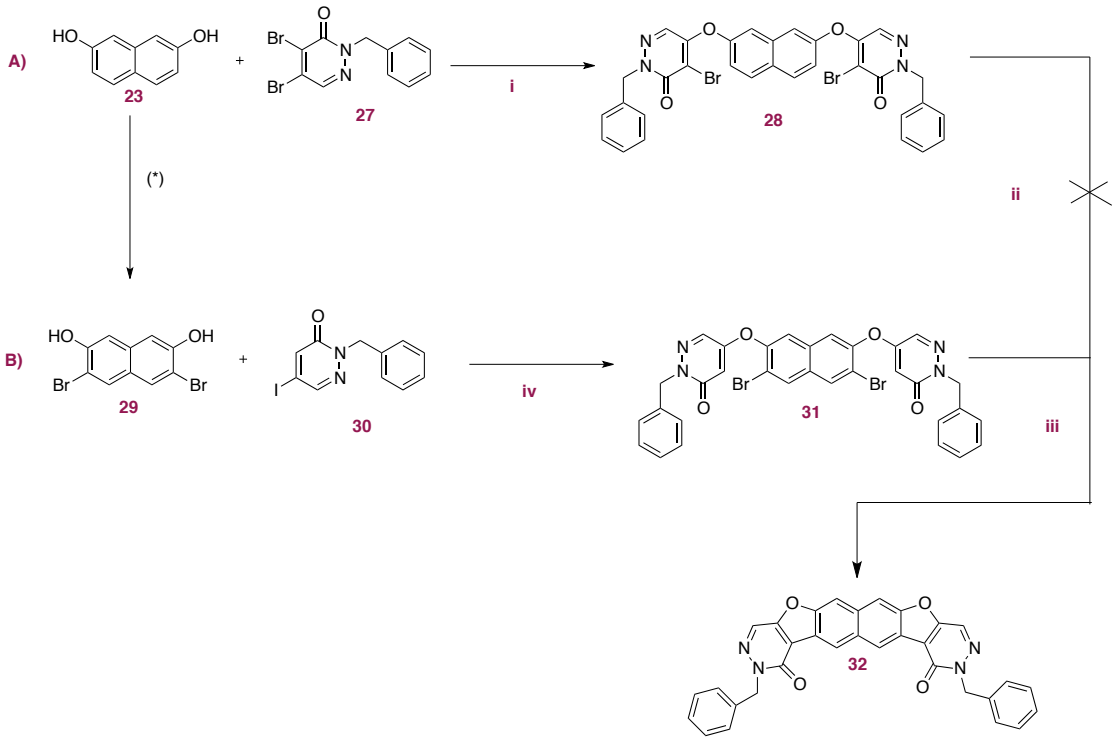

Scheme 6. **Synthesis of 5,5'-((3,6-dibromonaphthalene-2,7-diyl)bis(oxy))bis(2-benzylpyridazin-3(2*H*)-one) (31) and (32). (i) : $K^{+}(CH_3)_3CO^{-}$, dry DMF, r.t., 3hrs, 95% yield; (ii): $Pd(PPh_3)_2Cl_2$, NaOAcx3H_2O, DMA, 130 °C; (iii): $Pd(PPh_3)_2Cl_2$, NaOAcx3H_2O, DMA, 130 °C; (iv): K_2CO_3, CH_3CN, 3h MW, 60%.**

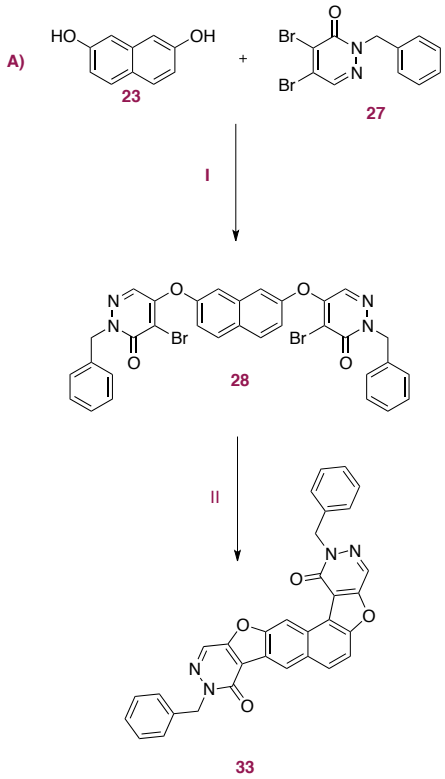

Scheme 7. **Synthesis of 5,5'-(naphthalene-2,7-diylbis(oxy))bis(2-benzyl-4-bromopyridazin-3(2*H*)-one) (28) and (33): (i): $K^{+}(CH_3)_3CO^{-}$, dry DMF, r.t., 3hrs, 95% yield; (ii): $Pd(PPh_3)_2Cl_2$, NaOAcx3H_2O, DMA, 130 °C, 100% yield.**

Noteworthy, in the synthetic pathway **A)** the nucleophilic substitution by 2,7-dihydroxy naphthalene **23** occurs on C-5 of 4,5-dibromo-2-*N*-benzylpyridazinone, ruling out any SN_2 on C-4 of 4,5-dihalo-2-*N*-benzylpyridazinone, which would result in the synthesis of a linear asymmetric molecule, if 2,7-dihydroxynaphthalene was differently substituted. This has been proven by the ^{1}H-NMR analysis reported hereinafter (fig.28). The relative HPLC chromatogram and elemental analysis (here not reported) fully support the NMR results (fig.28).

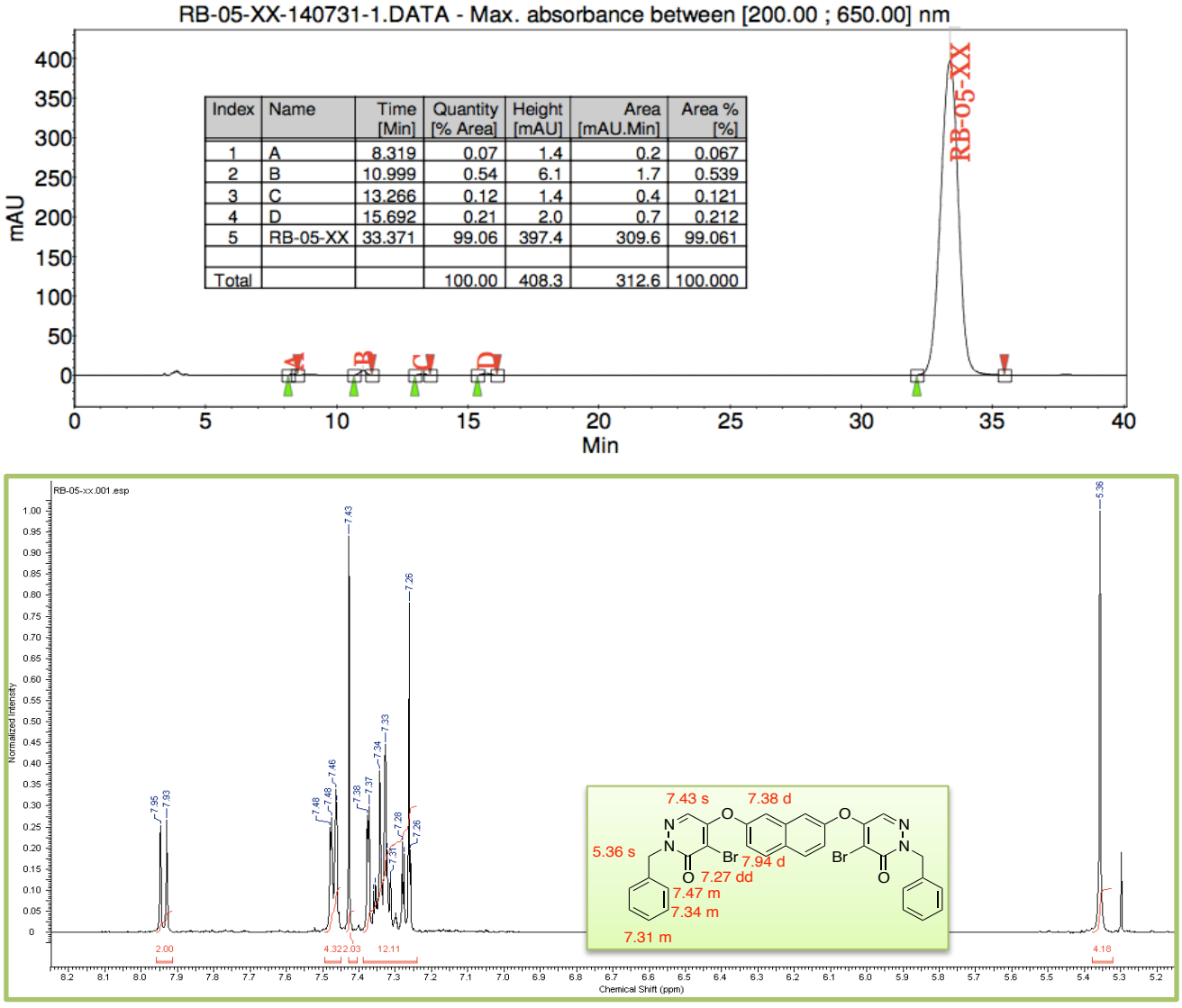

Figure 28. Compound 28: HPLC chromatogram and ^{1}H-NMR spectrum.

Compound **28** was synthesized under different conditions in order to improve both the yield and the reaction time. Therefore, as first attempt the reaction between **23**

and **27** was carried out in dry aceto nitrile, by using dry potassium carbonate as base and refluxing, affording 30% white chrystals. Then the yield was doubled when the same reaction was conducted in a microwave reactor over 2.30 hours, at 130 °C, 200 psi and 200 watt. Although a better reaction time and yield were accomplished, some 2-benzyl-4,5-dibromopyridazin-3(2*H*)-one resulted still unreacted. Thus, a new method was developed, using potassium tert butoxide as base, in dry DMF, at room temperature, over 3 hours, which afforded 95% yield.

Through this procedure all the starting materials disappeared over the reaction time above indicated. This result was important to achieve since it represented a great limit approached so far by any researcher who has had to face to the nucleophilic substitution reaction by a 4,5-dihalo-2-*N*-benzylpyridazinone.

The choice of both starting materials **23** and **29** and the entries **27** and **30**, together with the synthetic versatility of the pyridazinone compounds were crucial in order to get symmetrical or unsymmetrical final products after the ring closure reactions. Linear derivative **32** resulted from the strategic choise of 3,6-dibromo-2,7-dihydroxynaphthalene **29** as starting and 5-iodo-2-*N*-benzylpyridazinone **30** as entry. Compound **29** was synthesized according to the literature (103). The reaction between **29** and **30** was carried out under three different parallel conditions: a first attempt in dry aceto nitrile, using dry potassium carbonate as base and refluxing over 19 hours, yielded 60% white chrystals. A parallel reaction conducted in the microwave reactor over 2.30 hours, at 100 °C, 200 psi and 50 watt afforded the same yield. The last reaction conditions, which foresaw the use of potassium tert butoxide as base, in dry DMF, at room temperature, over 3 hours resulted too strong, hence unsuccessful.

The Heck-type intramolecular arylation of **28** linear derivative, gave the ring closure in C-3 and C-8 of the naphthalene ring (instead of C-3 and C-6 as it was expected), yielding the unsymmetrical derivative **33**. When the synthesis starts from 3,6-dibromo-2,7-dihydroxynaphthalene, only the symmetrical anellated naphthaleno-pyridazinone derivative **32** can be achieved. Unless **33**, all the above described derivatives show a C_{2v} symmetry feature (table 5).

Table 5. **Symmetry features of naphthaleno-pyridazine based derivatives.**

STARTING	ENTRY	LINEAR NAPHTHALENO-PYRIDAZINE-BASED DERIVATIVE	POINT GROUP SYMMETRY	ANELLATED NAPHTHALENO-PYRIDAZINE-BASED DERIVATIVE	POINT GROUP SYMMETRY
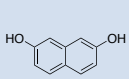	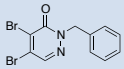	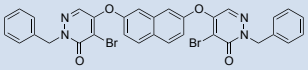	C_{2V}	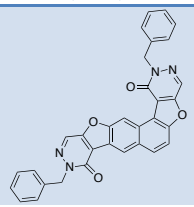	E
23	27	28		33	
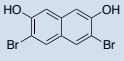	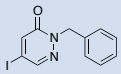	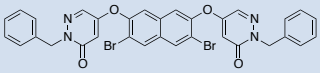	C_{2V}	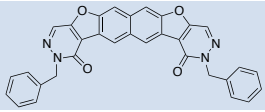	C_{2V}
29	30	31		32	

The synthesized compounds **28** and **31** were subjected to antiproliferative tests on HeLa cells, over 48 hours treatment. Noteworthy, the different position of the two bromo in **28** and **31** significantly affected the antiproliferative activity. Indeed, **28** and **31** respectively show >50 μM and 10.34 μM GI50 values. Even the di- and monohalo-2-*N*-benzyl pyridazinone compounds, **27** and **30** underwent the same antiproliferative assay. Interestingly **27** shows a 0.0027 μM GI50 value *vs* >50 μM shown by compound **30.** Derivatives **32** and **33** could not be assayed since these products were not soluble neither in DMSO nor in Ethanol as we could expected since their molecular structure.

In order to evaluate a potential effect of the substituent in compound **28**, derivative **40** was accomplished, as shown in the following reaction scheme:

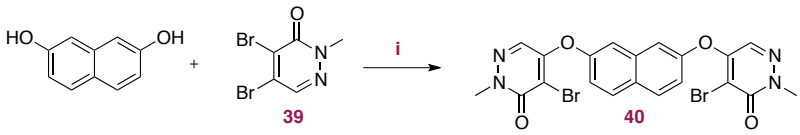

Scheme 8. **(i): K_2CO_3, CH_3CN, 8 h, refluxing, 20% yield.**

Table 6. GI50(mM) values, (HeLa cells, over 48 hrs treatment) related to compounds **28** and **40.**

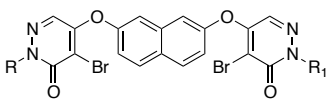

COMPOUND	$R=R_1$	GI50(μM) values, (HeLa cells, over 48 hrs treatment)
28	**-Bn**	>50
40	**-CH_3**	3.18

The growth inhibition of 50% resulted dramatically increased when the naphthaleno pyridazine-based derivative displayed in table 6, is symmetrically substituted by a methyl group instead of a benzyl one.

Due to its controllable regiochemistry, 2-Benzyl-4,5-dibromopyridazin-3(2*H*)-one **27** was chosen again as starting material for the synthesis of new other pyridazine-based derivatives. Compounds **34** and **35** were initially designed to be synthesized *via* nucleophilic substitution reaction and intramolecular Heck-type arylation, as previously above described.

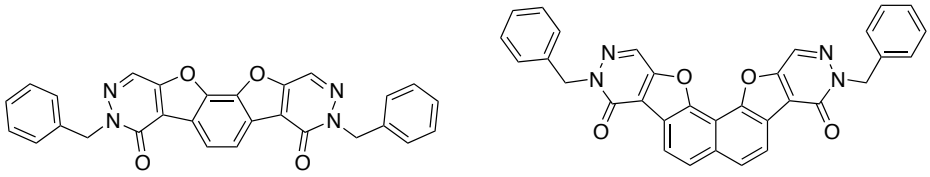

Figure 29. 1,2-Dihydroxy benzeno-pyridazinone anellated derivative (34); 1,8- dihydroxy naphthaleno pyridazinone derivative (35).

The nucleophlic substitution reaction afforded both symmetrical dihydroxy benzeno- and naphthaleno-pyridazinone angular derivatives (fig.29), since the substitution occurs on C_5 of 4,5-dibromo-2-*N*-benzylpyridazinone in the case of both hydroxyl groups, giving the best yield when the reactions were carried out using a microwave reactor.

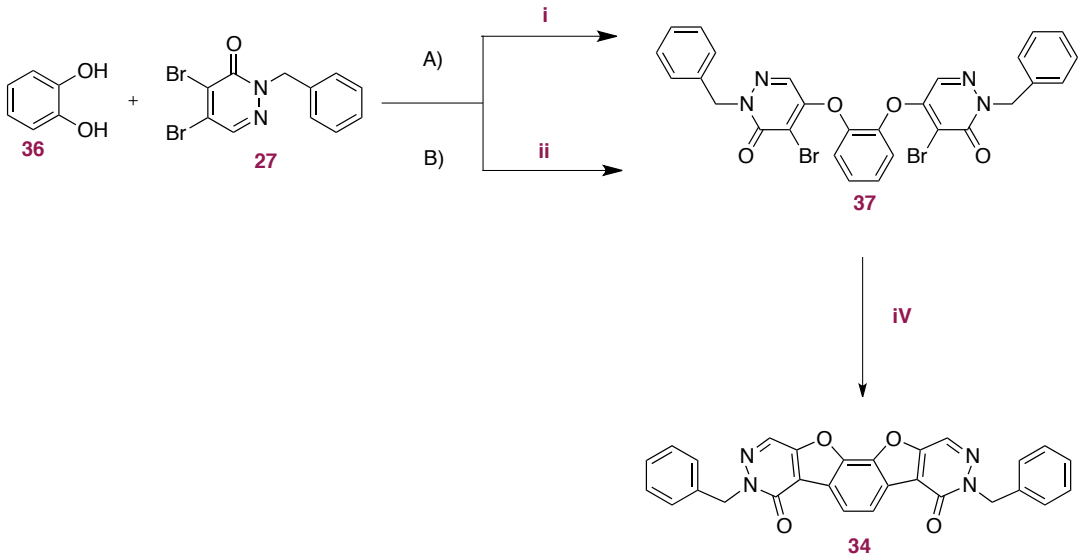

Scheme 9. (i): K_2CO_3, CH_3CN, 30 h, refluxing, 50% yield; (ii): K_2CO_3, CH_3CN, 3h MW, 60%; (iv): $Pd(PPH_3)_2Cl_2$, NaOAcx3H_2O, DMA, 100 °C, 100 WATT, Ar, MW.

Unfortunately Heck type intramolecular arylation in both case of **37** and **38** did not occur at the conditions used and derivatives **34** and **35** could not be accomplished.

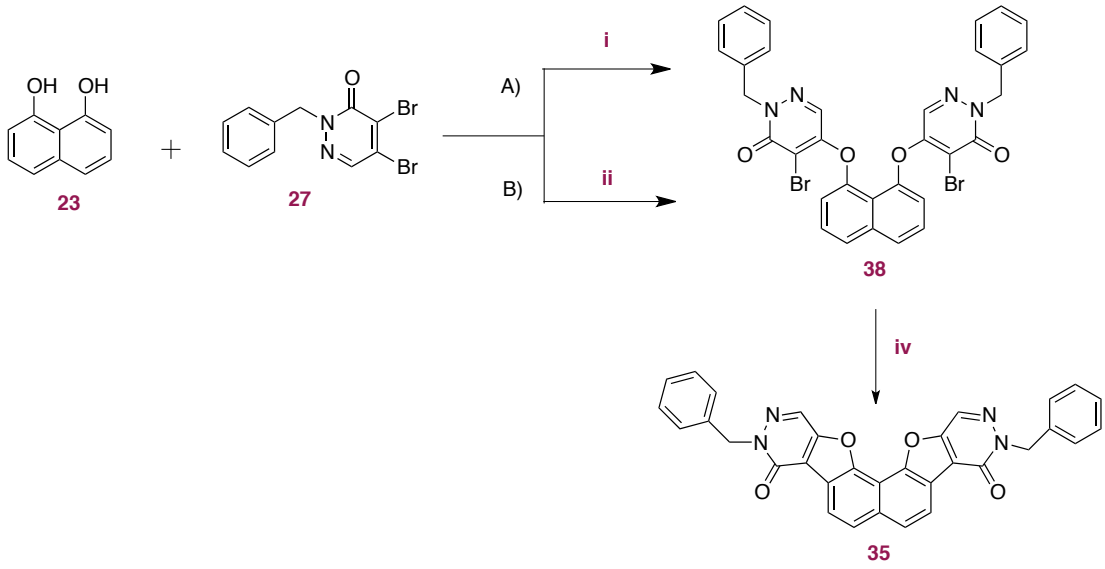

Scheme 10. **(i): K_2CO_3, CH_3CN, 8 h, refluxing, 20% yield; (ii): K_2CO_3, CH_3CN, 4h MW, 40%; (iv): $Pd(PPH_3)_2Cl_2$, NaOAcx3H_2O, DMA, 130 °C, 1h, Ar, MW.**

Compounds **37** and **38** were subjected to antiproliferative tests on HeLa cells, over 48 hours treatment. Interestingly, in this case a difference in dimension of the two cores, benzene in **37** and naphthalene in **38**, significantly affected the antiproliferative activity. Indeed, **37** shows 16.84 μM and **38** >50 μM GI50 values.

4. Conclusions And Perspectives

This PhD work aimed to the design, the synthesis, and the biological evaluation of novel heterocyclic small molecules able to halt tumor cell proliferation, both reproducing the mecanisms of action of the classical DNA-interactive drugs, namely the reversible binding to DNA through the formation of non-covalent interactions, and interacting with secondary structures of the DNA (G-quadruplexes), recently turned out as more appealing targets in anticancer drug discovery.

In the former work, the synthesis and the biological evaluation of the new benzo[*b*]thiophene series of type **10** and the related amino precursors **8 a-f** are reported. Generally, all tested compounds showed a good antiproliferative effect with GI50 values in a low micromolar range. Antiproliferative screening on HeLa tumor cell line underlined a significant growth inhibition effect of final imidazole-side chain compounds **10 a-l**. Methyl insertion on the imidazole ring resulted in a notable increase of activity for the TMB (**10d** *vs* **10j**) and the 3-chloro-4-fluoro-benzoylamino-benzo[*b*]thiophene derivatives (**10e** *vs* **10k**), while it was irrelevant in the other cases.

No differences were observed in the biological activity by changing the substituents on the benzoyl moiety (both electron-withdrawing and electron-releasing substituents), and the TMB derivatives **8d**, **10d**, and **10j** resulted the most active of each subgroup. To evaluate their potential influence on cell-cycle distribution, derivatives **8d**, **10j**, and **10l** were also tested in cell cycle perturbation experiments. After cell exposure to benzo[*b*]thiophene derivatives, a rapid accumulation of cells in the G2/M phase, with a concomitant reduction of cells in both the S and G0/G1 phases, was observed.

To rationalize biological results of selected hits on cell-cycle distribution, considering the structural features of the proposed derivatives of type 6 and 13, similar to known antimitotic agents, the benzothiophenes were analyzed through the *in silico* VLAK protocol. Compounds presenting the TMB moiety were classified as potential antimitotic agents, showing high affinity percentage for this mechanism of action class. The presence of the imidazole ring does not seem to affect the mechanism of action as previously observed by biological assays. This is also underlined by the presence of several imidazole derivatives as the best ranked antimitotic agents in table 2. Another important aspect to be underlined is the good percentage of affinity for topoisomerase II inhibitors showed by some other 3-benzoylamino-benzo[*b*]thiophene derivatives as **10b,d,h,j**. These findings could be in accordance with biological assays where a possible

antimitotic mechanism or a potential inhibition of the topoisomerase II enzyme could justify the cell cycle arrest at G2/M checkpoint.

In the latter work, the synthesis and the biological evaluation of the new benzo[*b*]furan series of type **11**, **12**, and **13** were reported. With respect to the previous issued benzo[*b*]thiophene series (**8** and **10**) and their antiproliferative activity, we replaced the thiophene central core with a furan ring, in order to evaluate the isosteric influence on the biological activity. As a general trend, the antiproliferative screening on HeLa and MCF7 tumor cell lines underlined a significant growth inhibition effect of final imidazole-side chain compounds **12a-f** and **13a-f**. Methyl insertion on the imidazole ring resulted in a notable increase of activity. The cytotoxic effect is remarkably interesting in the case of derivative **13f**, where GI_{50} values on both HeLa and MCF-7 tumour cell lines are respectively at 2.14 and 1.55 μM. No differences were observed in the biological activity by changing the substituents on the benzoyl portion, even though the presence of this moiety was crucial for the antiproliferative effects. Indeed the lack of activity observed in the biological screening of derivative **18** confirmed the importance of this moiety present in the whole benzo[*b*]furan series. To evaluate their potential influence on cell-cycle distribution, the methyl-imidazole side-chain compounds **13a-f** were also tested on HeLa cells, in cell cycle perturbation experiments, producing cell cycle arrest with proapoptotic effects.

As last, the design, the synthesis, and the biological evaluation on new potential G-quadruplex binders were reported.

Synthesis of *bis*-isoquinoline derivatives and double-chained naphthalenes were carried out. Spectroscopic tests on G4-DNA isoforms did not turn out the expected interaction, previously observed through molecular modelling studies.

Linear and annellated naphthaleno-pyridazinone derivatives were synthesized *via* nucleophilic substitution reaction and intramolecular Heck-type arylation exploiting as starting material, as in many of our synthetic pathways, the 2-benzyl-4,5-dibromopyridazin-3(2*H*)-one, because its controllable regiochemistry.

As shown in schemes 6-7**,** the strategical choise of starting materials **23** and **29**, and **27** and **30**, afforded respectively symmetrical and unsymmetrical anellated compounds **32** and **33.** In schemes 9-10 was important to accomplish linear, and eventually anellated compounds, showing two cores differently sized to evidence any difference in antiproliferative activity and/or in interaction with B-DNA and G4-DNA. Considerably

results were achieved. Indeed, the antiproliferative screening on HeLa tumor cell lines underlined a significant growth inhibition effect concerning compounds **31,** highlighting the importance of the different position of two bromo placed in C3 and C6, over the naphthalene core in **31** and on C4, over the pyridazinone in compound **28**; besides, the benzene core in **37** improved the GI50 value than that of the naphthalene one in compound **38**. Furthermore, a significant growth inhibition effect was provided by changing the benzyl group with a methyl one in compound **28.** Derivative **40** resulted the most active on HeLa tumor cell lines besides the commercially available **27** starting material. The anellated derivatives **34** and **35** above proposed to be achieved *via* Heck-type arylation, were assumed unable to C-C bond formation maybe due to both distance and strain issues.

The final aim was to evaluate any interaction of the anellated derivatives with B-DNA and G4-DNA, through UV-vis spectroscopy, circular dichroism (CD), fluorescence, viscosity, electrophoresis gel determination of binding constants studies. Unfortunately, due to some solubility issues, the anellated compounds achieved could not undergone any spectroscopic assays and antiproliferative screenings. Since some flat pyridazine-based compounds herein proposed, seems to be still promising as new potential G4-binders and stabilizers, in the near future might be interesting properly functionalize **32** and **33** derivatives, through the removal of the *N*-benzyl protective group, yielding the unsubstituted fused pyridazinone compounds to be decorated with proper side chains expected to bind the grooves of G4s.

The functionalization of these derivatives would afford interesting symmetrical and unsymmetrical disubstituted compounds, with improved chemical-physical features, useful to assess any interaction with B-DNA and G4-DNA.

5. Experimental Part

Chemistry

Materials and Methods

Unless otherwise indicated, all reagents and solvents were purchased from commercial sources and used without further purification. All melting points (°C) were determined on a Büchi Tottoli capillary apparatus and are uncorrected; IR spectra were determined in bromoform with a Jasco FT/IR 5300 spectrophotometer. ^{1}H NMR, ^{13}C NMR spectra were recorded, at 200 and 50.3 MHz respectively, in $CDCl_3$ or DMSO-d_6 solution, using a Bruker AC-E series 200 MHz spectrometer. Chemical shifts values are given in ppm and referred as the internal standard to tetramethylsilane (TMS). The following abbreviations are used: br s= broad signal, s= singlet, d= doublet, t= triplet, q= quartet, m = multiplet, rt= room temperature. The purity of all compounds screened in biological assays was determined to be >95% by HPLC/MS analysis. Mass spectra were performed using a GC and MS Shimadzu QP5050 with EI (75 ev). Microanalyses were in agreement with theoretical values ±0.4%. Thin layer chromatography was performed on precoated (0.25 mm) silica gel GF254 plates, compounds were detected with 254 nm UV lamp. Column chromatography was performed with Merck silica gel ASTM (230 and 400 mesh), or with a Biotage FLASH40i chromatography module (prepacked cartridge system). 2-fluorobenzonitrile (**3**) is commercially available. 2-fluoro-5-nitro-benzonitrile (**4**) was obtained following the procedure reported in literature (90).

Benzo[*b*]thiophene series. Synthesis of ethyl 3-amino-5-nitro-benzo[*b*]thiophene-2-carboxylate (5)

According to the literature procedure (93), ethyl thioglycolate (1.2 mL, 11 mmol) was added to a stirred mixture of NaH 60% dispersion in mineral oil (0.36 g, 15 mmol) in dry DMSO (10 mL). After stirring at room temperature for 20 min, a solution of 2- fluoro-5-nitrobenzonitrile (**4**) (1.66 g, 10 mmol) in dry DMSO (20 mL) was added dropwise. The reaction was stirred at room temperature for further 3 h and then was poured onto stirred water/ice. The precipitate was collected by filtration and dried to give orange-red needles of **5**, 2.48 g.

(5). Yield 93%. Mp 207-208 °C. IR ^{n}max: 3491, 3367 (NH_2), 1657 (CO) cm^{-1}. ^{1}H NMR ($CDCl_3$) d: 1.41 (t, 3H, J = 8.0Hz, CH_3), 4.42 (q, 2H, J = 8.0 Hz, CH_2), 6.03 (br s,

2H, exchange with D_2O, NH_2), 7.84 (d, 1H, J = 8.8 Hz, H-7), 8.29 (dd, 1H, J = 2.0, 8.8 Hz, H-6), 8.59 (d, 1H, J = 2.0 Hz, H-4); ^{13}C NMR (DMSO- *d*6) d: 14.3 (q), 60.2 (t), 96.9 (s), 119.4 (d), 122.0 (d), 124.3 (d), 131.4 (s), 144.5 (s), 144.9 (s), 149.7 (s), 163.9 (s). Anal. Calcd. (%) for $C_{11}H_{10}N_2O_4S$: C, 49.62; H, 3.79; N, 10.52; found: C, 49.64; H, 3.81; N, 10.48.

General procedure for the synthesis of ethyl 3-benzoylamino-5-nitro-benzo[*b*]thiophene-2-carboxylates 7a-f

To a suspension of amine **5** (0.37 mmol) and pyridine (0.56 mmol) was added the appropriate benzoyl chloride 11 (0.56 mmol). The reaction mixture was stirred at room temperature for about 12 h, and then poured onto stirred water/ice. The precipitate was collected by filtration, dried over night. The crude was crystallized from ethyl acetate.

Ethyl 3-benzoylamino-5-nitro-benzo[*b*]thiophene-2-carboxylate (**7a**). Yield 95%. Mp 200-201 –C. IR n_{max}: 3606 (NH), 1687, 1679 (CO) cm–^{1}. ^1H NMR ($CDCl_3$) d: 1.43 (t, 3H, J = 8.0 Hz, CH_3), 4.44 (q, 2H, J = 8.0 Hz, CH_2), 7.48-7.69 (m, 3H, H-3', H-4', H-5'), 7.89 (d, 1H, J = 8.8 Hz, H-7), 8.11 (dd, 2H, J = 2.0, 8.0 Hz, H-2', H-6'), 8.32 (dd, 1H, J = 2.0, 8.8 Hz, H-6), 9.24 (d, 1H, J = 2.0 Hz, H-4), 10.69 (s, 1H, NH). ^{13}C NMR ($CDCl_3$) d: 14.2 (q), 62.3 (t), 117.3 (s), 121.7 (d), 123.3 (d), 124.2 (d), 127.9 (d), 128.6 (s), 129.0 (d), 132.8 (d), 132.9 (s), 141.0 (s), 144.5 (s), 145.1 (s), 164.1 (s), 165.3 (s). Anal. Calcd. (%) for $C_{18}H_{14}N_2O_5S$: C, 58.37; H, 3.81; N, 7.56; found: C, 58.34; H, 3.84; N, 7.53.

Ethyl 3-(4-methoxy-benzoylamino)-5-nitro-benzo[*b*]thiophene-2-carboxylate (**7b**). Yield 82%. Mp 191-192 –C. IR n_{max}: 3601 (NH), 1696, 1672 (CO) cm–^{1}. ^1H NMR ($CDCl_3$) d: 1.43 (t, 3H, J = 8.0 Hz, CH_3), 3.91 (s, 3H, OCH_3), 4.44 (q, 2H, J = 8.0 Hz, CH_2), 7.05 (d, 2H, J 1⁄4 8.0 Hz, H-3' ,H-5'), 7.89 (d, 1H, J = 9.0 Hz, H-7), 8.07 (d, 2H, J = 8.0 Hz, H-2', H-6'), 8.32 (dd, 1H, J = 2.0, 9.0 Hz, H-6), 9.25 (d, 1H, J = 2.0 Hz, H-4), 10.64 (s, 1H, NH). ^{13}C NMR ($CDCl_3$) d: 14.2 (q), 55.6 (q), 62.3 (t), 114.1 (d), 114.2 (d), 121.2 (d), 121.6 (s), 121.8 (s), 126.8 (s), 132.3 (d), 132.8 (d), 141.3 (s), 141.8 (s), 144.5 (s), 145.0 (s), 164.2 (s), 164.8 (s). Anal. Calcd. (%) for $C_{19}H_{16}N_2O_6S$: C, 56.99; H,

4.03; N, 7.00; found: C, 56.95; H, 4.07; N, 7.03.

Ethyl 3-(4-methyl-benzoylamino)-5-nitro-benzo[*b*]thiophene-2-carboxylate (**7c**). Yield 98%. Mp 231-232 –C. IR n_{max}: 3607 (NH), 1700, 1677 (CO) cm–^{1}. ^{1}H NMR ($CDCl_3$) d: 1.43 (t, 3H, J = 8.0 Hz, CH_3), 2.47 (s, 3H, CH_3), 4.44 (q, 2H, J = 8.0 Hz, CH_2), 7.37 (d, 2H, J 1⁄4 8.8 Hz, H-3$^{'}$,H-5$^{'}$), 7.90 (d, 1H, J = 8.0 Hz, H-7), 8.00 (d, 2H, J 1⁄4 8.8 Hz, H-2$^{'}$, H-6$^{'}$), 8.33 (dd, 1H, J = 2.0, 8.0 Hz, H-6), 9.25 (d, 1H, J = 2.0 Hz, H-4), 10.66 (s, 1H, NH). ^{13}C NMR ($CDCl_3$) d: 14.2 (q), 21.6 (q), 62.3 (t), 118.5 (s), 121.7 (d), 123.3 (d), 124.2 (d), 128.0 (d), 129.7 (d), 130.3 (s), 132.9 (s), 141.2 (s), 143.6 (s), 144.5 (s), 145.1 (s), 164.1 (s), 165.3 (s). Anal. Calcd. (%) for $C_{19}H_{16}N_2O_5S$: C, 59.37; H, 4.20; N, 7.29; found: C, 59.40; H, 4.17; N, 7.32.

Ethyl 3-(3,4,5-trimethoxy-benzoylamino)-5-nitro-benzo[*b*]thiophene-2-carboxylate (**7d**). Yield 99%. Mp 211-213 –C. IR n_{max}: 3607 (NH), 1680, 1668 (CO) cm–^{1}. ^{1}H NMR ($CDCl_3$) d: 1.46 (t, 3H, J = 8.0 Hz, CH_3), 3.98 (s, 3H, OCH_3), 4.02 (s, 6H, 2 OCH_3), 4.45 (q, 2H, J = 8.0 Hz, CH_2), 7.38 (s, 2H, H-2$^{'}$,H-6$^{'}$), 7.93 (d, 1H, J = 8.0 Hz, H-7), 8.36 (dd, 1H, J = 2.0, 8.0 Hz, H-6), 9.32 (d, 1H, J = 2.0 Hz, H-4), 10.72 (s, 1H, NH). ^{13}C NMR ($CDCl_3$) d: 14.2 (q), 56.4 (q), 61.0 (t), 62.3 (q), 105.3 (d), 117.0 (s), 117.5 (d), 121.7 (d), 121.9 (d), 128.4 (s), 131.3 (s), 132.8 (s), 141.1 (s), 145.1 (s), 145.6 (s), 153.4 (s), 164.2 (s), 165.0 (s). Anal. Calcd. (%) for $C_{21}H_{20}N_2O_8S$: C, 54.78; H, 4.38; N, 6.08; found: C, 54.76; H, 4.40; N, 6.10.

Ethyl 3-(4-trifluoromethyl-benzoylamino)-5-nitro-benzo[*b*]thiophene-2-carboxylate (**7e**). Yield 74%. Mp 236-237 –C. IR n_{max}: 3616 (NH), 1695, 1684 (CO) cm–^{1}. ^{1}H NMR ($CDCl_3$) d: 1.44 (t, 3H, J = 8.0Hz, CH_3), 4.46(q,2H, J = 8.0Hz, CH_2), 7.85 (d, 2H, J = 8.0Hz, H-3$^{'}$, H-5$^{'}$), 7.92 (d, 1H, J = 8.0 Hz, H-7), 8.23 (d, 2H, J = 8.0 Hz, H-2$^{'}$, H-6$^{'}$), 8.36 (dd, 1H, J = 2.0, 8.0 Hz, H-6), 9.27 (d, 1H, J = 2.0 Hz, H-4), 10.83 (s, 1H, NH). ^{13}C NMR ($CDCl_3$) d: 14.2 (q), 62.5 (t), 117.7 (s), 120.9 (s), 121.9 (d), 123.5 (s), 124.1 (d), 125.0 (s), 126.1 (d), 128.4 (d), 130.6 (d), 132.7 (s), 140.5 (s), 144.4 (s), 151.5 (s), 164.0 (s), 164.2 (s). Anal. Calcd. (%) for $C_{19}H_{13}F_3N_2O_5S$: C, 52.06; H, 2.99; N, 6.39; found: C, 52.10; H, 2.93; N, 6.42.

Ethyl 3-(3-chloro-4-fluoro-benzoylamino)-5-nitro-benzo[*b*]thiophene-2-carboxylate (**7f**). Yield 57.4%. Mp 218-219 –C. IR n_{max}: 3620 (NH), 1693, 1684 (CO) cm–^{1}. ^{1}H NMR ($CDCl_3$) d: 1.47 (t, 3H, J = 8.0 Hz, CH_3), 4.49 (q, 2H, J = 8.0 Hz, CH_2), 7.36 (t, 1H, J = 10.0 Hz, H-5$^{'}$), 7.94 (d, 1H, J = 8.0 Hz, H-7), 8.03 (dq, 1H, J = 2.0, 10.0 Hz, H-6$^{'}$), 8.23 (dd, 1H, J = 2.0, 8.0 Hz, H-6), 8.37 (dd, 1H, J = 2.0, 10.0 Hz, H- 2$^{'}$), 9.24 (d, 1H, J = 2.0 Hz, H-4), 10.83 (s, 1H, NH). ^{13}C NMR ($CDCl_3$) d: 14.2 (q), 62.5 (t), 117.3 (d, J = 5 Hz), 117.4 (s), 121.8 (d), 122.5 (s), 123.4 (s), 123.9 (d), 128.1 (d), 130.3 (s), 131.4 (s), 132.6 (d), 140.5 (s), 144.4 (s), 145.2 (s), 161.0 (d, J = 30 Hz), 163.2 (s), 164.2 (s). Anal. Calcd. (%) for $C_{18}H_{12}ClFN_2O_5S$: C, 51.13; H, 2.86; N, 6.63; found: C, 51.16; H, 2.90; N, 6.65.

General procedure for the synthesis of ethyl 5-amino-3 benzoylaminobenzo[*b*]thiophene-2-carboxylates 8 a-f

A suspension of 5-nitro compound **7 a-f** (1 mmol), 10% Pd/C (0.05 g) in ethanol was subjected to hydrogenation using a Parr Hydrogenation apparatus at 500 psi for 2 h. After then, the catalyst was removed by filtration and the filtrate was concentrated under reduced pressure. The crude was recrystallized from ethanol.

Ethyl 5-amino-3-benzoylamino-benzo[*b*]thiophene-2-carboxylate (**8a**). Yield 91%. Mp 184-185 –C. IR n_{max}: 3612, 3356 (NH_2), 3293 (NH), 1688, 1664 (CO) cm–^{1}. ^{1}H NMR ($CDCl_3$) d: 1.42 (t, 3H, J = 8.0 Hz, CH_3), 4.41 (q, 2H, J = 8.0 Hz, CH_2), 4.83 (br s, 2H, NH_2) 6.96 (dd, 1H, J = 2.0, 8.0 Hz, H-6), 7.49 (d, 1H, J = 2.0 Hz, H-4), 7.52-7.63 (m, 5H, C_6H_5), 8.10 (d, 1H, J = 8.0 Hz, H-7), 10.48 (s, 1H, NH). ^{13}C NMR ($CDCl_3$) d: 14.3 (q), 61.6 (t), 111.0 (d), 119.0 (d), 123.2 (d), 127.8 (d), 128.9 (d), 130.4 (s), 131.1 (s), 132.4 (d), 133.9 (s), 139.1 (s), 143.6 (s), 146.6 (s), 161.2 (s), 165.9 (s). Anal. Calcd. (%) for $C_{18}H_{16}N_2O_3S$: C, 63.51; H, 4.74; N, 8.23; found: C, 63.53; H, 4.72; N, 8.21.

Ethyl 5-amino-3-(4-methoxy-benzoylamino)-benzo[b]thio- phene-2-carboxylate (**8b**). Yield 98%. Mp 160-161 –C. IR n_{max}: 3613, 3360 (NH_2), 3296 (NH), 1683, 1660 (CO) cm–^{1}. ^{1}H NMR (DMSO-d_6) d: 1.19 (t, 3H, J = 8.0 Hz, CH_3), 3.91 (s, 3H, OCH_3), 4.24 (q, 2H, J = 8.0 Hz, CH_2), 5.08 (br s, 2H, NH_2) 6.94 (d, 1H, J = 2.0 Hz, H-4), 7.09-

7.17 (m, 3H, H-6, H-3', H-5'), 7.50 (d, 1H, J = 8.0 Hz, H-7), 8.07 (d, 2H, J = 8.8 Hz, H-2', H-6'), 10.04 (s, 1H, NH). ^{13}C NMR (DMSO-*d*6) d: 13.9 (q), 55.6 (q), 60.8 (t), 113.5 (d), 113.7 (d), 118.8 (d), 119.2 (d), 126.3 (s), 127.2 (s), 129.6 (d), 130.2 (s), 134.2 (s), 138.8 (s), 139.7 (s), 161.7 (s), 161.9 (s), 164.9 (s). Anal. Calcd. (%) for $C_{19}H_{18}N_2O_4S$: C, 61.61; H, 4.90; N, 7.56; found: C, 61.59; H, 4.93; N, 7.52.

Ethyl 5-amino-3-(4-methyl-benzoylamino)-benzo[*b*]thiophene-2-carboxylate (**8c**). Yield 70%. Mp 208-209 –C. IR n_{max}: 3613, 3360 (NH_2), 3297 (NH), 1682, 1665 (CO) cm–^{1}. ^{1}H NMR (DMSO-*d*6): d 1.18 (t, 3H, J = 8.0 Hz, CH_3), 2.42 (s, 3H, CH_3), 4.23 (q, 2H, J = 8.0 Hz, CH_2), 5.32 (br s, 2H, NH_2) 6.90-6.95 (m, 2H, H-4, H- 6), 7.38 (d, 2H, J 1⁄4 8.0 Hz, H-3', H-5'), 7.64 (d, 1H, J = 8.0 Hz, H-7), 7.97 (d, 2H, J = 8.8 Hz, H-2', H-6'), 10.20 (s, 1H, NH). ^{13}C NMR (DMSO-*d*6) d: 14.5 (q), 21.5 (q), 61.3 (t), 105.8 (d), 118.3 (d), 123.0 (d), 125.9 (s), 127.8 (d), 129.0 (d), 131.0 (s), 135.5 (s), 137.1 (s), 141.9 (s), 146.5 (s), 161.9 (s), 163.0 (s), 165.2 (s). Anal. Calcd. (%) for $C_{19}H_{18}N_2O_3S$: C, 64.39; H, 5.12; N, 7,90; found: C, 64.42; H, 5.15; N, 7.93.

Ethyl 5-amino-3-(3,4,5-trimethoxy-benzoylamino)-benzo[*b*]thiophene-2-carboxylate (**8d**). Yield 93%. Mp 182-183 –C. IR n_{max}: 3404, 3316 (NH_2), 3213 (NH), 1696, 1655 (CO) cm–^{1}. ^{1}H NMR (DMSO-*d*6) d: 1.20 (t, 3H, J = 8.0 Hz, CH_3), 3.76 (s, 3H, OCH_3), 3.88 (s, 6H, 2 OCH_3), 4.22 (q, 2H, J = 8.0 Hz, CH_2), 5.34 (br s, 2H, NH_2) 6.87 (d, 1H, J = 2.0 Hz, H-4), 6.93 (dd, 1H, J = 2.0, 8.0 Hz, H-6), 7.41 (s, 2H, H-2', H-6'), 7.65 (d, 1H, J = 8.0 Hz, H-7), 10.22 (s, 1H, NH). ^{13}C NMR (DMSO-*d*6) d: 14.0 (q), 56.1 (q), 60.1 (q), 60.8 (t), 99.5 (s), 105.3 (d), 105.7 (d), 118.3 (s), 123.0 (d), 125.8 (d), 128.9 (s), 135.2 (s), 137.1 (s), 140.5 (s), 146.5 (s), 152.7 (s), 161.8 (s), 164.6 (s). Anal. Calcd. (%) for $C_{21}H_{22}N_2O_6S$: C, 58.59; H, 5.15; N, 6.51; found: C, 58.63; H, 5.17; N, 6.55.

Ethyl 5-amino-3-(4-trifluoromethyl-benzoylamino)-benzo[*b*]thiophene-2-carboxylate (**8e**). Yield 80%. Mp 198-199 –C. IR n_{max}: 3612, 3356 (NH_2), 3293 (NH), 1688, 1664 (CO) cm–^{1}. ^{1}H NMR (DMSO-*d*6) d: 1.18 (t, 3H, J = 8.0 Hz, CH_3), 4.22 (q, 2H, J = 8.0 Hz, CH_2), 5.34 (br s, 2H, NH_2) 6.89 (d, 1H, J = 2.0 Hz, H-4), 6.93 (dd, 1H, J = 2.0, 8.0 Hz, H-6), 7.66 (d, 1H, J = 8.0 Hz, H-7), 7.98 (d, 2H, J = 8.8 Hz, H-3', H-5'),

8.25 (d, 2H, J = 8.8 Hz, H-2', H-6'), 10.54 (s, 1H, NH). ^{13}C NMR (DMSO-d_6) d: 14.0 (q), 60.9 (t), 119.1 (s), 118.3 (d), 120.8 (s), 123.1 (d), 123.7 (s), 125.5 (d), 126.9 (s), 128.6 (d), 129.1 (d), 134.4 (s), 137.1 (s), 146.6 (s), 147.9 (s), 161.7 (s), 164.3 (s). Anal. Calcd. (%) for $C_{19}H_{15}F_3N_2O_3S$: C, 55.88; H, 3.70; N, 6.86; found: C, 55.84; H, 3.73; N, 6.82.

Ethyl 5-amino-3-(3-chloro-4-fluoro-benzoylamino)-benzo[*b*]thiophene-2-carboxylate (**8f**). Yield 52%. Mp 226-227 –C. IR n_{max}: 3615, 3360 (NH_2), 3290 (NH), 1689, 1667 (CO) cm–^{1}. ^{1}H NMR ($CDCl_3$) d: 1.18 (t, 3H, J = 8.0 Hz, CH_3), 4.23 (q, 2H, J = 8.0 Hz, CH_2), 5.35 (br s, 2H, NH_2), 6.87 (d, 1H, J = 2.0 Hz, H-4), 6.93 (dd, 1H, J = 2.0, 10.0Hz,H-2'), 7.65 (d, 1H, J = 8.0Hz,H-7), 7.66 (t, 1H, J = 10.0Hz,H-5'), 8.08 (dq, 1H, J = 2.0, 10.0 Hz, H-6'), 8.29 (dd, 1H, J = 2.0, 8.0 Hz, H-6), 10.34 (s, 1H, NH). ^{13}C NMR (DMSO-d_6) d: 14.0 (q), 61.1 (t), 99.5 (s), 117.3 (d), 118.5 (s), 120.0 (d), 122.6 (s), 123.2 (s), 125.8 (d), 128.9 (d), 131.5 (s), 134.3 (d), 137.0 (s), 141.1 (s), 146.6 (s), 161.6 (d), 163.2 (s), 164.3 (s). Anal. Calcd. (%) for $C_{18}H_{14}ClFN_2O_3S$: C, 55.03; H, 3.59; N, 7.13; found: C, 55.04; H, 3.60; N, 7.22.

General procedure for the synthesis of ethyl 3-benzoylamino- 5-[(1H-imidazol-4-yl-methyl)-amino]-benzo[*b*]thiophene-2- carboxylates 10 a-l

To a suspension of the **8 a-f** (1.25 mmol) and the appropriate aldehyde (1.6 mmol) in dry ethanol (10 mL) was added acetic acid up to pH 4. The mixture was stirred for 30 min, and then $NaCNBH_3$ (1.6 mmol) was added by stirring at room temperature for further 6-24 h. The reaction solvent was removed under reduced pressure and the crude product was purified by chromatography column using dichloromethane/methanol 98:2 as eluent. Recrystallized from ethanol.

Ethyl 3-benzoylamino-5-[(1H-imidazol-4-yl-methyl)-amino]- benzo[*b*]thiophene-2-carboxylate (**10a**). Yield 76%. Mp 184-185 –C. IR n_{max}: 3301, 3245 (NH), 1684, 1668 (CO) cm–^{1}. ^{1}H NMR (DMSO-d_6) d: 1.19 (t, 3H, J = 8.0 Hz, CH_3), 4.24 (q, 2H, J = 8.0 Hz, CH_2), 4.52-4.54 (m, 3H, NH, NCH_2) 6.89 (s, 1H, H-5''), 7.19 (s, 1H, H-2''), 7.29 (dd, 1H, J = 2.0, 8.0 Hz, H-6), 7.56-7.65 (m, 5H, C_6H_5), 7.73 (d, 2H, J = 8.0 Hz, H-7),

8.04 (d, 1H, J = 2.0 Hz, H-4) 10.39 (s, 1H, NH), 12.10 (br s, 1H, NH). ^{13}C NMR (DMSO-*d*6) d: 13.5 (q), 46.1 (t), 60.4 (t), 100.3 (d), 119.7 (s), 122.8 (s), 122.9 (d), 125.9 (s), 128.4 (d), 129.5 (d), 131.1 (s), 132.5 (s), 134.4 (d), 135.1 (d), 135.7 (d), 137.0 (d), 146.2 (s), 149.5 (s), 161.6 (s), 165.9 (s). Anal. Calcd. (%) for $C_{22}H_{20}N_4O_3S$: C, 62.84; H, 4.79; N, 13.32; found: C, 62.86; H, 4.80; N, 13.35.

Ethyl5-[(1H-imidazol-4-yl-methyl)-amino]-3-(4-methoxy-benzoylamino)-benzo[*b*]thiophene-2-carboxylate (**10b**). Yield 62%. Mp 124-125 – C. IR n_{max}: 3306, 3243 (NH), 1682, 1667 (CO) cm–^{1}. ^{1}H NMR (DMSO-*d*6) d: 1.15 (t, 3H, J = 8.0 Hz, CH_3), 3.86 (s, 3H, OCH_3), 4.20 (q, 2H, J = 8.0 Hz, CH_2), 4.28 (d, 2H, J = 2.0 Hz, NCH_2) 5.34 (t, 1H, J = 2.0 Hz, NH), 6.91 (s, 1H, H-5''), 7.04-7.16 (m, 4H, H-3' , H-5' , H-2'' , H-6), 7.54 (d, 1H, J = 8.0 Hz, H-7), 7.58 (d, 1H, J = 2.0 Hz, H-4), 8.06 (d, 2H, J = 8.0 Hz, H-2', H-6') 10.06 (s, 1H, NH), 11.96 (br s, 1H, NH). ^{13}C NMR (DMSO-*d*6) d: 14.0 (q), 40.1 (t), 55.4 (q), 60.8 (t), 99.5 (s), 103.5 (d), 113.6 (d), 113.7 (s), 117.7 (d), 122.0 (s), 122.5 (s), 122.9 (d), 126.2 (d), 129.7 (d), 134.8 (d), 135.6 (s), 137.0 (s), 146.6 (s), 161.9 (s), 162.0 (s), 164.9 (s). Anal. Calcd. (%) for $C_{23}H_{22}N_4O_4S$: C, 61.32; H, 4.92; N, 12.44; found: C, 61.31; H, 4.94; N, 12.48.

Ethyl5-[(1H-imidazol-4-yl-methyl)-amino]-3-(4-methyl-benzoylamino)-benzo[*b*]thiophene-2-carboxylate (**10c**). Yield 58%. Mp 138-139 – C. IR n_{max}: 3307, 3253 (NH), 1680, 1669 (CO) cm–^{1}. ^{1}H NMR (DMSO-*d*6) d: 1.18 (t, 3H, J ¼ 8.0 Hz, CH_3), 2.42 (s, 3H, CH_3), 4.14 (d, 2H, J = 2.0 Hz, NCH_2), 4.23 (q, 2H, J = 8.0 Hz, CH_2), 6.11 (t, 1H, J = 2.0 Hz, NH), 6.91-6.93 (m, 2H, H-4, H-5''), 7.06 (dd, 1H, J = 2.0, 8.0 Hz, H-6), 7.38 (d, 2H, J = 8.0 Hz, H-3' , H-5'), 7.56 (s, 1H, H-2''), 7.68 (d, 1H, J = 8.0 Hz, H-7), 7.97 (d, 2H, J = 8.0 Hz, H-2', H-6'), 10.23 (s, 1H, NH), 11.93 (br s, 1H, NH). ^{13}C NMR (DMSO-*d*6) d: 14.0 (q), 21.0 (q), 40.4 (t), 60.8 (t), 103.4 (d), 117.4 (d), 117.7 (d), 122.7 (s), 122.9 (d), 126.1 (s), 127.8 (d), 129.0 (d), 131.3 (s), 134.8 (d), 135.3 (s), 137.0 (s), 141.8 (s), 146.6 (s), 161.9 (s), 165.3 (s), 172.0 (s). Anal. Calcd. (%) for $C_{23}H_{22}N_4O_3S$: C, 63.58; H, 5.10; N, 12.89; found: C, 63.60; H, 5.12; N, 12.85.

Ethyl5-[(1H-imidazol-4-yl-methyl)-amino]-3-(3,4,5-trimethoxy-benzoylamino)-

benzo[*b*]thiophene-2-carboxylate (**10d**). Yield 94%. Mp 165-166 –C. IR: 3301, 3245 (NH), 1684, 1668 (CO) cm–^{1}. ^{1}H NMR (DMSO-d_6) d: 1.20 (t, 3H, J = 7.0 Hz, CH_3), 3.76 (s, 3H, OCH_3), 3.89 (s, 6H, 2 OCH_3), 4.34 (d, 2H, J = 1.8 Hz, NCH_2), 4.24 (q, 2H, J 1⁄4 7.0 Hz, CH_2), 6.14 (t,1H, J = 1.8 Hz, NH), 6.89 (d,1H, J = 1.8 Hz, H-4) 6.95 (s, 1H, H-5''), 7.07 (dd, 1H, J = 1.8, 8.8 Hz, H-6), 7.40 (s, 2H, H-2', H-6'), 7.58 (s, 1H, H-2''), 7.70 (d, 1H, J = 8.8 Hz, H-7), 10.25 (s, 1H, NH), 12.22 (br s, 1H, NH). ^{13}C NMR (DMSO-d_6) d: 14.0 (q), 40.2 (t), 56.0 (q), 60.1 (q), 60.2 (t), 99.5 (s), 103.3 (s), 105.3 (d), 117.7 (d), 122.9 (d), 126.1 (d), 129.1 (s), 129.5(s), 134.8 (s), 135.2 (d), 137.0 (s), 140.4 (s), 146.6 (s), 152.6 (d), 156.9 (s), 161.8 (s), 164.9 (s). Anal. Calcd. (%) for $C_{25}H_{26}N_4O_6S$: C, 58.81; H, 5.13; N, 10.97; found: C, 58.83; H, 5.14; N, 10.95.

Ethyl5-[(1H-imidazol-4-yl-methyl)-amino]-3-(4-trifluoromethyl-benzoylamino)-benzo[*b*]thiophene-2-carboxylate (**10e**). Yield 84%. Mp 192-193 –C. IR n_{max}: 3298, 3233 (NH), 1679, 1665 (CO) cm–^{1}. ^{1}H NMR (DMSO-d_6) d: 1.21 (t, 3H, J = 6.0 Hz, CH_3), 4.25 (q, 2H, J = 6.0 Hz, CH_2), 4.53-4.56 (m, 3H, NCH_2, NH), 6.90 (1, 1H, H-5''), 7.19 (d, 1H, J = 2.0 Hz, H-4), 7.57 (s, 1H, H-2''), 7.74 (d, 1H, J = 8.0 Hz, H-7), 7.99 (d, 2H, J = 10.0 Hz, H-3', H-5'), 8.22 (d, 2H, J = 10.0 Hz, H-2', H-6'), 10.56 (s, 1H, NH), 11.93 (br s, 1H, NH). ^{13}C NMR (DMSO-d_6) d: 14.0 (q), 40.0 (t), 60.9 (t), 99.5 (s), 113.0 (d), 117.9 (d), 121.1 (d), 125.4 (s), 125.5 (s), 126.2 (d), 128.6 (d), 129.0 (s), 130.6 (d), 134.4 (d), 134.8 (s), 136.9 (s), 137.8 (s), 146.7 (s), 161.7 (s), 164.5 (s), 166.3 (s). Anal. Calcd. (%) for $C_{23}H_{19}F_3N_4O_3S$: C, 56.55; H, 3.92; N, 11.47; found: C, 56.53; H, 3.91; N, 11.49.

Ethyl 5-[(1H-imidazol-4-yl-methyl)-amino]-3-(3-chloro-4- fluoro-benzoylamino)-benzo[*b*]thiophene-2-carboxylate (**10f**). Yield 43%. Mp 162-163 –C. IR n_{max}: 3306, 3253 (NH), 1690, 1669 (CO) cm–^{1}. ^{1}H NMR ($CDCl_3$) d: 1.34 (t, 3H, J = 8.0 Hz, CH_3), 4.26-4.30 (m, 3H, NH, NCH_2), 4.32 (q, 2H, J = 8.0 Hz, CH_2), 6.82 (dd, 1H, J = 2.0, 8.0 Hz, H-6), 6.96 (s, 1H, H-5''), 7.24 (t, 1H, J = 8.0 Hz, H-5'), 7.43 (d, 1H, J = 8.0 Hz, H-7), 7.47 (s, 1H, H-2''), 7.73 (d, 1H, J = 2.0 Hz, H-4), 7.89 (dq, 1H, J = 2.0, 8.0 Hz, H-6'), 8.07 (dd, 1H, J = 2.0, 8.0 Hz, H-2'), 9.73 (s, 1H, NH), 10.45 (br s, 1H, NH). ^{13}C

NMR (DMSO-*d*6) d: 14.0 (q), 40.6 (t), 60.9 (t), 103.0 (d), 117.0 (d), 117.9 (d), 119.6 (s), 120.0 (s), 123.0 (d), 123.4 (s), 126.1 (s), 129.0 (d), 129.1 (d), 130.3 (d), 131.7 (s), 134.4 (s), 134.8 (d), 136.9 (s), 146.8 (s), 161.7 (s), 163.3 (s), 172.2 (s). Anal. Calcd. (%) for $C_{22}H_{18}ClFN_4O_3S$: C, 55.87; H, 3.84; N, 11.85; found: C, 55.91; H, 3.81; N, 11.88.

Ethyl 3-benzoylamino-5-[(5-methyl-1H-imidazol-4-yl- methyl)-amino]-benzo[*b*]thiophene-2-carboxylate (**10g**). Yield 49%. Mp 169-171 – C. IR n_{max}: 3607, 3336 (NH), 1671, 1543 (CO) cm^{-1}. ^1H NMR (DMSO-*d*6) d: 1.22 (t, 3H, J = 6.0 Hz, CH_3), 2.24 (s, 3H, CH_3), 4.22-4.33 (m, 4H, OCH_2, NCH_2), 5.27 (t, 1H, J = 4.0 Hz, NH), 7.27 (d, 1H, J = 8.0 Hz, H-7), 7.52 (s, 1H, H-2''), 7.60-7.66 (m, 5H, C_6H_5), 8.12 (d, 1H, J = 2.0 Hz, H-4), 8.15 (dd, 1H, J = 2.0, 8.0 Hz, H-6), 10.25 (s, 1H, NH), 11.96 (br s, 1H, NH). ^{13}C NMR (DMSO-*d*6) d: 10.0 (q), 14.0 (q), 39.0 (t), 60.8 (t), 102.8 (d), 117.9 (d), 122.9 (s), 123.5 (d), 125.0 (s), 125.9 (s), 127.8 (d), 128.4 (d), 129.2 (d), 131.0 (s), 132.3 (s), 132.7 (d), 146.5 (s), 147.5 (s), 160.8 (s), 165.4 (s), 171.9 (s). Anal. Calcd. (%) for $C_{23}H_{22}N_4O_3S$: C, 63.58; H, 5.10; N, 12.89; found: C, 63.54; H, 5.06; N, 12,86.

Ethyl 5-[(5-methyl-1H-imidazol-4-yl-methyl)-amino]-3-(4- methoxy-benzoylamino)-benzo[*b*]thiophene-2-carboxylate (**10h**). Yield 34%. Mp 165-1667 °C. IR n_{max}: 3603, 3328 (NH), 1670, 1611 (CO) cm^{-1}. ^1H NMR (DMSO-*d*6) d: 1.18 (t, 3H, J = 6.2 Hz, CH_3), 2.09 (s, 3H, CH_3), 3.87 (s, 3H, OCH_3), 4.06 (br s, 2H, CH_2), 4.22 (q, 2H, J = 6.2 Hz, CH_2), 6.07 (br s, 1H, NH), 6.87 (s, 1H, H-4), 7.00-7.18 (m, 3H, H-6, H-3', H-5'), 7.51 (s, 1H, H-2''), 7.67 (d, 1H, J = 8.2 Hz, H-7), 8.06 (d, 2H, J = 8.0 Hz, H-2' , H-6'), 10.17 (s, 1H, NH), 11.36 (s, 1H, NH). ^{13}C NMR (DMSO-*d*6) d: 10.0 (q), 14.0 (q), 40.1 (t), 55.4 (q), 60.7 (t), 99.5 (s), 102.9 (d), 110.5 (s), 113.6 (s), 117.9 (d), 121.3 (s), 122.5 (d), 122.8 (s), 126.1 (d), 129.5 (s), 129.7 (d), 133.1 (d), 135.6 (s), 137.0 (s), 146.5 (s), 162.0 (s), 164.8 (s). Anal. Calcd. (%) for $C_{24}H_{24}N_4O_4S$: C, 62.05; H, 5.21; N, 12.06; found: C, 62.09; H, 5.24; N, 12.10.

Ethyl 5-[(5-methyl-1H-imidazol-4-yl-methyl)-amino]-3-(4- methyl-benzoylamino)-benzo[b]thiophene-2-carboxylate (**10i**). Yield 32%. Mp 164-166 °C. IR n_{max}: 3615, 3360 (NH), 1689, 1667 (CO) cm^{-1}. ^1H NMR (DMSO-*d*6) d: 1.18 (t, 3H, J = 6.2 Hz,

CH_3), 2.09 (s; 3H, CH_3), 2.42 (s, 3H, CH_3), 4.06 (br, s, 2H, CH_2), 4.22 (q, 2H, J = 6.2 Hz, CH_2), 6.05 (br s, 1H, NH), 6.88 (d, 1H, J = 2.0 Hz, H-4), 7.06 (dd, 1H, J = 2.0, 8.6 Hz, H-6), 7.38 (d, 2H, J = 8.0 Hz, H-3', H-5'), 7.44 (s, 1H, H-2''), 7.67 (d, 1H, J = 8.6 Hz, H-7), 8.98 (d, 2H, J = 8.0 Hz, H- 2', H-6'), 10.23 (s, 1H, NH), 11.84 (br s, 1H, NH). ^{13}C NMR (DMSO-*d*6) d: 10.1 (q), 14.0 (q), 21.0 (q), 39.0 (t), 60.8 (t), 102.8 (d), 117.9 (d), 122.8 (d), 126.1 (s), 127.8 (d), 128.9 (d), 129.6 (s), 131.2 (s), 133.1 (d), 135.4 (s), 137.0 (s), 141.8 (s), 146.6 (s), 161.9 (s), 165.3 (s), 171.1 (s), 172.1 (s). Anal. Calcd. (%) for $C_{24}H_{24}N_4O_3S$: C, 64.27; H, 5.39; N, 12.49; found: C, 64.31; H, 5.36; N, 12.51.

Ethyl 5-[(5-methyl-1H-imidazol-4-yl-methyl)-amino]-3- (3,4,5-trimethoxy-benzoylamino)-benzo[*b*]thiophene-2-carboxylate (**10j**). Yield 56%. Mp 167-168 °C. IR n_{max}: 3617, 3363 (NH), 1690, 1665 (CO) cm–1. ^1H NMR (DMSO-*d*6) d: 1.25 (t, 3H, J = 6.2 Hz, CH_3), 2.16 (s; 3H, CH_3), 3.81 (s, 3H, OCH_3), 3.94 (s, 6H, OCH_3x2), 4.35 (d, 2H, J = 1.6 Hz, CH_2), 4.29 (q, 2H, J = 7.0 Hz, CH_2), 6.23 (t, 1H, J = 1.6Hz, NH), 6.85 (d, 1H, J = 1.6Hz, H-4), 7.11 (dd, 1H, J = 2.0, 8.8 Hz, H-6), 7.46 (s, 2H, H-2', H-6'), 7.62 (s, 1H, H-2''), 7.74 (d. 1H, J = 8.8 Hz, H-7), 10.27 (s, 1H, NH), 12.09 (br s, 1H, NH). ^{13}C NMR (DMSO-*d*6) d: 14.0 (q), 21.0 (q), 40.1 (t), 56.0 (q), 60.1 (q), 60.8 (t), 99.5 (s), 102.7 (s), 105.3 (d), 117.9 (s), 123.0 (d), 126.1 (s), 129.1 (s), 133.2 (d), 135.2 (s), 137.0 (s), 140.3 (s), 140.4 (s), 146.6 (s), 152.6 (d), 161.8 (s), 164.8 (s), 172.0 (s). Anal. Calcd. (%) for $C_{26}H_{28}N_4O_6S$: C, 59.53; H, 5.38; N, 10.68; found: 59.56; H, 5.40; N, 10.66.

Ethyl5-[(5-methyl-1H-imidazol-4-yl-methyl)-amino]-3-(4-trifluoromethyl-benzoylamino)-benzo[*b*]thiophene-2-carboxylate (**10k**). Yield 34%. Mp 171-173 °C. IR n_{max}: 3612, 3294 (NH), 1691, 1644 (CO) cm–1. ^1H NMR (DMSO-*d*6) d: 1.18 (t, 3H, J = 7.0 Hz, CH_3), 2.08 (s, 3H, CH_3), 4.05 (br s, 2H, CH_2), 4.22 (q, 2H, J = 7.0 Hz, CH_2), 6.03 (br s, 1H, NH), 6.88 (d, 1H, J = 2.0 Hz, H-4), 7.06 (dd, 1H, J = 2.0, 8.6 Hz, H-6), 7.44 (s, 1H, H-2''), 7.68 (d, 1H, J = 8.6 Hz, H-7), 7.97 (d, 2H, J = 8.2 Hz, H-3', H-5'), 8.20 (d, 2H, J = 8.2 Hz, H-2', H-6'), 10.53 (s, 1H, NH), 11.67 (br s, 1H, NH). ^{13}C NMR (DMSO-*d*6): d 10.3 (q), 14.0 (q), 39.1 (t), 60.9 (t), 99.5 (s), 102.4 (d), 118.1 (d), 122.9 (d), 123.6 (s), 125.4 (s), 125.5 (d), 126.1 (s), 128.7 (d), 131.9 (s), 133.1 (d), 134.5

(s), 137.0 (s), 137.9 (s), 146.8 (s), 161.7 (s), 164.5 (s), 172.0 (s). Anal. Calcd. (%) for $C_{24}H_{21}F_3N_4O_3S$: C, 57.36; H, 4.21; N, 12.15; found: C, 57.46; H, 4.31; N, 12.25.

Ethyl5-[(5-methyl-1H-imidazol-4-yl-methyl)-amino]-3-(3-chloro-4-fluoro-benzoylamino)-benzo[*b*]thiophene-2-carboxylate (**10l**). Yield 35%. Mp 184.7-186 °C. IR n_{max}: 3607, 3332 (NH), 1701, 1655 (CO) cm^{-1}. ^1H NMR (DMSO-d_6) d: 1.24 (t, 3H, J = 7.1 Hz, CH_3), 2.15 (s, 3H, CH_3), 4.11 (br s, 2H, CH_2), 4.28 (q, 2H, J = 7.1 Hz, CH_2), 6.10 (br s, 1H, NH), 6.92 (d, 1H, J = 1.7 Hz, H-4), 7.12 (dd, 1H, J = 8.8 Hz, H-6), 7.47 (s, 1H, H-2''), 7.66-7.75 (m, 2H, H-7, H-2'), 8.13 (dd, 1H, J = 2.1, 13.3 Hz, H-6'), 8.34 (dd, 1H, J = 2.0, 7.1 Hz, H-5'), 10.50 (s, 1H, NH) 11.96 (br s, 1H, NH). ^{13}C NMR (DMSO-d_6) d: 10.5 (q), 14.0 (q), 39.1 (t), 60.9 (t), 99.5 (s), 102.4 (d), 116.9 (d), 117.4 (d), 118.1 (d), 119.6 (s), 119.9 (s), 123.0 (d), 123.5 (s), 126.1 (s), 129.2 (d), 130.3 (d), 131.7 (s), 134. 5 (s), 137.0 (s), 146.8 (s), 161.7 (s), 163.3 (s), 172.2 (s). Anal. Calcd. (%) for $C_{23}H_{20}ClFN_4O_3S$: C, 56.73; H, 4.14; N, 11.50; found: C, 56.77; H, 4.10; N, 11.54.

Biology

Chemicals and reagents

Propidium iodide, ribonuclease A (RNAse A), 3-(4,5-dimethyl-2- thiazolyl)-2,5-diphenyl-2H-tetrazolium bromide (MTT), and DMSO were obtained from Sigma Aldrich (St. Louis, MO, USA). RPMI, fetal bovine serum (FBS), phosphate buffered saline (PBS), L-glutamine solution (200 mM), trypsin-EDTA solution (170.000 U/l trypsin and 0.2 g/l EDTA) and penicillin-streptomycin solution (10.000 U/ml penicillin and 10 mg/ml streptomycin) were purchased from Lonza (Verviers, Belgium).

Cell culture

The cancer cell line HeLa (Human epithelial cervical cancer) was obtained from American Type Culture Collection (ATCC) (Rockville, MD, USA). The cells were cultured in RPMI supplemented with 5% FBS, 2 mM L-glutamine, 50 IU/ml penicillin, and 50 mg/ml streptomycin and maintained in a humidified atmosphere with 5% CO_2 at 37 °C. The cells were routinely cultured in 75 cm^2 culture flasks and were trypsinized using trypsin-EDTA when the cells reached approximately 80% confluence.

Exponentially growing cells were used for experiments.

Antiproliferative evaluation assay

3-benzoylamino-benzo[*b*]thiophene derivatives 10 **a-l** and **8 a-f** were submitted to the MTT assay to assess the growth inhibition activity against HeLa cells. The MTT assay is a measurement of cell metabolic activity, quite effective in estimating cell proliferation, which is based on the protocol first described by Mossmann (104). The assay was performed as previously described (105). The cells were seeded into a series of standard 96-well plates in 100 ml of complete culture medium at 1.0 10^4 cells/cm^2. Cells were incubated for 24 h under 5% CO_2 at 37 °C and the medium was then replaced with 100 ml of fresh medium supplemented by 5% (v/ v) FBS containing the treatments. Benzothiophene derivatives were previously dissolved in DMSO to obtain 20 mM stock solutions. Working solutions were freshly prepared on the day of testing by dilutions of the stock solutions in the complete culture medium. For the experiments a concentration range from 50 to 0.05 mM was used. 24 h after seeding aliquots of 100 ml of different solutions at the appropriate concentrations were added to the appropriate wells and the cells were incubated for 48 h without renewal of the medium. In each experiment, DMSO concentration never exceeded 0.25% and culture medium with 0.25% DMSO was used as control. After the incubation time, cells were washed and 100 mL FBS-free medium containing 0.5 mg/mL of MTT was added. The medium was discarded after a 4 h incubation at 37 °C and formazan blue formed in the cells was dissolved in DMSO. The absorbance (optical density, OD) at 570 nm of MTT-formazan was measured in a microplate reader. As the absorbance is directly proportional to the number of living, metabolically active cells, the percentage of growth (PG) to with respect to untreated cell control for each drug concentrations was calculated according to one of the following two expressions:

if $(OD_{test} - Od_{tzero}) \geq 0$; then

$PG = 100 \times (OD_{test} - Od_{tzero})/(OD_{ctr} - Od_{tzero})$

if $(OD_{test} \_ OD_{tzero}) < 0$; then

$PG = 100 (OD_{test} - Od_{tzero})/OD_{tzero}$

where OD_{tzero} is the average of optical density measurements before exposure of cells to the test compound, OD_{test} is the average of optical density measurements after the desired period of time, and OD_{ctr} is the average of optical density measurements after the desired period of time with no exposure of cells to the test compound. The concentration necessary for 50% of growth inhibition (GI50) for each derivative was calculated from concentration-response curves using linear regression analysis by fitting the test concentrations that give PG values above and below the reference value (50%). Each result was the mean value of three separate experiments performed in quadruplicate.

Cell-cycle analysis

Effects of 3-benzoylamino-benzo[*b*]thiophene derivatives **8d, 10j, and 10l** exposure on cell-cycle were performed by DNA staining with propidium iodide (PI) and flow cytometry analysis. HeLa cells were seeded on 12 well plates at a density of 2.0 10^4 cells/cm^2, and treated 24 h after seeding without or with indicated concentrations of the test compound for 24 h. Following the treatments, cells were collected, washed in PBS and stained with staining solution (20 mg/ml propidium iodide, 200 mg/ml RNAse A and 0.1% Triton X-100 in PBS), for 30 min at 37 °C. The DNA contents of more than 10,000 cells were subjected to fluorescence-activated cell sorting (FACS) analysis (Coulter® Epics® XLTM, Beckman) and the percentage of cells belonging to the different compartments of the cell cycle was determined. All experiments were performed in duplicate and reproduced two times.

Statistical analysis

All data are expressed as mean ± SD. Statistical difference was calculated using unpaired Student's t-test. Bonferroni least significance difference test was used to examine difference between group means. Values of p lower than 0.05 were considered significant.

Computational details

The compounds of the Anti-Cancer Agents Mechanism Database (NCI ACAM Database) (96)(97)(98), were drawn and optimized in vacuo by Ligprep software of MAESTRO SUITE (106). The NCI ACAM Database entries containing cations or

consisting of a mix of two structures were excluded. Thus the starting database was constituted from 114 compounds classified in six mechanism of action: 30, Alkylating Agents; 13, Antimitotic Agents; 24, Topoisomerase I Inhibitors; 15, Topoisom- erase II Inhibitors; 16, RNA/DNA Antimetabolites; 16, DNA Anti- metabolites (**Table 2**). 2D and 3D molecular descriptors were calculated for all structures to achieve all the structural information useful for building a lock model database. Each descriptor value range is delimited by μDj(MA) ± sDj(MA), where (MA) is a specific mechanism of action, mDj(MA) is the molecular descriptor j average value and sDj(MA) is the standard deviation of descriptor j. When the molecular descriptor value Dj of a tested structure X falls within the defined range (mDj ± sDj) a = 1 (i.e. D1, D3, and Dj), otherwise a = 0. Therefore, after processing descriptor values as mentioned above, every training set database structure is converted into a binary sequence. Then all of the binary values are summed, so the higher is the number of fitted pins (descriptors with a = 1), the higher will be the affinity of the investigated compound to a specific class with potential anticancer mechanism. Thus, the percentage of affinity A% (Eq. (1)) for each compound belonging to training set database has been defined for each class (MA) as:

$$A\% = Sai; j(MA)\ D_{tot}*100 \qquad \text{Equation (1)}$$

where Sai, j (MA) is the sum of all fitted molecular descriptors for the MA class and D_{tot} is the total of the molecular descriptors used in the VLAK protocol.

Acknowledgments

This work was in part supported by an FFR2012 e University of Palermo grant (CUP:B78C12000380001).

Benzo[*b*]furan series

Synthesis of ethyl 3-amino-5-nitro-benzo[b]furan-2-carboxylate (16)

To a solution of 2-fluoro-5-nitrobenzonitrile (**4**) (0.3 g, 1.8 mmol) in dry DMF (5 mL), ethyl glycolate (0.3 mL, 3.2 mmol) and potassium carbonate (0.95 g, 6.8 mmol) were added at room temperature, and the mixture was heated at 100°C for 12h. After the reaction was completed, the reaction mixture was cooled and poured in water/ice. The precipitate was collected by filtration and dried to give orange-red needles of **16**. Yield 63%. Mp 195-196 °C. IR ν_{max}: 3453, 3450 (NH_2), 1675 (CO) cm^{-1}. ^1H NMR ($CDCl_3$) δ:

1.46 (t, J= 6.0 Hz, 3H, CH_3), 4.47 (q, J= 6.0 Hz, 2H, CH_2), 5.14 (br s, 2H, NH_2), 7.56 (d, J= 9.6 Hz, 1H, H-7), 8.37 (dd, J= 2.0, 9.6 Hz, 1H, H-6), 8.59 (d, 1H, J= 2.0Hz, H-4); ^{13}C NMR ($CDCl_3$) δ: 14.6, 61.0, 113.2, 116.9, 122.0, 123.9, 131.6, 141.6, 143.4, 156.3, 161.4. Anal. Calcd. (%) for $C_{11}H_{10}N_2O_5$: C, 52.80; H, 4.03; N, 11.23; found: C, 52.85; H, 4.07; N, 11.26.

General procedure for the synthesis of ethyl 3-benzoylamino-5-nitro-benzo[b]furan-2-carboxylates 17a-f

To a suspension of amine **16** (0.37 mmol) and pyridine (0.56 mmol) was added the appropriate benzoyl chloride **6** (0.56 mmol). The reaction mixture was stirred at room temperature for about 12h, and then poured onto stirred water/ice. The precipitate was collected by filtration, dried over night. The crude was recrystallized from ethylacetate.

Ethyl 3-benzoylamino-5-nitro-benzo[b]furan-2-carboxylate (17a)

Yield 84%. Mp 172-174 °C. IR ν_{max}: 3607 (NH), 1695, 1672 (CO), 1529, 1343 (NO_2) cm^{-1}. ^1H NMR ($CDCl_3$) δ: 1.50 (t, J= 6.0 Hz, 3H, CH_3), 4.44 (q, J= 6.0 Hz, 2H, CH_2), 7.50 (d, J= 8.0 Hz, 1H, H-7), 7.56-7.64 (m, 5H, C_6H_5), 8.06 (dd, J= 2.0, 8.0 Hz, 1H, H-6), 8.65 (d, J= 2.0 Hz, 1H, H-4), 10.69 (s, 1H, NH). ^{13}C NMR ($CDCl_3$) δ: 14.3, 62.3, 112.8, 121.5, 124.1, 124.7, 127.7, 129.1, 132.1, 132.4, 132.7, 132.9, 144.0, 156.5, 161.4, 164.7. Anal. Calcd. (%) for $C_{18}H_{14}N_2O_6$: C, 61.02; H, 3.98; N, 7.91; found: C, 61.13; H, 3.88; N, 7.87.

Ethyl3-(4-methoxy-benzoylamino)-5-nitro-benzo[b]furan-2-carboxylate (17b). Yield 81%. Mp 218-219 °C. IR ν_{max}: 3610 (NH), 1697, 1675 (CO), 1546, 1345 (NO_2) cm^{-1}. ^1H NMR (DMSO-d_6) δ: 1.30 (t, J= 6.0 Hz, 3H, CH_3), 3.88 (s, 3H, OCH_3), 4.38 (q, J= 6.0 Hz, 2H, CH_2), 7.15 (d, J= 8.0 Hz, 2H, H-3',H-5'), 8.00 (d, J= 8.0 Hz, 1H, H-7), 8.07 (d, J= 8.0 Hz, 2H, H-2', H-6'), 8.43 (dd, J=2.0, 8.0 Hz, 1H, H-6), 8.98 (d, J= 2.6 Hz, 1H, H-4), 10.50 (s, 1H, NH). ^{13}C NMR (DMSO-d_6) δ: 14.0, 55.7, 61.5, 113.7, 114.6, 120.1, 123.2, 124.9, 127.9, 129.9, 131.3, 132.6, 143.6, 155.6, 162.1, 164.5, 167.0. Anal. Calcd. (%) for $C_{19}H_{16}N_2O_7$: C, 59.38; H, 4.20; N, 7.29; found: C, 59.42; H, 4.31; N, 7.19.

Ethyl 3-(4-methyl-benzoylamino)-5-nitro-benzo[b]furan-2-carboxylate (17c) Yield 62%. Mp 219-220 °C. IR ν_{max}: 3606 (NH), 1697, 1674 (CO), 1528, 1345 (NO_2) cm^{-1}. ^1H NMR (DMSO-d_6) δ: 1.30 (t, J= 6.9 Hz, 3H,

CH_3), 2.44 (s, 3H, CH_3), 4.38 (q, J= 6.9 Hz, 2H, CH_2), 7.43 (d, J= 8.0 Hz, 2H, H-3',H-5'), 7.99 (d, J= 8.0 Hz, 2H, H-2', H-6'), 8.02 (d, J= 7.8 Hz, 1H, H-7), 8.44 (dd, J= 2.0, 7.8 Hz, 1H, H-6), 8.98 (d, J= 2.0 Hz, 1H, H-4), 10.54 (s, 1H, NH). ^{13}C NMR (DMSO-d_6) δ: 14.2, 21.1, 62.3, 112.7, 121.4, 128.0, 129.1, 129.3, 129.9, 130.4, 132.1, 132.7, 143.0, 144.6, 145.7, 164.2, 165.3. Anal. Calcd. (%) for $C_{19}H_{16}N_2O_6$: C, 61.95; H, 4.38; N, 7.61; found: C, 61.83; H, 4.42; N, 7.67.

Ethyl 3-(3,4,5-trimethoxy-benzoylamino)-5-nitro-benzo[b]furan-2-carboxylate (17d). Yield 82%. Mp 215-216 °C. IR ν_{max}: 3603 (NH), 1680, 1668 (CO), 1550, 1333 (NO_2) cm^{-1}. ^{1}H NMR (DMSO-d_6) δ: 1.32 (t, J= 6.0 Hz, 3H, CH_3), 3.78 (s, 3H, OCH_3), 3.91 (s, 6H, 2xOCH_3), 4.35 (q, J= 6.0 Hz, 2H, CH_2), 7.24 (s, 2H, H-2',H-6'), 8.03 (d, J= 8.9 Hz, 1H, H-7), 8.44 (dd, J=2.0, 8.9 Hz, 1H, H-6), 8.86 (d, J= 2.0 Hz, 1H, H-4), 10.52 (s, 1H, NH). ^{13}C NMR (DMSO-d_6) δ: 14.2, 55.8, 60.1, 60.2, 106.2, 113.4, 115.7, 123.6, 124.2, 125.8, 127.9, 132.4, 141.2, 144.2, 144.9, 152.6, 162.1, 166.9. Anal. Calcd. (%) for $C_{21}H_{20}N_2O_9$: C, 56.76; H, 4.54; N, 6.30; found: 56.82; H, 4.57; N, 6.39.

Ethyl 3-(4-trifluoromethyl-benzoylamino)-5-nitro-benzo[b]furan-2-carboxylate (17e). Yield 81%. Mp 236-237 °C. IR ν_{max}: 3616 (NH), 1695, 1684 (CO), 1493, 1339 (NO_2) cm^{-1}. ^{1}H NMR ($CDCl_3$) δ: 1.42 (t, J= 6.0 Hz, 3H, CH_3), 4.47 (q, J= 6.0 Hz, 2H, CH_2), 7.56 (d, J= 8.6 Hz, 2H, H-3', H-5'), 7.76 (d, J= 8.0 Hz, 1H, H-7), 8.10 (d, J= 8.6 Hz, 2H, H-2', H-6'), 8.36 (dd, J=2.0, 8.0 Hz, 1H, H-6), 9.55 (d, J= 2.0 Hz, 1H, H-4), 10.44 (s, 1H, NH).^{13}C NMR (DMSO-d_6) δ: 14.0, 61.6, 113.7, 120.4, 123.6, 125.6, 125.7, 126.5, 126.6, 128.8, 136.8, 137.7, 143.8, 155.5, 158.5, 163.9, 167.9. Anal. Calcd. (%) for $C_{19}H_{13}F_3N_2O_6$: C, 54.04; H, 3.10; N, 6.63; found: C, 54.14; H, 3.17; N, 6.59.

Ethyl 3-(3-chloro-4-fluoro-benzoylamino)-5-nitro-benzo[b]furan-2-carboxylate (17f). Yield 86%. Mp 212-213 °C. IR ν_{max}: 3606 (NH), 1700, 1674 (CO) 1497, 1335 (NO_2) cm^{-1}. ^{1}H NMR ($CDCl_3$) δ: 1.43 (t, J= 6.7 Hz, 3H, CH_3), 4.48 (q, J= 6.7 Hz, 2H, CH_2), 7.25 (t, J= 9.8 Hz, 1H, H-5'), 7.56 (d, J= 9.6 Hz, 1H, H-7), 7.87 (dq, J= 2.0, 3.9, 9.6 Hz, 1H, H-6'),

8.08 (dd, J=3.9, 8.0 Hz, 1H, H-2'), 8.34 (dd, J= 2.0, 9.6 Hz, 1H, H-6), 9.50 (d, J= 2.0 Hz, 1H, H-4), 10.30 (s, 1H, NH). ^{13}C NMR ($CDCl_3$) δ: 14.6, 61.0, 113.2, 115.0, 117.0, 120.9, 122.0, 123.9, 128.8, 130.0, 131.5, 131.7, 138.2, 143.4, 156.3, 160.0, 161.0, 165.3. Anal. Calcd. (%) for $C_{18}H_{12}ClFN_2O_6$: C, 53.15; H, 2.97; N, 6.89; found: C, C, 53.21; H, 2.92; N, 6.94.

General procedure for the synthesis of ethyl 5-amino-3-benzoylamino-benzo[b]furan-2-carboxylates 11a-f

A suspension of 5-nitro compound **17a-f** (1 mmol), 10% Pd/C (0.05 g) in ethanol was subjected to hydrogenation using a *Parr* Hydrogenation apparatus at 500 psi for 2h. After then, the catalyst was removed by filtration and the filtrate was concentrated under reduced pressure. The crude was crystallized from ethanol.

Ethyl 5-amino-3-benzoylamino-benzo[b]furan-2-carboxylate (11a)

Yield 84%. Mp 173-174 °C. IR ν_{max}:3411, 3368 (NH_2), 3293 (NH), 1688, 1667 (CO) cm^{-1}. ^{1}H NMR ($CDCl_3$): δ 1.46 (t, J= 6.3 Hz, 3H, CH_3), 3.30 (br s, 2H, NH_2), 4.45 (q, J= 6.3 Hz, 2H, CH_2), 6.91 (dd, J= 2.0, 8.7 Hz, 1H, H-6), 7.32 (d, J= 8.7 Hz, 1H, H-7), 7.49-7.65 (m, 3H, H-3', H-4', H-5'), 7.81 (d, J=2.0 Hz, 1H, H-4), 8.03 (dd, J= 1.6, 8.4 Hz, 2H, H-2', H-6'), 10.31 (s, 1H, NH).^{13}C NMR (DMSO-d_6) δ: 14.0, 60.7, 104.3, 112.2, 117.8, 124.5, 126.9, 127.6, 128.6, 132.1, 133.4, 135.2, 145.1, 146.7, 159.2, 164.6. Anal. Calcd. (%) for $C_{18}H_{16}N_2O_4$: C, 66.66; H, 4.97; N, 8.64; found: C, 66.57; H, 4.87; N, 8.69.

Ethyl 5-amino-3-(4-methoxy-benzoylamino)-benzo[b]furan-2-carboxylate (11b). Yield 57%. Mp 146-147 °C. IR ν_{max}: 3613, 3357 (NH_2), 3296 (NH), 1718, 1667 (CO) cm^{-1}. ^{1}H NMR ($CDCl_3$): δ 1.46 (t, J= 6.7 Hz, 3H, CH_3), 2.83 (br s, 2H, NH_2), 3.89 (s, 3H, OCH_3), 4.49 (q, J= 6.7 Hz, 2H, CH_2), 6.91 (dd, J= 2.0, 8.0 Hz, 1H, H-6), 7.02 (d, J= 8.0 Hz, 2H, H-3', H-5'), 7.31 (d, J= 8.0 Hz, 1H, H-7), 7.82 (d, J= 2.0 Hz, 1H, H-4), 8.01 (d, J= 8.0 Hz, 2H, H-2', H-6'), 10.24 (s, 1H, NH). ^{13}C NMR (DMSO-d_6) δ: 14.1, 55.5, 60.8, 104.5, 112.1, 113.9, 115.4, 117.8, 120.5, 129.6, 132.6, 135.7, 143.3, 145.0, 146.7, 159.3, 162.3. Anal. Calcd. (%) for $C_{19}H_{18}N_2O_5$: C, 64.40; H, 5.12; N, 7.91;found.: C, 64.47; H, 5.09; N, 7.98.

Ethyl 5-amino-3-(4-methyl-benzoylamino)-benzo[b]furan-2-carboxylate (11c). Yield 93%. Mp 208-209 °C. IR ν_{max}: 3607, 3370 (NH_2), 3307 (NH), 1692, 1662 (CO) cm^{-1}. ^1H NMR (DMSO-d_6) δ: 1.27 (t, J= 6.0 Hz, 3H, CH_3), 2.42 (s, 3H, CH_3), 4.31 (q, J= 6.0 Hz, 2H, CH_2), 5.25 (br s, 2H, NH_2), 6.84-6.93 (m, 2H, H-6, H-7), 7.37 (d, J= 2.0 Hz, 1H, H-4), 7.39 (d, J= 8.0 Hz, 2H, H-3', H-5'), 7.96 (d, J= 8.0 Hz, 2H, H-2', H-6'), 10.17 (s, 1H, NH). ^{13}C NMR (DMSO-d_6) δ: 14.0, 21.0, 60.8, 104.6, 112.1, 117.8, 124.5, 127.1, 127.7, 129.2, 130.6, 134.9, 142.2, 144.7, 146.7, 159.3, 164.3. Anal. Calcd. (%) for $C_{19}H_{18}N_2O_4$: C, 67.44; H, 5.36; N, 8.28; found: C, 67.53; H, 5.42; N, 8.23.

Ethyl 5-amino-3-(3,4,5-trimethoxy-benzoylamino)-benzo[b]furan-2-carboxylate (11d) Yield 36%. Mp 176-177 °C. IR ν_{max}: 3404, 3316 (NH_2), 3213 (NH), 1691, 1654 (CO) cm^{-1}. ^1H NMR (DMSO-d_6): δ 1.27 (t, J= 6.0 Hz, 3H, CH_3), 3.76 (s, 3H, OCH_3), 3.88 (s, 6H, 2xOCH_3), 4.31 (q, J= 6.0 Hz, 2H, CH_2), 5.35 (br s, 2H, NH_2), 6.81-6.88 (m, 2H, H-6, H-7), 7.36-7.41 (m, 3H, H-4, H-2', H-6'), 10.18 (s, 1H, NH). ^{13}C NMR (DMSO-d_6) δ: 14.0, 56.0, 60.1, 60.8, 104.1, 105.2, 106.4, 112.2, 117.8, 124.7, 128.5, 135.6, 140.5, 144.9, 146.7, 152.7, 164.2, 166.9. Anal. Calcd. (%) for $C_{21}H_{22}N_2O_7$: C, 60.86; H, 5.35; N, 6.76; found: C, 60.86; H, 5.35; N, 6.76.

Ethyl 5-amino-3-(4-trifluoromethyl-benzoylamino)-benzo[b]furan-2-carboxylate (11e). Yield 60%. Mp 198-199 °C. IR ν_{max}: 3612, 3356 (NH_2), 3293 (NH), 1688, 1664 (CO) cm^{-1}. ^1H NMR ($CDCl_3$): δ 1.39 (t, J= 6.0 Hz, 3H, CH_3), 2.72 (br s, 2H, NH_2), 4.42 (q, J= 6.0 Hz, 2H, CH_2), 6.85 (dd, J= 2.0, 8.0 Hz, 1H, H-6), 7.25 (d, J= 8.0 Hz, 1H, H-7), 7.72 (d, J= 2.0 Hz, 1H, H-4), 7.73 (d, J= 8.0 Hz, 2H, H-3', H-5'), 8.07 (d, J= 8.0 Hz, 2H, H-2', H-6'), 10.34 (s, 1H, NH). ^{13}C NMR (DMSO-d_6) δ: 14.0, 60.8, 112.3, 117.8, 124.6, 125.6, 126.0, 128.6, 130.1, 131.5, 132,1, 135.9, 137.3, 145.2, 146.7, 159.0, 163.7. Anal. Calcd. (%) for $C_{19}H_{15}F_3N_2O_4$: C, 58.17; H, 3.85; N 7.14; found: C, 58.23; H, 3.81; N 7.07.

Ethyl 5-amino-3-(3-chloro-4-fluoro-benzoylamino)-benzo[b]furan-2-carboxylate (11f). Yield 81%. Mp 193-195 °C. IR ν_{max}: 3615, 3360

(NH_2), 3342 (NH), 1672, 1623 (CO) cm^{-1}. ^1H NMR (DMSO-d_6) δ: 1.29 (t, J= 6.0 Hz, 3H, CH_3), 3.59 (br s, 2H, NH_2), 4.36 (q, J= 6.0 Hz, 2H, CH_2), 7.42-7.51 (m, 2H, H-2', H-5'), 7.76 (d, J= 2.0 Hz, 1H, H-4), 7.78 (d, J= 6.8 Hz, 1H, H-7), 8.12-8.22 (m, 2H, H-6, H-6'), 10.54 (s, 1H, NH). ^{13}C NMR (DMSO-d_6) δ: 14.1, 61.0, 104.3, 112.3, 115.0, 117.9, 120.9, 123.6, 128.8, 130.0, 131.7, 137.2, 142.9, 146.3, 149.0, 160.0, 162.6, 165.8. Anal. Calcd. (%) for $C_{18}H_{14}ClFN_2O_4$: C, 57.38; H, 3.75; N, 7.44; found: C, 57.43; H, 3.84; N, 7.37.

General procedure for the synthesis of ethyl 3-benzoylamino-5-[(1H-imidazol-4-yl-methyl)-amino]-benzo[b]furan-2-carboxylates 12a-f and 13a-f

To a suspension of the **11a-f** (1.25 mmol) and the appropriate aldehyde (1.6 mmol) in dry ethanol (10 mL) was added acetic acid up to pH 4. The mixture was stirred for 30 min, and then $NaCNBH_3$ (1.6 mmol) was added continuing the stirring at room temperature for further 6-24h. The reaction solvent was removed under reduced pressure and the crude product was purified by chromatography column using dichloromethane/methanol 98:2 as eluent. Recrystallization from ethanol. When is employed the carbaldehyde **9b** from the crude it was also possible to isolate the methyl-imidazole side-chain derivative **18** in variable yields (10-23%).

Ethyl 5-[(5-methyl-1H-imidazol-4-yl-methyl)-amino]-3-amino-benzo[b]furan-2-carboxylate (18). Mp 140-141 °C. IR ν_{max}: 3311, 3234 (NH), 1683, (CO) cm^{-1}. ^1H NMR (DMSO-d_6) δ: 1.30 (t, J= 6.7 Hz, 3H, CH_3), 2.17 (s, 3H, CH_3), 4.05 (s, 2H, CH_2), 4.26 (q, J=6.7 Hz, 2H, CH_2), 5.54 (br s, 1H, NH), 6.11 (s, 2H, NH_2), 6.94 (dd, J=2.0, 8.0 Hz, 1H, H-6), 7.03 (d, J=2.0 Hz, 1H, H-4), 7.20 (d, J=8.0 Hz, 1H, H-7), 7.48 (s, 1H, H-2'). ^{13}C NMR (DMSO-d_6) δ: 9.7, 14.1, 40.7, 60.8, 101.5, 112.9, 117.4, 121.3, 124.7, 125.2, 126.0, 135.8, 139.6, 142.1, 159.5, 164.7. Anal. Calcd. (%) for $C_{16}H_{18}N_4O_3$: C, 61.14; H, 5.77; N, 17.82; found: C, 61.17; H, 5.79; N, 17.86.

Ethyl 3-benzoylamino-5-[(1H-imidazol-4-yl-methyl)-amino]-benzo[b]furan-2-carboxylate (12a). Yield 50%. Mp 184-185 °C. IR ν_{max}: 3301, 3245 (NH), 1684, 1668 (CO) cm^{-1}. ^1H NMR (DMSO-d_6) δ: 1.25 (t,

J= 6.7 Hz, 3H, CH_3), 4.14 (br s, 2H, CH_2), 4.30 (q, J= 6.7 Hz, 2H, CH_2), 5.92 (t, J= 4.0 Hz, 1H, NH), 6.86-7.08 (m, 3H, H-4, H-6, H-5"), 7.44 (d, J= 7.8 Hz, 1H, H-7), 7.53-7.69 (m, 4H, H-3', H-4', H-5', H-2"), 8.05 (d, J= 8.0 Hz, 2H, H-2', H-6'), 10.29 (s, 1H, NH), 12.03 (br s, 1H, NH). ^{13}C NMR (DMSO-d_6) δ: 14.0, 40.7, 60.8, 101.5, 112.3, 116.5, 117.5, 124.4, 126.8, 127.3, 127.7, 128.6, 132.1, 133.5, 134.8, 135.3, 145.3, 146.8, 159.2, 164.9. Anal. Calcd. (%) for $C_{22}H_{20}N_4O_4$: C, 65.34; H, 4.98; N, 13.85; found: C, 65.39; H, 4.45; N, 13.79.

Ethyl 5-[(1H-imidazol-4-yl-methyl)-amino]-3-(4-methoxy-benzoylamino)-benzo[b]furan-2-carboxylate (12b). Yield 24%. Mp 124-125 °C. IR ν_{max}: 3306, 3243 (NH),1682, 1667 (CO) cm^{-1}. ^{1}H NMR (DMSO-d_6): δ 1.26 (t, J= 6.0 Hz, 3H, CH_3), 3.87 (s, 3H, OCH_3), 4.14 (d, J= 2.0 Hz, 2H, CH_2), 4.30 (q, J= 6.0 Hz, 2H, CH_2), 5.91 (t, J= 2.0 Hz, 1H, NH), 6.92-7.04 (m, 3H, H-4, H-6, H-5"), 7.12 (d, J= 8.0 Hz, 2H, H-3', H-5'), 7.43 (d, J=8.0 Hz, 1H, H-7), 7.58 (s, 1H, H-2"), 8.04 (d, J= 8.0 Hz, 2H, H-2', H-6') 10.13 (s, 1H, NH), 11.93 (br s, 1H, NH). ^{13}C NMR (DMSO-d_6) δ: 14.0, 40.3, 55.4, 60.8, 101.9, 107.2, 112.3, 113.9, 116.6, 117.5, 124.3, 125.5, 127.1, 129.7, 134.8, 134.9, 145.0, 146.9, 159.3, 162.3, 164.4. Anal. Calcd. (%) for $C_{23}H_{22}N_4O_5$: C, 63.59; H, 5.10; N, 12.90; found: C, 63.66; H, 5.18; N, 12.88.

Ethyl 5-[(1H-imidazol-4-yl-methyl)-amino]-3-(4-methyl-benzoylamino)-benzo[b]furan-2-carboxylate (12c). Yield 65%. Mp 138-139 °C. IR ν_{max}: 3307, 3253 (NH), 1680, 1669 (CO) cm^{-1}. ^{1}H NMR (DMSO-d_6) δ: 1.26 (t, J= 6.3 Hz, 3H, CH_3), 2.42 (s, 3H, CH_3), 4.14 (s, 2H, CH_2), 4.30 (q, J= 6.3 Hz, 2H, CH_2), 5.92 (br t, J= 3.7 Hz, 1H, NH), 6.92-7.04 (m, 3H, H-4, H-6, H-5"), 7.37-7.45 (m, 3H, H-7, H-3', H-5'), 7.58 (s, 1H, H-2"), 7.92 (d, J= 8.1 Hz, 2H, H-2', H-6') 10.20 (s, 1H, NH), 12.02 (br s, 1H, NH). ^{13}C NMR (DMSO-d_6) δ: 14.0, 21.0, 40.4, 60.8, 101.7, 112.3, 117.5, 124.3, 124.5, 126.9, 127.7, 129.2, 130.6, 135.1, 138.2, 142.3, 145.2, 146.9, 159.3, 162.2, 164.7. Anal. Calcd. (%) for $C_{23}H_{22}N_4O_4$: C, 66.02; H, 5.30; N, 13.39; found: C, 66.13; H, 5.27; N, 13.31.

Ethyl 5-[(1H-imidazol-4-yl-methyl)-amino]-3-(3,4,5-trimethoxy-benzoylamino)-benzo[b]furan-2-carboxylate (12d). Yield 30%. Mp 137-139 °C. IR ν_{max}: 3307, 3250 (NH), 1687, 1670 (CO) cm^{-1}. ^1H NMR (DMSO-d_6) δ: 1.32 (t, J= 6.0 Hz, 3H, CH_3), 3.73 (s, 3H, OCH_3), 3.83 (s, 3H, 2xOCH_3), 4.28 (d, J= 2.0 Hz, 2H, CH_2), 4.35 (q, J= 6.0 Hz, 2H, CH_2), 6.64 (br s, 1H, NH), 7.24 (s, 2H, H-2', H-6'), 7.41 (s, 1H, H-5"), 7.62 (s, 1H, H-2"), 8.02 (d, J= 9.7 Hz, 1H, H-7), 8.44 (dd, J= 3.0, 9.7 Hz, 1H, H-6), 8.87 (d, J= 3.0 Hz, 1H, H-4) 10.37 (s, 1H, H-2"), 10.52 (s, 1H, NH), 12.94 (br s, 1H, NH). ^{13}C NMR (DMSO-d_6) δ: 14.2, 40.5, 55.8, 60.1, 60.8, 105.5, 106.3, 113.7, 117.7, 123.6, 124.9, 125.9, 127.4, 128.0, 137.2, 140.2, 141.2, 143.7, 152.6, 155.6, 158.6, 165.3, 166.9, 172.0. Anal. Calcd. (%) for $C_{25}H_{26}N_4O_7$: C, 60.72; H, 5.30; N, 11.33; found: C, 60.77; H, 5.36; N, 11.25.

Ethyl 5-[(1H-imidazol-4-yl-methyl)-amino]-3-(4-trifluoromethyl-benzoylamino)-benzo[b]furan-2-carboxylate (12e). Yield 23%. Mp 169-171 °C. IR ν_{max}: 3293, 3229 (NH), 1674, 1668 (CO) cm^{-1}. ^1H NMR (DMSO-d_6) δ: 1.24 (t, J= 6.3 Hz, 3H, CH_3), 4.14 (s, 2H, CH_2), 4.30 (q, J= 6.3 Hz, 2H, CH_2), 5.96 (br s, 1H, NH), 6.84 (s, 1H, H-5"), 6.94-7.07 (m, 2H, H-4, H-6), 7.45 (d, J= 7.8 Hz, 1H, H-7), 7.62 (s, 1H, H-2"), 7.98 (d, J= 8.2 Hz, 2H, H-3', H-5'), 8.24 (d, J= 8.2 Hz, 2H, H-2', H-6') 10.54 (s, 1H, NH), 12.04 (br s, 1H, NH). ^{13}C NMR (DMSO-d_6) δ: 14.0, 60.7, 100.8, 112.4, 117.6, 124.6, 125.6, 126.0, 128.7, 130.0, 134.8, 135.8, 135.0, 135.5, 135.9, 137.4, 145.5, 146.7, 158.9, 163.8, 166.3. Anal. Calcd. (%) for $C_{23}H_{19}F_3N_4O_4$: C, 58.48; H, 4.05; N, 11.86; found: C, 58.56; H, 4.13; N, 11.79.

Ethyl 5-[(1H-imidazol-4-yl-methyl)-amino]-3-(3-chloro-4-fluoro-benzoylamino)-benzo[b]furan-2-carboxylate (12f). Yield 57%. Mp 162-163 °C. IR ν_{max}: 3306, 3253 (NH), 1690, 1669 (CO) cm^{-1}. ^1H NMR ($CDCl_3$) δ: 1.26 (t, 3H, J= 6.6 Hz, CH_3), 4.16 (s, 2H, CH_2), 4.31 (q, J= 6.6 Hz, 2H, CH_2), 5.93 (br s, 1H, NH), 6.82 (dd, J= 2.0, 8.0 Hz, 1H, H-6), 6.96 (s, 1H, H-5"), 7.25 (t, 1H, J= 8.0 Hz, H-5'), 7.46 (d, J= 8.0Hz, 1H, H-7), 7.47 (s, 1H, H-2"), 7.73 (d, J= 2.0 Hz, 1H, H-4), 7.89 (dq, J= 2.0,

8.0 Hz, 1H, H-6'), 8.07 (dd, J= 2.0, 8.0 Hz, 1H, H-2'), 10.35 (s, 1H, NH). ^{13}C NMR (DMSO-d_6) δ: 14.0, 40.6, 60.9, 103.0, 117.0, 117.9, 119.6 (s), 120.0, 123.0, 123.4, 126.1, 129.0, 129.1, 130.3, 131.7, 134.4, 134.8, 136.9, 146.8, 161.7, 163.3, 172.2. Anal. Calcd. (%) for $C_{22}H_{18}ClFN_4O_4$: C, 57.84; H, 3.97; N, 12.26; found: C, 57.87; H, 3.93; N, 12.23.

Ethyl 3-benzoylamino-5-[(5-methyl-1H-imidazol-4-yl-methyl)-amino]-benzo[b]furan-2-carboxylate (13a). Yield 30%. Mp 183-184 °C. IR ν_{max}: 3311, 3248 (NH), 1687, 1664 (CO) cm^{-1}. ^{1}H NMR (DMSO-d_6) δ: 1.26 (t, J= 6.0 Hz, 3H, CH_3), 2.19 (s, 3H, CH_3), 4.14 (br s, 2H, CH_2), 4.31 (q, J= 6.0 Hz, 2H, CH_2), 5.98 (br s, 1H, NH), 6.82 (d, J= 2.0 Hz, 1H, H-4), 6.99 (dd, J= 2.0, 8.0 Hz, 1H, H-6), 7.54-7.72 (m, 3H, H-3', H-4', H-5'), 8.00-8.13 (m, 3H, H-2', H-6', H-2"), 10.28 (s, 1H, NH), 13.12 (br s, 1H, NH). ^{13}C NMR (DMSO-d_6) δ: 9.1, 14.0, 54.9, 60.8, 101.7, 112.5, 117.6, 124.3, 125.7, 126.5, 127.0, 127.3, 127.7, 128.7, 132.9, 133.4, 135.2, 144.7, 147.1, 159.2, 164.9. Anal. Calcd. (%) for $C_{23}H_{22}N_4O_4$: C, 66.02; H, 5.30; N, 13.39; found: C, 66.06; H, 5.34; N, 13.35.

Ethyl 5-[(5-methyl-1H-imidazol-4-yl-methyl)-amino]-3-(4-methoxy-benzoylamino)-benzo[b]furan-2-carboxylate (13b). Yield 34%. Mp 154-155 °C. IR ν_{max}: 3310, 3247 (NH), 1691, 1665 (CO) cm^{-1}. ^{1}H NMR (DMSO-d_6): δ 1.26 (t, J= 6.0 Hz, 3H, CH_3), 2.14 (s, 3H, CH_3), 3.87 (s, 3H, OCH_3), 4.05 (br s, 2H, CH_2), 4.29 (q, J= 6.0 Hz, 2H, CH_2), 5.83 (br s, 1H, NH), 6.85 (d, J= 2.0 Hz, 1H, H-4), 7.00 (dd, J= 2.0, 9.7 Hz, 1H, H-6), 7.12 (d, J= 8.0 Hz, 2H, H-2', H-6'), 7.43 (d, J= 9.7 Hz, 1H, H-7), 7.53 (s, 1H, H-2"), 8.04 (d, J= 8.0 Hz, 2H, H-3', H-5'), 10.13 (s, 1H, NH). ^{13}C NMR (DMSO-d_6) δ: 10.1, 14.0, 39.4, 55.5, 60.7, 101.4, 105.8, 112.2, 113.8, 124.4, 125.7, 127.3, 129.7, 133.1, 135.0, 144.1, 145.3, 146.8, 159.3, 162.2, 164.1, 172.0. Anal. Calcd. (%) for $C_{24}H_{24}N_4O_5$: C, 64.28; H, 5.39; N, 12.49; found: C, 64.24; H, 5.35; N, 12.47.

Ethyl 5-[(5-methyl-1H-imidazol-4-yl-methyl)-amino]-3-(4-methyl-benzoylamino)-benzo[b]furan-2-carboxylate (13c). Yield 15%. Mp 168-169 °C. IR ν_{max}: 3311, 3258 (NH), 1681, 1670 (CO) cm^{-1}. ^{1}H NMR (DMSO-d_6) δ: 1.26 (t, J= 6.0 Hz, 3H, CH_3), 1.82 (s, 3H, CH_3), 1.92 (s,

1H, CH_3), 4.15 (s, 2H, CH_2), 4.30 (q, J= 6.0 Hz, 2H, CH_2), 6.12 (br s, 1H, NH), 6.85 (d, J= 2.0 Hz, H-4), 7.00 (dd, J= 2.0, 8.0 Hz, 1H, H-6), 7.40 (d, J= 8.0 Hz, 1H, H-7), 7.45 (d, J= 8.0 Hz, 2H, H-3', H-5'), 7.97 (d, J= 8.0 Hz, 2H, H-2', H-6'), 8.08 (s, 1H, H-2"), 10.21 (s, 1H, NH). ^{13}C NMR (DMSO-d_6) δ: 9.5, 14.1, 21.0, 38.4, 60.8, 101.7, 112.4, 117.6, 124.3, 125.7, 127.2, 127.7, 129.2, 130.6, 133.0, 135.0, 142.2, 144.9, 147.0, 159.3, 164.5, 172.1. Anal. Calcd. (%) for $C_{24}H_{24}N_4O_4$: C, 66.65; H, 5.59; N, 12.96; found: C, 66.67; H, 5.54; N, 12.98.

Ethyl 5-[(5-methyl-1H-imidazol-4-yl-methyl)-amino]-3-(3,4,5-trimethoxy-benzoylamino)-benzo[b]furan-2-carboxylate (13d). Yield 27%. Mp 162-163 °C. IR ν_{max}: 3307, 3239 (NH), 1686, 1665 (CO) cm^{-1}. ^{1}H NMR (DMSO-d_6) δ: 1.27 (t, J= 6.0 Hz, 3H, CH_3), 2.21 (s, 3H, CH_3), 3.77 (s, 3H, OCH_3), 3.89 (s, 3H, 2xOCH_3), 4.17 (s, 2H, CH_2), 4.28 (q, J= 6.0 Hz, 2H, CH_2), 6.02 (br s, 1H, NH), 6.24 (d, J= 2.0 Hz, 1H, H-4), 6.99 (dd, J= 2.0, 8.0 Hz, 1H, H-6), 7.40 (s, 2H, H-2', H-6'), 7.47 (d, J= 8.0 Hz, 1H, H-7), 8.23 (s, 1H, H-2"), 10.21 (s, 1H, NH).^{13}C NMR (DMSO-d_6) δ: 10.0, 14.1, 39.7, 55.7, 60.1, 60.8, 105.3, 113.4, 117.6, 123.3, 124.8, 125.8, 127.3, 128.7, 131.9, 135.0, 140.2, 141.2, 143.7, 152.6, 155.3, 158.3, 165.0, 166.7, 172.0. Anal. Calcd. (%) for $C_{26}H_{28}N_4O_7$: C, 61.41; H, 5.55; N, 11.02; found: C, 61.43; H, 5.57; N, 11.05.

Ethyl 5-[(5-methyl-1H-imidazol-4-yl-methyl)-amino]-3-(4-trifluoromethyl-benzoylamino)-benzo[b]furan-2-carboxylate (13e). Yield 90%. Mp 183-184 °C. IR ν_{max}: 3287, 3230 (NH), 1670, 1661 (CO) cm^{-1}. ^{1}H NMR (DMSO-d_6) δ: 1.25 (t, J= 6.0 Hz, 3H, CH_3), 2.10 (s, 3H, CH_3), 4.32 (s, 2H, CH_2), 4.49 (q, J= 6.0 Hz, 2H, CH_2), 6.83 (br s, 1H, NH), 7.07 (dd, J= 2.0, 8.0 Hz, 1H, H-6), 7.41-7.51 (m, 2H, H-4, H-7), 7.99-8.02 (m 3H, H-3', H-5' H-2"), 8.24 (d, J= 8.6 Hz, 2H, H-2', H-6') 10.54 (s, 1H, NH). ^{13}C NMR (DMSO-d_6) δ: 11.1, 14.1, 40.2, 60.8, 112.3, 117.5, 124.4, 124.9, 125.3, 126.2, 128.7, 130.1, 134.7, 135.3, 135.7, 135.9, 137.2, 145.7, 146.2, 158.6, 163.9, 167.5. Anal. Calcd. (%) for $C_{24}H_{21}F_3N_4O_4$: C, 59.26; H, 4.35; N, 11.52; found: C, 59.28; H, 4.33; N, 11.57.

Ethyl 5-[(5-methyl-1H-imidazol-4-yl-methyl)-amino]-3-(3-chloro-4-fluoro-benzoylamino)-benzo[b]furan-2-carboxylate (13f). Yield 54%. Mp 139-141 °C. IR ν_{max}: 3307, 3232 (NH), 1693, 1655 (CO) cm^{-1}. ^{1}H NMR (DMSO-d_6) δ: 1.25 (t, J= 6.7 Hz, 3H, CH_3), 2.13 (s, 3H, CH_3), 4.05 (s, 2H, CH_2), 4.29 (q, J=6.7 Hz, 2H, CH_2), 5.84 (br s, 1H, NH), 6.75 (d, J=2.0 Hz, 1H, H-4), 7.01 (dd, J=2.0, 8.0 Hz, 1H, H-6), 7.44 (d, J=8.0 Hz, 1H, H-7), 7.47 (s, 1H, H-2"), 7.67 (t, J=9.0 Hz, 1H, H-5'), 8.07 (dq, J=2.0, 9.0 Hz, 1H, H-6'), 8.29 (dd, J=2.0, 8.0 Hz, 1H, H-2'), 10.44 (s, 1H, NH). ^{13}C NMR (DMSO-d_6) δ: 10.1, 14.0, 39.7, 60.7, 99.5, 102.5, 112.3, 113.5, 115.9, 117.5, 119.7, 120.6, 124.7, 125.9, 129.0, 130.3, 131.2, 133.1, 136.0, 145.6, 146.7, 158.8, 162.7. Anal. Calcd. (%) for $C_{23}H_{20}ClFN_4O_4$: C, 58.67; H, 4.28; N, 11.90; found: C, 58.65; H, 4.26; N, 11.95.

Biology

Propidium iodide, ribonuclease A (RNAse A), 3-(4,5-dimethyl-2-thiazolyl)-2,5-diphenyl-2H-tetrazolium bromide (MTT), and DMSO were obtained from Sigma Aldrich (St. Louis, MO, USA). RPMI, fetal bovine serum (FBS), phosphate buffered saline (PBS), L-glutamine solution (200 mM), trypsin-EDTA solution (170.000 U/l trypsin and 0.2 g/l EDTA) and penicillin-streptomycin solution (10.000 U/ml penicillin and 10 mg/ml streptomycin) were purchased from Lonza (Verviers, Belgium).

Cell culture

The tumor cell lines HeLa (human epithelial cervical cancer) and MCF-7 (human epithelial breast cancer), were obtained from American Type Culture Collection (ATCC) (Rockville, MD, USA). The cells were cultured as monolayers and maintained in a humidified atmosphere with 5% CO_2 at 37 °C. MCF-7 cells were grown in DMEM while HeLa cells in RPMI. Both medium were supplemented with 5% FBS, 2 mM L-glutamine, 50 IU/ml penicillin, and 50 µg/ml streptomycin. The cells were routinely cultured in 75 cm^2 culture flasks and were trypsinized using trypsin-EDTA when the cells reached approximately 80% confluence. Exponentially growing cells were used for experiments.

Antiproliferative Evaluation Assay

3-benzoylamino-benzo[*b*]furan derivatives **11a-f, 12a-f** and **13a-f** were submitted to the MTT assay to assess the growth inhibition activity against HeLa and MCF-7 tumor cell lines. The MTT assay is based on the protocol first described by Mosmann (107). It is a measurement of cell metabolic activity, and correlates quite well with cell proliferation. The assay was performed as previously described.[15] The cells were seeded into a series of standard 96-well microtiter plates in 100 µl of complete culture medium, at a plating density depending on the doubling times of individual cell line. MCF-7 cells were seeded at 1.5×10^4 cells/cm^2, while HeLa cells were seeded at 1.0×10^4 cells/cm^2. Cells were incubated for 24 h under 5% CO_2 at 37 °C and the medium was then replaced with 100 µl of fresh medium containing the treatments. Benzo[*b*]furan derivatives were previously dissolved in DMSO to obtain 20 mM stock solutions. Working solutions were freshly prepared on the day of testing by dilutions of the stock solutions in the complete culture medium and the synthetized derivatives were tested in the 50–0.1 µM concentration range. 24 h after seeding aliquots of 100 µl of different solutions at the appropriate concentrations were added to the appropriate microtiter wells and the cells were incubated for 48 h, without renewal of the medium. In each experiment DMSO concentration never exceeded 0.25%. and culture medium with 0.25% DMSO was used as control. After the incubation time, cells were washed, and 50 µL FBS-free medium containing 0.5 mg/mL of methyl thiazolyl tetrazolium (MTT) reagent was added. The medium was discarded after to 3h incubation at 37 °C, and formazan blue formed in the cells was dissolved in DMSO. The absorbance (OD, optical density) at 570 nm of MTT-formazan was measured in a microplate reader. The absorbance is directly proportional to the number of living, metabolically active cells.

The percentage of growth (PG) to respect untreated cell control for each drug concentrations was calculated according to one of the following two expressions:

if $(OD_{test} - OD_{tzero}) \geq 0$, then

$PG = 100 \times (OD_{test} - OD_{tzero})/(OD_{ctrl} - OD_{tzero})$;

if $(OD_{test} - OD_{tzero}) < 0$, then

$PG = 100 \times (OD_{test} - OD_{tzero})/OD_{tzero}$,

where OD_{tzero} is the average of optical density measurements before exposure of cells to the test compound, OD_{test} is the average of optical density measurements after the desired period of time, and OD_{ctrl} is the average of optical density measurements after the desired period of time with no exposure of cells to the test compound.

The concentration necessary for 50% of growth inhibition (GI_{50}) for each compound were calculated from concentration−response curves using linear regression analysis by fitting the test concentrations that give PG values above and below the reference value (i.e., 50%). If, however, for a given cell line all of the tested concentrations produce PGs exceeding the respective reference level of, then the highest tested concentration is assigned as the default value, which is preceded by a ">" sign. Each result is a mean value of three separate experiments.

Cell-cycle analysis

Effects of the 3-benzoylamino-benzo[b]furan derivatives **13a-f** exposure on cell-cycle were evaluated by DNA staining with propidium iodide and flow cytometry analysis. HeLa cells were seeded on 6 well plates at a density of 2.5 10^4 cells/cm^2, and treated 24 hours after seeding with or without various concentrations of test compounds. Following the treatments, cells were collected, washed in PBS, fixed in ice-cold 70% ethanol and kept at -20 °C. Fixed cells were centrifuged, resuspended in PBS and stained with staining solution (20 µg/ml propidium iodide, 200 µg/ml RNAse A and Triton X-100 in PBS), for 30 min at 37°C. The DNA contents of more than 10000 cells were subjected to fluorescence-activated cell sorting (FACS) analysis (Coulter® Epics® XL™, Beckman) and the percentage of cells belonging to the different compartments of the cell cycle was determined. All experiments were performed in duplicate and reproduced at least two times.

Acknowledgments

This work was in part supported by an FFR2012 – University of Palermo grant (CUP:B78C12000380001).

Experimental part (G4-binders)

General. All reaction solvents were purified in accordance with Purification of Laboratory Chemicals (Fourth Edition) prior to use. All reagents were used as purchased without further purification. The solvents were removed under reduced pressure using standard rotary evaporators.

All of the reactions were monitored by TLC using Merck's silica gel 60 F_{254}-precoated aluminum sheets. Visualization was accomplished with UV light (254 or 365 nm). Solvent mixtures used for chromatography are always given in a vol/vol ratio. Flash column chromatography was generally performed using Silica Gel 60 (Merck, spherical, 40-63 μm).

Melting points were determined on a Büchi-540 capillary melting point apparatus and are uncorrected.

The high-resolution accurate masses (HRMS) were determined with an Agilent 6230 time-of-flight mass spectrometer. Samples were introduced by the Agilent 1260 Infinity LC system. The mass spectrometer was operated in conjunction with a Jet Stream electrospray ion source in positive ion mode. Reference masses of *m/z* 121.050873 and 922.009798 were used to calibrate the mass axis during analysis. Mass spectra were processed using Agilent MassHunter B.02.00 software.

High-performance liquid chromatography (HPLC) was performed on a Jasco 2080 Plus isocratic binary pump, using a Jasco 2075 Plus variable wavelength absorbance detector and Jasco ChromPass v.1.8.6.1 software.

Elemental analyses were performed on an Elementar VarioEL III apparatus. MW irradiation experiments were carried out in a monomode CEM-Discover MW reactor, using the standard configuration as delivered, including proprietary software. The experiments were executed in 10 or 80 mL MW process vials with control of the temperature by infrared detection. After completion of the reaction, the vial was cooled to 50 °C by air jet cooling.

^{1}H and ^{13}C nuclear magnetic resonance (NMR) spectra were recorded at ambient temperature (if not indicated otherwise), in the solvent indicated, on a Varian Mercury Plus 400 spectrometer at frequency of 400 and 100 MHz or on a Bruker Avance III 500 spectrometer at frequency of 500 and 125 MHz respectively. Chemical shifts are given using the δ-scale (in ppm) relative to tetramethylsilane or the residual solvent signal as an internal reference. Coupling constants are indicated in Hertz (Hz). The

following abbreviations are used for spin multiplicity: s=singlet, d=doublet, t=triplet, q=quartet, m=multiplet, ovl. m=overlapping multiplet, br=broad, dd = doublet doublet, dm = doublet multiplet and tm = triplet multiplet. The signification of the one star (*) in the ^{13}C NMR means tentative assignments.

Biology

Chemicals and reagents

Propidium iodide, ribonuclease A (RNAse A), 3-(4,5-dimethyl-2- thiazolyl)-2,5-diphenyl-2H-tetrazolium bromide (MTT), and DMSO were obtained from Sigma Aldrich (St. Louis, MO, USA). RPMI, fetal bovine serum (FBS), phosphate buffered saline (PBS), L-glutamine solution (200 mM), trypsin-EDTA solution (170.000 U/l trypsin and 0.2 g/l EDTA) and penicillin-streptomycin solution (10.000 U/ml penicillin and 10 mg/ml streptomycin) were purchased from Lonza (Verviers, Belgium).

Cell culture

The cancer cell line HeLa (Human epithelial cervical cancer) was obtained from American Type Culture Collection (ATCC) (Rockville, MD, USA). The cells were cultured in RPMI supplemented with 5% FBS, 2 mM L-glutamine, 50 IU/ml penicillin, and 50 mg/ml streptomycin and maintained in a humidified atmosphere with 5% CO_2 at 37 $^{\circ}C$. The cells were routinely cultured in 75 cm^2 culture flasks and were trypsinized using trypsin-EDTA when the cells reached approximately 80% confluence. Exponentially growing cells were used for experiments.

Antiproliferative evaluation assay

Compounds were submitted to the MTT assay to assess the growth inhibition activity against HeLa cells. The MTT assay is a measurement of cell metabolic activity, quite effective in estimating cell proliferation, which is based on the protocol first described by Mossmann (104). The assay was performed as previously described (105). The cells were seeded into a series of standard 96-well plates in 100 ml of complete culture medium at 1.0 10^4 cells/cm^2. Cells were incubated for 24 h under 5% CO_2 at 37 $^{\circ}C$ and the medium was then replaced with 100 ml of fresh medium supplemented by 5% (v/ v) FBS

containing the treatments. The derivatives were previously dissolved in DMSO to obtain 20 mM stock solutions. Working solutions were freshly prepared on the day of testing by dilutions of the stock solutions in the complete culture medium. For the experiments a concentration range from 50 to 0.05 mM was used. 24 h after seeding aliquots of 100 ml of different solutions at the appropriate concentrations were added to the appropriate wells and the cells were incubated for 48 h without renewal of the medium. In each experiment, DMSO concentration never exceeded 0.25% and culture medium with 0.25% DMSO was used as control. After the incubation time, cells were washed and 100 mL FBS-free medium containing 0.5 mg/mL of MTT was added. The medium was discarded after a 4 h incubation at 37 °C and formazan blue formed in the cells was dissolved in DMSO. The absorbance (optical density, OD) at 570 nm of MTT-formazan was measured in a microplate reader. As the absorbance is directly proportional to the number of living, metabolically active cells, the percentage of growth (PG) to with respect to untreated cell control for each drug concentrations was calculated according to one of the following two expressions:

if $(OD_{test} - Od_{tzero}) \geq 0$; then

$PG = 100 \times (OD_{test} - Od_{tzero})/(OD_{ctr} - Od_{tzero})$

if $(OD_{test} \_ OD_{tzero}) < 0$; then

$PG = 100 (OD_{test} - Od_{tzero})/OD_{tzero}$

where OD_{tzero} is the average of optical density measurements before exposure of cells to the test compound, OD_{test} is the average of optical density measurements after the desired period of time, and OD_{ctr} is the average of optical density measurements after the desired period of time with no exposure of cells to the test compound. The concentration necessary for 50% of growth inhibition (GI50) for each derivative was calculated from concentration-response curves using linear regression analysis by fitting the test concentrations that give PG values above and below the reference value (50%). Each result was the mean value of three separate experiments performed in quadruplicate.

General procedure for the synthesis of bis isoquinoline derivatives 22a-b

To a solution of **20a-b** (2.5 mmol) in acetonitrile, 1,3-dichloro-2-propanol (1.25) was added. The mixture was stirred within a Shlenk flask over 10-20 hours at 140 °C. The reaction solvent was removed by filtration under reduced pressure.

(22a). Yield 95%. Mp 279-283 °C. ^{1}H NMR ($CDCl_3$) δ: 10.23 (s, J= 1.5 Hz, 1H, CH), 8.62 (t, J= 7.5 Hz, 1H, CH), 8.55 (m, 1H, CH), 8.42 (m, 1H, CH), 8.10 (m, 1H, CH), 4.85 (s, J= 7.0 Hz, 2H, CH_2), 8.89 (d, J= 7.5 Hz, H), 3.2 (q, J= 7.0 Hz, 1H), 3.58 (s, OH). ^{13}C NMR ($CDCl_3$) δ: 23.53, 45.82, 70.75, 119.07, 125.92, 126.58, 128.81, 127, 74, 130.80, 136.74, 151.46, 174.90. Anal. Calcd. (%) for $C_{21}H_{20}N_2O^{2+}$: C, 79.72; H, 6.37; N, 8.85; O, 5.06; found: C, 79.75; H, 6.31; N, 8.82; O, 5.08.

(22b). Yield 90%. Mp 271-278 °C. ^{1}H NMR (DMSO-d_6) δ: 10.31 (s, J= 1.5 Hz, 1H, CH), 8.04 (t, J= 1.5 Hz, 1H, CH), 8.55 (m, 1H, CH), 8.42 (m, 1H, CH), 8.10 (m, 1H, CH), 4.85 (s, J= 7.0 Hz, 2H, CH_2), 2.91 (s, 3H, CH_3), 3.2 (q, J= 7.0 Hz, 1H), 3.58 (s, OH). ^{13}C NMR ($CDCl_3$) δ: 20.8, 58.1, 64.7, 124.8, 127.2, 127.3, 128.4, 140.3, 143.2, 155.1. Anal. Calcd. (%) for $C_{23}H_{24}N_2O^{2+}$: C, 80.20; H, 7.02; N, 8.13; O, 4.64 found: C, 80.22; H, 7.07; N, 8.16; O, 4.60.

Synthesis of compound (24)

Under inert atmosphere, to a suspension of **23** in DCM pyridine was added at 0 °C. Then, trifluoromethansulfonic anhydride was added dropwise. The mixture was reacted overnight, at room temperature. A satured solution of $NaHCO_3$ was added until neutralization. The mixture was extracted (3x20ml) with DCM and the collected fraction dried over Na_2SO_4, then filtered and concentrated under reduced pressure. The crude was purified by column chromatography (PE/EtOAc 95:5) to afford a white solid. Recrystallization from ethanol.

(24). Yield 60%. Mp 58.9-60.2 °C. ^{1}H-NMR (DMSO-d_6) δ: 7.91 (d, J= 7.5 Hz, 1H, CH), 7.26 (s, J= 1.5 Hz, 1H, CH), 7.05 (d, J= 1.5 Hz, 1H, CH). ^{13}C NMR ($CDCl_3$) δ: 107.8, 115.2, 117.8, 124.4, 129.6, 137.5, 153.7. Anal. Calcd. (%) for $C_{12}H_6F_6O_6S_2$: C, 33.97; H, 1.43; F, 26.87; O, 22.63; S, 15.11 found: C, 33.95; H, 1.41; F, 26.89; O, 22.65; S, 15.18.

Synthesis of 2,7-bis(4-bromobut-1-yn-1-yl)naphthalene (25)

To a solution of **24** (2.36 mmol) and $Pd(PPh_3)Cl_2$ (0.35 mmol) in DMF was added under N_2, at room temperature a mixture of 4-bromo-1-butyne (4.72 mmol) in THF (8ml), DIPEA (2.5 ml) , CuI (0.3 mmol) and dry DMF (8 ml). The mixture was reacted over 30 min. After that time, the mixture was diluted with DCM and the organic phase extracted with a satured solution of NH_4Cl (1X) followed by extraction with distilled water (2X). The collected organic phases were dried over Na_2SO_4, filtered and dried under reduced pressure to afford a brownish oil. Purification by column cromatography (PE).

(25). Yield 40%. Mp 58.9-60.2 °C. ^{1}H-NMR (DMSO-*d*$_6$) δ: 8.29 (s, 1H, CH), 7.78 (d, J= 1.5 Hz, 1H, CH), 7.53 (d, J= 7.5 Hz, 1H, CH), 3.47 (t, J= 7.5 Hz, 2H, CH_2), 2.53 (t, J= 7.5 Hz, 2H, CH_2). ^{13}C NMR ($CDCl_3$) δ: 24.1, 29.4, 81.9, 102.6, 119.7, 127.7, 129.5, 131.8, 133.2, 135.0. Anal. Calcd. (%) for $C_{18}H_{14}Br_2$: C, 55.42; H, 3.62; Br, 40.96 found: C, 55.40; H, 3.65; Br, 40.97.

Synthesis of 2,7-bis(4-morpholinobut-1-yn-1-yl)naphthalene (26)

To a solution of **25** (5.12 mmol) in dry DCM is added a solution of morpholine (1.12) in dry DCM at room temperature, dropwise. The mixture was reacted refluxing over 3 hours. After cooling, the solvent reaction was removed under reduced pressure and the crude was purified on silica gel (PE/EtOAc 7:3) to give a white solid.

(26). Yield 30%. Mp 80.9-91.5 °C. ^{1}H-NMR (DMSO-*d*$_6$) δ: 8.29 (s, 1H, CH), 7.78 (d, J= 1.5 Hz, 1H, CH), 7.53 (d, J= 7.5 Hz, 1H, CH), 2.53 (t, J= 7.1 Hz, 2H, CH_2), 2.13 (t, J= 7.5 Hz, 2H, CH_2), 2.36 (d, J= 7.1 Hz, 2H, CH_2), 3.65 (d, J= 7.5 Hz, 2H, CH_2). ^{13}C NMR (DMSO-*d*$_6$) δ: 17.1, 55.2, 58.9, 66.7, 81.9, 102.6, 119.7, 127.7, 129.5, 131.8, 133.2, 135.0. Anal. Calcd. (%) for $C_{26}H_{30}N_2O_2$: C, 77.58; H, 7.51; N, 6.96; O, 7.95 found: C, 77.6; H, 7.53; N, 6.93; O, 7.94.

Synthesis of 5,5'-(naphthalene-2,7-diylbis(oxy))bis(2-benzyl-4-bromopyridazin-3(2*H*)-one) (28)

2,7-Dihydroxynaphthalene (0.31 mmol) was dissolved in DMF and $K^+(CH_3)CO^-$ (0.94 mmol) was added. After 30min, **27** (0.62 mmol) was added to the mixture and it was refluxed for 3 hours. The solvent was removed under reduced pressure. Distilled water was added to the mixture that was extracted with DCM (5X30 ml). The collected organic phases were subsequently dried over Na_2SO_4 and concentrated. The solvent was

evaporated under reduced pressure and the compounds were purified by column chromatography (Hexane/EtOAc 7:3). Recrystallization from diethyl ether.

28. Yield 95%. Mp 115.1-120.3 °C. ^{1}H-NMR (DMSO-*d*$_6$) δ: 7.91 (d, J= 7.5 Hz 1H, CH), 7.68 (m, 1H, CH), 7.50 (s, 1H, CH), 7.33 (m, 1H, CH), 7.26 (m, 1H, CH), 7.26 (s, J= 1.5 Hz, 1H, CH), 6.10 (d, J= 7.5 Hz, 2H, CH_2). ^{13}C NMR (DMSO-*d*$_6$) δ: 34.7, 107.8, 115.2, 124.4, 126.4, 126.7, 126.9, 128.5, 129.6, 133.2, 134.5, 137.5, 148.8, 153.9, 155.4. Anal. Calcd. (%) for $C_{32}H_{22}Br_2N_4O_4$: C, 56.00; H, 3.23; Br, 23.28; N, 8.16; O, 9.32 found: C, 56.04; H, 3.26; Br, 23.31; N, 8.18; O, 9.37.

Synthesis compound (33).

A mixture of **28** (0.06 mmol), $Pd(PPh_3)_2Cl_2$ (20%mol), and NaOAcx3H_2O (0.15 mmol)in DMA was stirred at 110 °C under Ar atmosphere over 3 hours. The mixture was evaporated to dryness in vacuo. Distilled water was added and the mixture was subsequently extracted with chloroform. The combined organic phases were dried over Na_2SO_4. The solvent was evaporated under reduced pressure to afford a grey powder.

(33) Yield 100%. Mp 269.1-273.5 °C. ^{1}H-NMR (DMSO-*d*$_6$) δ: 7.80 (s, J= 1.5 Hz, 1H, CH), 7.73 (s, 1H, CH), 7.68 (m, 1H, CH), 7.69 (m, 1H, CH), 7.66 (d, J= 7.5 Hz, 1H, CH), 7.59 (d, J= 7.5 Hz 1H, CH), 7.50 (s, 1H, CH), 7.51 (s, 1H, CH), 6.10 (s, 2H, CH_2). ^{13}C NMR (DMSO-*d*$_6$) δ: 51.5, 111.5, 113.4, 120.4, 121.2, 123.1, 126.7, 126.9, 128.3, 128.5, 130.6, 134.5, 138.5, 143.0, 154.7, 158.4, 158.5. Anal. Calcd. (%) for $C_{32}H_{20}N_4O_4$: C, 73.27; H, 3.84; N, 10.68; O, 12.20 found: C, 73.29; H, 3.82; N, 10.66; O, 12.23.

Synthesis of 5,5'-((3,6-dibromonaphthalene-2,7-diyl)bis(oxy))bis(2-benzylpyridazin-3(2*H*)-one) (31).

3,6-Dibromo-2,7-dihydroxynaphthalene (0.63 mmol) was dissolved in dry CH_3CN and K_2CO_3 (3.15 mmol) was added. After 30min, **30** (1.26 mmol) was added to the mixture and it was refluxed for 3 hours in a microwave reactor. The solvent was removed under reduced pressure. Distilled water was added to the mixture that was extracted with DCM (5X30 ml). The collected organic phases were subsequently dried over Na_2SO_4 and concentrated. The solvent was evaporated under reduced pressure and the compound was purified by column chromatography (Hexane/EtOAc 7:3). Recrystallization from diethyl ether.

(31) Yield 60%. Mp 141.7-143.9 °C. ^{1}H-NMR (DMSO-d_6) δ: 8.13 (s, J= 1.5 Hz, 1H, CH), 7.68 (m, 1H, CH), 7.50 (s, 1H, CH), 7.33 (m, 1H, CH), 7.26 (m, 1H, CH), 7.09 (s, 1H, CH) 6.10 (s, 2H, CH_2), 5.12 (s, 1H, CH). ^{13}C NMR (DMSO-d_6) δ: 35.4, 109.0, 110.8, 113.5, 126.7, 126.9, 127.1, 128.5, 130.3, 130.5, 134.5, 138.9, 157.0, 159.4, 161.5. Anal. Calcd. (%) for $C_{32}H_{22}Br_2N_4O_4$: C, 56.00; H, 3.23; Br, 23.28; N, 8.16; O, 9.32 found: C, 56.04; H, 3.21; Br, 23.29; N, 8.19; O, 9.36.

Synthesis compound (32)

A mixture of **31** (0.7 mmol), $Pd(PPh_3)_2Cl_2$ (20%mol), and NaOAcx3H_2O (1.75 mmol) in DMA was stirred at 130 °C under N_2 atmosphere over 3 hours. The mixture was evaporated to dryness in vacuo. Distilled water was added and the mixture was subsequently extracted with chloroform. The combined organic phases were dried over Na_2SO_4. The solvent was evaporated under reduced pressure to afford a yellow powder.

(32) Yield 40%. Mp 159.7-163.5 °C. ^{1}H-NMR (DMSO-d_6) δ: 7.80 (s, J= 1.5 Hz, 1H, CH), 7.73 (s, J= 1.5 Hz, 1H, CH), 7.68 (m, 1H, CH), 7.50 (s, 1H, CH), 7.33 (m, 1H, CH), 7.26 (m, 1H, CH), 6.10 (s, 2H, CH_2). ^{13}C NMR (DMSO-d_6) δ: 51.5, 120.4, 121.2, 123.1, 126.7, 126.9, 128.5, 128.3, 128.7, 129.7, 134.5, 143.0, 154.7, 158.4, 158.5, Anal. Calcd. (%) for $C_{32}H_{20}N_4O_4$: C, 73.27; H, 3.84; N, 10.68; O, 12.20 found: C, 73.24; H, 3.82; N, 10.67; O, 12.19.

Synthesis of 5,5'-(1,2-phenylenebis(oxy))bis(2-benzyl-4-bromopyridazin-3(2*H*)-one) (37)

1,2-Dihydroxybenzene (9.1 mmol) was dissolved in dry CH_3CN and dry K_2CO_3 (73 mmol) was added. After 30min, **27** (18.2 mmol) was added to the mixture and it was refluxed for 3 hours, at 85 °C, 200 PSI, 50 watt in a microwave reactor. The solvent was removed under reduced pressure. Distilled water was added to the mixture that was extracted with DCM (5X30 ml). The collected organic phases were subsequently dried over Na_2SO_4 and concentrated. The solvent was evaporated under reduced pressure and the compound was purified by column chromatography (Hexane/EtOAc 7:3). Recrystallization from diethyl ether.

(37) Yield 50%. Mp 189.1-189.6 °C. ^{1}H-NMR (DMSO-d_6) δ: 7.68 (m, 1H, CH), 7.50 (s, 1H, CH), 7.50 (s, 1H, CH), 7.33 (m, 1H, CH), 7.26 (m, 1H, CH), 6.84 (d, J= 7.5 Hz, 1H, CH), 6.78 (d, J= 7.5 Hz, 1H, CH), 6.10 (s, 2H, CH_2). ^{13}C NMR (DMSO-d_6) δ: 34.7, 116.3, 123.6, 126.4, 126.7, 126.9, 128.5, 133.2, 134.5, 142.8, 148.8, 155.4, Anal. Calcd.

(%) for $C_{28}H_{20}Br_2N_4O_4$: C, 52.85; H, 3.17; Br, 25.12; N, 8.81; O, 10.06 found: C, 52.83; H, 3.11; Br, 25.15; N, 8.80; O, 10.04.

Synthesis of 5,5'-(naphthalene-1,8-diylbis(oxy))bis(2-benzyl-4-bromopyridazin-3(2*H*)-one) (38)

1,8-Dihydroxynaphthalene (3.75 mmol) was dissolved in dry CH_3CN and dry K_2CO_3 (18.75 mmol) was added. After 30min, **27** (1.26 mmol) was added to the mixture and it was refluxed for 4 hours, at 100 °C, 200 PSI, 50 watt in a microwave reactor. The solvent was removed under reduced pressure. Distilled water was added to the mixture that was extracted with DCM (5X30 ml). The collected organic phases were subsequently dried over Na_2SO_4 and concentrated. The solvent was evaporated under reduced pressure and the compound was purified by column chromatography (Hexane/EtOAc 7:3). Recrystallization from diethyl ether.

(38) Yield 50%. Mp 246.9-247.4 ^oC. ^1H-NMR (DMSO-d_6) δ: 7.73 (d, 1H, CH), 7.68 (m, 1H, CH), 7.50 (s, 1H, CH), 7.43 (t, 1H, CH), 7.33 (m, 1H, CH), 7.26 (m, 1H, CH), 6.71 (d, J= 7.5 Hz, 1H, CH), 6.78 (m, 1H, CH), 6.10 (s, 2H, CH_2). ^{13}C NMR (DMSO-d_6) δ: 34.7, 109.7, 110.6, 114.9, 126.4, 126.7, 126.9, 128.5, 133.2, 134.5, 134.6, 146.2, 148.8, 155.4. Anal. Calcd. (%) for $C_{28}H_{20}Br_2N_4O_4$: C, 52.85; H, 3.17; Br, 25.12; N, 8.81; O, 10.06 found: C, 52.83; H, 3.11; Br, 25.15; N, 8.80; O, 10.04.

Synthesis of 5,5'-(naphthalene-2,7-diylbis(oxy))bis(4-bromo-2-methylpyridazin-3(2*H*)-one) (40)

2,7-Dihydroxybenzene (1.25 mmol) was dissolved in dry CH_3CN and dry K_2CO_3 (6.25 mmol) was added. After 30min, **39** (2.50 mmol) was added to the mixture and it was refluxed for 19 hours. The solvent was removed under reduced pressure. Distilled water was added to the mixture that was extracted with DCM (5X30 ml). The collected organic phases were subsequently dried over Na_2SO_4 and concentrated. The solvent was evaporated under reduced pressure and the compound was purified by column chromatography (Hexane/EtOAc 7:3). Recrystallization from diethyl ether.

(40) Yield 30%. Mp 170.9-172.4 ^oC. ^1H-NMR (DMSO-d_6) δ: 7.91 (d, 1H, CH), 7.50 (s, 1H, CH), 7.26 (s, 1H, CH), 7.05 (d, 1H, CH), 2.74 (s, 1H, NH). ^{13}C NMR (DMSO-d_6) δ: 39.9, 107.8, 115.2, 124.4, 126.4, 133.2, 137.5, 148.8, 153.9, 155.4. Anal. Calcd. (%) for $C_{28}H_{20}Br_2N_4O_4$: C, 52.85; H, 3.17; Br, 25.12; N, 8.81; O, 10.06 found: C, 52.83; H, 3.11; Br, 25.15; N, 8.80; O, 10.04.

6. References

1. Hannon MJ. Supramolecular DNA recognition. *Chem Soc Rev*. **2007**;36(2), 280–95.

2. Li X, Mishra SK, Wu M, Zhang F, Zheng J. Syn-Lethality: An Integrative Knowledge Base of Synthetic Lethality towards Discovery of Selective Anticancer Therapies. *Bio. Med. Res. Int*. **2014**;2014:1–7.

3. Morandell S, Yaffe MB. Exploiting Synthetic Lethal Interactions Between DNA Damage Signaling, Checkpoint Control, and p53 for Targeted Cancer Therapy. In: Progress in *Mol. Biol. Translational Science Elsevier*; **2012** p. 289–314. Available from: http://linkinghub.elsevier.com/retrieve/pii/B9780123876652000110

4. Waldman T, Zhang Y, Dillehay L, Yu J, Kinzler K, Vogelstein B, et al. Cell-cycle arrest versus cell death in cancer therapy. *Nat. Med*. **1997**;3(9):1034–6.

5. Borison, H.L., Brand, E.D., Orkand, R.K. Am. *J. Physiol*. Emetic action of nitrogen mustard (mechloretamine hydrochloride) in dogs and cats. **1958**;192:410–6.

6. Pittillo RF, Schabel FM, Wilcox WS, Skipper HE. Experimental evaluation of potential anticancer agents. XVI. Basic study of effects of certain anticancer agents on kinetic behavior of model bacterial cell populations. *Cancer Chemother Rep*. **1965**;47:1–26.

7. Silverman RB. The organic chemistry of drug design and drug action. 2nd ed. Amsterdam ; Boston: Elsevier Academic Press; **2004**. 617 p.

8. Hendry LB, Mahesh VB, Bransome ED, Ewing DE. Small molecule intercalation with double stranded DNA: Implications for normal gene regulation and for predicting the biological efficacy and genotoxicity of drugs and other chemicals. *Mutat Res*, *Fundam Mol Mech Mutagen*. **2007**;623(1-2):53–71.

9. Zeglis BM, Pierre VC, Barton JK. Metallo-intercalators and metallo-insertors. *Chem Commun.* **2007**;(44):4565–79.

10. Balasubramanian S, Hurley LH, Neidle S. Targeting G-quadruplexes in gene promoters: a novel anticancer strategy? *Nat Rev Drug Discov*. **2011**;10(4):261–75.

11. Dickerson RE, Drew HR, Conner BN, Wing RM, Fratini AV, Kopka ML. The anatomy of A-, B-, and Z-DNA. *Science*. **1982**;216(4545):475–85.

12. Saenger W. Principles of nucleic acid structure. New York: Springer-Verlag; **1984**.

13. Beak P. Energies and alkylations of tautomeric heterocyclic compounds: old problems - new answers. *Acc. Chem. Res*. **1977**,10(5):186–92.

14. Wolfenden RV. Tautomeric equilibria in inosine and adenosine. *J. Mol. Biol*.

1969;40(2):307–10.

15. Chenon MT, Pugmire RJ, Grant DM, Panzica RP, Townsend LB. Carbon-13 magnetic resonance. XXV. Basic set of parameters for the investigation of tautomerism in purines established from carbon-13 magnetic resonance studies using certain purines and pyrrolo[2,3-d]pyrimidines. *J.A.C.S*. **1975**;97(16):4627–36.

16. Kool ET. Replacing the Nucleobases in DNA with Designer Molecules. *Acc. Chem. Res.*. **2002**;35(11):936–43.

17. Khakshoor O, Wheeler SE, Houk KN, Kool ET. Measurement and Theory of Hydrogen Bonding Contribution to Isosteric DNA Base Pairs. *J.A.C.S.***2012**;134(6):3154–63.

18. Schweitzer BA, Kool ET. Aromatic Nonpolar Nucleosides as Hydrophobic Isosteres of Pyrimidines and Purine Nucleosides. *J.O.C.* **1994**;59(24):7238–42.

19. Kool ET. Hydrogen bonding, base stacking, and steric effects in dna replication. *Annu. Rev. Biophys. Biomol. Struct*. **2001**;30:1–22.

20. Kool ET. Active site tightness and substrate fit in DNA replication. *Annu Rev Biochem.* **2002**;71:191–219.

21. Guckian KM, Kool ET. Highly Precise Shape Mimicry by a Difluorotoluene Deoxynucleoside, a Replication-Competent Substitute for Thymidine. *Angew. Chem. Int. Ed.* **1997**;36(24):2825–8.

22. Guckian KM, Krugh TR, Kool ET. Solution structure of a DNA duplex containing a replicable difluorotoluene-adenine pair. *Nat. Struct. Biol*. **1998**;5(11):954–9.

23. Moran S, Ren RX-F, Rumney S, Kool ET. Difluorotoluene, a Nonpolar Isostere for Thymine, Codes Specifically and Efficiently for Adenine in DNA Replication. *J. Am. Chem. Soc.* **1997**;119(8):2056–7.

24. Kunkel TA, Bebenek K. DNA replication fidelity. *Annu. Rev. Biochem.* **2000**;69:497–529.

25. Goodman MF. Hydrogen bonding revisited: Geometric selection as a principal determinant of DNA replication fidelity. Proceedings of the National Academy of Sciences. **1997**;94(20):10493–5.

26. Lauria A, Terenzi A, Bartolotta R, Bonsignore R, Perricone U, Tutone M, et al. Does Ligand Symmetry Play a Role in the Stabilization of DNA G-Quadruplex Host-Guest Complexes? *Current Medicinal Chemistry*. **2014**;21(23):2665–90.

27. Collie GW, Parkinson GN. The application of DNA and RNA G-quadruplexes to

therapeutic medicines. *Chem Soc Rev.* **2011**;40(12):5867–92.

28. Aisner D. Telomerase regulation: not just flipping the switch. *Curr. Opin. Genet. Dev.* **2002**;12(1):80–5.

29. Düchler M. G-quadruplexes: targets and tools in anticancer drug design. *J. Drug. Targ*. **2012**;20(5):389–400.

30. Shalaby T, Fiaschetti G, Nagasawa K, Shin-ya K, Baumgartner M, Grotzer M. G-Quadruplexes as Potential Therapeutic Targets for Embryonal Tumors. *Molecules.* **2013**;18(10):12500–37.

31. Dexheimer TS, Sun D, Hurley LH. Deconvoluting the Structural and Drug-Recognition Complexity of the G-Quadruplex-Forming Region Upstream of the bcl-2 P1 Promoter. *J. Am. Chem. Soc*. **2006**;128(16):5404–15.

32. Sun D, Guo K, Rusche JJ, Hurley LH. Facilitation of a structural transition in the polypurine/polypyrimidine tract within the proximal promoter region of the human VEGF gene by the presence of potassium and G-quadruplex-interactive agents. *Nucl Acids Res*. **2005**;33(18):6070–80.

33. De Armond R, Wood S, Sun D, Hurley LH, Ebbinghaus SW. Evidence for the Presence of a Guanine Quadruplex Forming Region within a Polypurine Tract of the Hypoxia Inducible Factor 1α Promoter†. *Biochem*. **2005**;44(49):16341–50.

34. Palumbo SL, Memmott RM, Uribe DJ, Krotova-Khan Y, Hurley LH, Ebbinghaus SW. A novel G-quadruplex-forming GGA repeat region in the c-myb promoter is a critical regulator of promoter activity. *Nucl. Acids. Res*. **2008**;36(6):1755–69.

35. Cogoi S, Paramasivam M, Spolaore B, Xodo LE. Structural polymorphism within a regulatory element of the human KRAS promoter: formation of G4-DNA recognized by nuclear proteins. *Nucl. Acids. Res*. **2008**;36(11):3765–80.

36. Paramasivam M, Membrino A, Cogoi S, Fukuda H, Nakagama H, Xodo LE. Protein hnRNP A1 and its derivative Up1 unfold quadruplex DNA in the human KRAS promoter: implications for transcription. *Nucl. Acids. Res*. **2009**;37(9):2841–53.

37. McElligott R, Wellinger RJ. The terminal DNA structure of mammalian chromosomes. *EMBO J.* **1997**;16(12):3705–14.

38. Wright WE, Tesmer VM, Huffman KE, Levene SD, Shay JW. Normal human chromosomes have long G-rich telomeric overhangs at one end. *Genes & Dev.* **1997**;11(21):2801–9.

39. De Lange T. Shelterin: the protein complex that shapes and safeguards human

telomeres. *Genes & Dev*. **2005**;19(18):2100–10.

40. Moyzis RK, Buckingham JM, Cram LS, Dani M, Deaven LL, Jones MD, et al. A highly conserved repetitive DNA sequence, (TTAGGG)n, present at the telomeres of human chromosomes. *Proc Natl Acad Sci U S A*. **1988**;85(18):6622–6.

41. Griffith JD, Comeau L, Rosenfield S, Stansel RM, Bianchi A, Moss H, et al. Mammalian Telomeres End in a Large Duplex Loop. *Cell*. **1999**;97(4):503–14.

42. Artandi SE, DePinho RA. Telomeres and telomerase in cancer. *Carcinogenesis*. **2009**;31(1):9–18.

43. Greider CW, Blackburn EH. A telomeric sequence in the RNA of Tetrahymena telomerase required for telomere repeat synthesis. *Nature*. **1989**;337(6205):331–7.

44. Mergny JL. Natural and pharmacological regulation of telomerase. *Nucl Acids Res*. **2002**;30(4):839–65.

45. Meyerson M, Counter CM, Eaton EN, Ellisen LW, Steiner P, Caddle SD, et al. hEST2, the Putative Human Telomerase Catalytic Subunit Gene, Is Up-Regulated in Tumor Cells and during Immortalization. *Cell*. **1997**;90(4):785–95.

46. Kirkpatrick KL, Mokbel K. The significance of human telomerase reverse transcriptase (hTERT) in cancer. *Eur. J. Surgic. Oncol*. **2001**;27(8):754–60.

47. Chen J-L, Blasco MA, Greider CW. Secondary Structure of Vertebrate Telomerase RNA. *Cell*. **2000**;100(5):503–14.

48. Neumann AA, Reddel RR. Opinion: Telomere maintenance and cancer - look, no telomerase. *Nat. Rev. Cancer*. **2002**;2(11):879–84.

49. Cesare AJ, Reddel RR. Alternative lengthening of telomeres: models, mechanisms and implications. *Nat Rev Genet*. **2010;**11(5):319–30.

50. Oganesian L, Karlseder J. Telomeric armor: the layers of end protection. *J Cell Sci*. **2009**;122(22):4013–25.

51. Lei M, Podell ER, Cech TR. Structure of human POT1 bound to telomeric single-stranded DNA provides a model for chromosome end-protection. *Nat. Struct. Mol. Biol.* **2004**;11(12):1223–9.

52. Zahler AM, Williamson JR, Cech TR, Prescott DM. Inhibition of telomerase by G-quartet DMA structures. Nature. 1991 Apr 25;350(6320):718–20.

53. Reed JE, Arola-Arnal A, Neidle S, Vilar R. Stabilization of G-quadruplex DNA and inhibition of telomerase activity by square-planar nickel(II) complexes. J Am Chem Soc. 2006;128(18):5992–3.

54. Neidle S, Parkinson G. Telomere maintenance as a target for anticancer drug discovery. *Nat. Rev. Drug. Disc*. **2002**;1(5):383–93.

55. Cairns D, Anderson R, Perry P, Jenkins T. Design of Telomerase Inhibitors for the Treatment of Cancer. *Curr Pharm Des*. **2002**;8(27):2491–504.

56. Hurley LH. DNA and its associated processes as targets for cancer therapy. *Nat Rev Cancer*. **2002**;2(3):188–200.

57. Florencia Sassano M. Identification of G-Quadruplex Inducers Usinga Simple, Inexpensiveand Rapid High Throughput Assay, and TheirInhibition of Human Telomerase. *Open Med. Chem. J.* **2012**;6(1):20–8.

58. Dua R, Shrivastava S, Sonwane S.K, Shrivastava S.K. Pharmacological significance of synthetic heterocycles scaffold: a review. *Adv Biol Res*. **2011**;5:120–44.

59. Karcher W, Devillers J, editors. Practical applications of quantitative structure-activity relationships (QSAR) in environmental chemistry and toxicology. Dordrecht ; Boston: Kluwer Academic Publishers; **1990**. 475 p.

60. Langmuir I. Isomorphism, isosterism and covalence. *J.A.C.S.* **1919**;41(10):1543–59.

61. Ali G Fazal Subhan, Nazar Ul Islam, Inamullah Khan, Khalid Rauf, Samiullah, Muzaffar Abbas, Abdur Rauf. Input of Isosteric and Bioisosteric Approach in Drug Design. *J Chem Soc Pak*. **2014**;36, No.1.

62. Brown N, editor. Bioisosteres in medicinal chemistry. Weinheim, Germany: Wiley-VCH; **2012**. 237 p.

63. Williams DA, Lemke TL. Foye's Principi di Chimica Farmaceutica. IV ediz. **2004.**

64. Neidle S. Human telomeric G-quadruplex: The current status of telomeric G-quadruplexes as therapeutic targets in human cancer. *FEBS J.* **2010**;277(5):1118–25.

65. Rezler EM, Bearss DJ, Hurley LH. Telomere Inhibition and Telomere Disruption as Processes for Drug Targeting. *Annu Rev Pharmacol Toxicol*. **2003**;43(1):359–79.

66. Cuesta J, Read M, Neidle S. The Design of G-quadruplex Ligands as Telomerase Inhibitors. *Mini Rev. Med. Chem*. **2003** Feb 1;3(1):11–21.

67. Rohs R, West SM, Sosinsky A, Liu P, Mann RS, Honig B. The role of DNA shape in protein–DNA recognition. *Nature*. **2009**;461(7268):1248–53.

68. Da Ros T, Spalluto G, Prato M, Saison-Behmoaras T, Boutorine A, Cacciari B. Oligonucleotides and oligonucleotide conjugates: A new approach for cancer treatment. *Curr. Med. Chem*. **2005**;12(1):71–88.

69. Thuong NT, Helene C. Sequence-Specific Recognition and Modification of Double-Helical DNA by Oligonucleotides. *Angew. Chem.,* Int Ed. **1993**;32(5):666–90.

70. Bando T, Sugiyama H. Synthesis and Biological Properties of Sequence-Specific DNA-Alkylating Pyrrole−Imidazole Polyamides. *Acc. Chem. Res*. **2006**;39(12):935–44.

71. Burridge JM, Quarendon P, Reynolds CA, Goodford PJ. Electrostatic potential and binding of drugs to the minor groove of DNA. *J. Mol. Graph*. **1987**;5(3):165–6.

72. Kopka ML, Yoon C, Goodsell D, Pjura P, Dickerson RE. The molecular origin of DNA-drug specificity in netropsin and distamycin. *Proc. Natl. Acad. Sci.* **1985**;82(5):1376–80.

73. Lerman LS. Structural considerations in the interaction of DNA and acridines. *J. Mol. Biol*. **1961**;3:18–30.

74. Topcu Z. DNA topoisomerases as targets for anticancer drugs. *J. Clin. Pharm. Ther.* **2001**;26(6):405–16.

75. Ulukan H, Swaan PW. Camptothecins: a review of their chemotherapeutic potential. Drugs. **2002**;62(14):2039–57.

76. Liu LF. DNA topoisomerase poisons as antitumor drugs. *Annu Rev Biochem.* **1989**;58:351–75.

77. Sobell HM. Actinomycin and DNA transcription. *Proc. Natl. Acad. Sci. U S A*. **1985**;82(16):5328–31.

78. Zittoun R, Bury J, Stryckmans P, Lowenberg B, Peetermans M, Rozendaal KY, et al. Amsacrine with high-dose cytarabine in acute leukemia. *Canc. Treat. Rep*. **1985**;69(12):1447–8.

79. Gewirtz DA. A critical evaluation of the mechanisms of action proposed for the antitumor effects of the anthracycline antibiotics adriamycin and daunorubicin. *Biochem. Pharmacol*. **1999**;57(7):727–41.

80. Biological alkylating agents. W. C. J. Ross, Butterworth Inc. *J. Pharm. Sci*. **1962**;51(10):1016–1016.

81. Krumbhaar EB, Krumbhaar HD. The Blood and Bone Marrow in Yelloe Cross Gas (Mustard Gas) Poisoning: Changes produced in the Bone Marrow of Fatal Cases. *J. Med. Res.* **1919**;40(3):497–508.3.

82. Gilman A, Philips FS. The Biological Actions and Therapeutic Applications of the B-Chloroethyl Amines and Sulfides. *Science*. **1946**;103(2675):409–36.

83. Burger AM. The G-Quadruplex-Interactive Molecule BRACO-19 Inhibits Tumor

Growth, Consistent with Telomere Targeting and Interference with Telomerase Function. *Cancer Res.* **2005**;65(4):1489–96.

84. Martorana A, Gentile C, Perricone U, Piccionello AP, Bartolotta R, Terenzi A, et al. Synthesis, antiproliferative activity, and in silico insights of new 3-benzoylamino-benzo[b]thiophene derivatives. *Eur. J. of Med. Chem*. **2015**;90:537–46.

85. Lu Y, Chen J, Xiao M, Li W, Miller DD. An Overview of Tubulin Inhibitors That Interact with the Colchicine Binding Site. *Pharm. Res.* **2012**;29(11):2943–71.

86. Penthala NR, Sonar VN, Horn J, Leggas M, Yadlapalli JSKB, Crooks PA. Synthesis and evaluation of a series of benzothiophene acrylonitrile analogs as anticancer agents. *Med. Chem. Comm*. **2013**;4(7):1073.

87. Nakagawa-Goto K, Wu P-C, Lai C-Y, Hamel E, Zhu H, Zhang L, et al. Antitumor Agents. 284. New Desmosdumotin B Analogues with Bicyclic B-Ring as Cytotoxic and Antitubulin Agents. *J. Med. Chem*. **2011**;54(5):1244–55.

88. Romagnoli R, Baraldi PG, Lopez-Cara C, Preti D, Aghazadeh Tabrizi M, Balzarini J, et al. Concise Synthesis and Biological Evaluation of 2-Aroyl-5-Amino Benzo[b]thiophene Derivatives As a Novel Class of Potent Antimitotic Agents. *J. Med. Chem.* **2013**;56(22):9296–309.

89. Romagnoli R, Baraldi PG, Kimatrai Salvador M, Preti D, Aghazadeh Tabrizi M, Bassetto M, et al. Synthesis and Biological Evaluation of 2-(Alkoxycarbonyl)-3-Anilinobenzo[b]thiophenes and Thieno[2,3- b]pyridines as New Potent Anticancer Agents. *J. Med. Chem*. **2013**;56(6):2606–18.

90. Bridges AJ, Zhou H. Synthesis of [1]benzothieno[3,2-d]pyrimidines substituted with electron donating substituents on the benzene ring. *J. Heterocycl. Chem.* **1997**;34(4):1163–72.

91. Lauria A, Tutone M, Almerico AM. Virtual lock-and-key approach: The in silico revival of Fischer model by means of molecular descriptors. *Eur. J. Med. Chem*. **2011**;46(9):4274–80.

92. Lauria A, Tutone M, Barone G, Almerico AM. Multivariate analysis in the identification of biological targets for designed molecular structures: The BIOTA protocol. *Eur. J. Med. Chem*. **2014**;75:106–10.

93. Lauria A, Abbate I, Patella C, Martorana A, Dattolo G, Almerico AM. New annelated thieno[2,3-e][1,2,3]triazolo[1,5-a]pyrimidines, with potent anticancer activity, designed through VLAK protocol. *Eur. J. Med. Chem*. **2013**;62:416–24.

94. Lauria A, Alfio A, Bonsignore R, Gentile C, Martorana A, Gennaro G, et al. New benzothieno[3,2-d]-1,2,3-triazines with antiproliferative activity: Synthesis, spectroscopic studies, and biological activity. *Bioorg & Med. Chem. Lett*. **2014**;24(15):3291–7.

95. Mingoia F, Di Sano C, Di Blasi F, Fazzari M, Martorana A, Almerico AM, et al. Exploring the anticancer potential of pyrazolo[1,2-a]benzo[1,2,3,4]tetrazin-3-one derivatives: The effect on apoptosis induction, cell cycle and proliferation. *Eur. J. Med. Chem*. **2013**;64:345–56.

96. Monks A, Scudiero D, Skehan P, Shoemaker R, Paull K, Vistica D, et al. Feasibility of a High-Flux Anticancer Drug Screen Using a Diverse Panel of Cultured Human Tumor Cell Lines. *JNCI*. **1991**;83(11):757–66.

97. Weinstein JN, Kohn KW, Grever MR, Viswanadhan VN, Rubinstein LV, Monks AP, et al. Neural computing in cancer drug development: predicting mechanism of action. *Science*. **1992**;258(5081):447–51.

98. Van Osdol WW, Myers TG, Paull KD, Kohn KW, Weinstein JN. Use of the Kohonen Self-organizing Map to Study the Mechanisms of Action of Chemotherapeutic Agents. *JNCI*, **1994**;86(24):1853–9.

99. Lauria A, Ippolito M, Almerico AM. Combined Use of PCA and QSAR/QSPR to Predict the Drugs Mechanism of Action. An Application to the NCI ACAM Database. *QSAR Comb. Sci*. **2009**;28(4):387–95.

100. Romagnoli R, Baraldi PG, Salvador MK, Prencipe F, Lopez-Cara C, Schiaffino Ortega S, et al. Design, Synthesis, in Vitro, and in Vivo Anticancer and Antiangiogenic Activity of Novel 3-Arylaminobenzofuran Derivatives Targeting the Colchicine Site on Tubulin. *J. Med. Chem*. **2015**;58(7):3209–22.

101. Florencia Sassano M. Identification of G-Quadruplex Inducers Usinga Simple, Inexpensiveand Rapid High Throughput Assay, and TheirInhibition of Human Telomerase. *Open Med. Chem. J*. **2012**;6(1):20–8.

102. Mátyus P, Horváth K. Alpha-adrenergic approach in the medical management of benign prostatic hyperplasia. *Med Res Rev*. **1997**;17(6):523–35.

103. Tate DJ, Abdelbasit M, Kilner CA, Shepherd HJ, Warriner SL, Bushby RJ. A simple route to derivatives of benzo[j]fluoranthene. *Tetrahedron.* **2014**;70(1):67–74.

104. Mosmann T. Rapid colorimetric assay for cellular growth and survival: Application to proliferation and cytotoxicity assays. *J. Immun. Meth*. **1983**;65(1–2):55–63.

105. Aleksić M, Bertoša B, Nhili R, Uzelac L, Jarak I, Depauw S, et al. Novel Substituted Benzothiophene and Thienothiophene Carboxanilides and Quinolones: Synthesis, Photochemical Synthesis, DNA-Binding Properties, Antitumor Evaluation and 3D-Derived QSAR Analysis. *J. Med. Chem.* **2012**;55(11):5044–60.
106. LigPrep, Version 2.4, Schroedinger LLC, New York, NY, 2010. 2010;
107. Mosmann T. Rapid colorimetric assay for cellular growth and survival: application to proliferation and cytotoxicity assays. *J. Immunol. Methods*. **1983**;65(1-2):55–63.